**TECHNICAL UNIVERSITY OF CRETE**

**SCHOOL OF MINERAL RESOURCES ENGINEERING**

**MSc PETROLEUM ENGINEERING**

MASTER THESIS:

**EVALUATION OF THE PERFORMANCE OF PHYSICAL MODEL BASED MISCIBLE DISPLACEMENT MODELLING TECHNIQUES**

**Ioannis Tiptiris**

**Supervisor: Varotsis Nikolaos, Professor TUC**
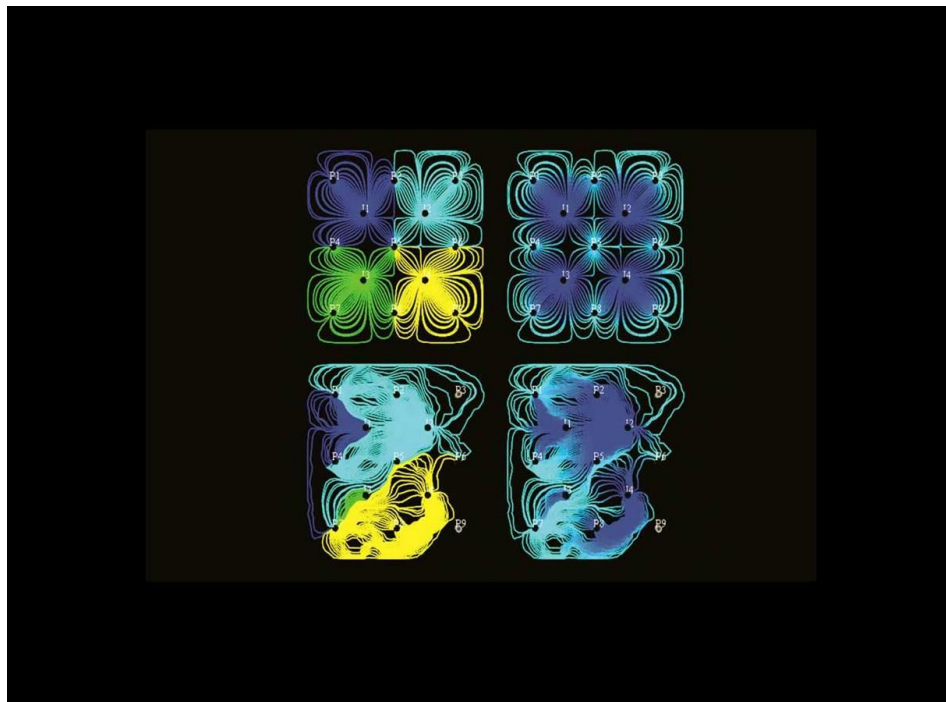


**Examination Committee: Gaganis Vassilios, Varotsis Nikolaos, Pasadakis Nikolaos**

**January 2020**

## ACKNOWLEDGEMENTS

This thesis marks the end of a very busy and full period in many different levels and also the end of a brief but very didactic time in TUC. There are certain people I would personally like to thank.

First and for most, I would like to thank Mr. Vasilis Gaganis, Assistant Professor of both TUC and NTUA, who supervised this thesis. For almost 6 months he stood by me and helped me overcome any problem I encountered. He did everything in order to make my life easier and more productive and helped me understand concepts I would never have on my own. I want to thank him for all that and for being one of the best teachers I ever had in my academic career and one of the greatest people I have ever had the pleasure to meet.

Next, I want to thank of course my parents, Mary and Dimitris, who helped me in all kinds of ways anyone could think throughout not only this time, but my whole life.

Finally, I would like to thank from my heart my friends from Athens, who even though I was in Chania, stood by me in so many different ways. My friends from NTUA, Maria, Georgia, and George, my friends Nick and Hercules and my "Bears" group and everyone else who helped me go through all this.

I feel blessed for being surrounded by such beautiful people and I thank you all for all the help and support you've given me throughout this time.

# Short Abstract

The oil and gas industry has developed over the years powerful and reliable tools (e.g. reservoir simulators) to simulate the oil recovery process. Complex production scenaria, such as EOR projects, specifically $CO_2$ injection ones, can be simulated in detail. Such tools however are very complex and require very detailed data as input which in many cases is not available. What is more significant is that time and resources (both human and economic) need to be spent to evaluate production scenaria that might prove to be not profitable at all. The need for the development of quick and low-cost tools to make a first screening in order to decide whether the project is a potential, profitable candidate, or if no further research is required due to very low expected recovery, is due. The objective of this thesis is to combine two existing simulation methodologies, one relying on basic analytical relationships and the other on fundamental 2D-simulation techniques, into such an integrated screening tool which will allow the engineer to make a first sort and decide which projects require further detailed investigation.

The first part of the integrated screening tool is based on Zero-Dimensional Mapping, a volumetric technique comprising of simple Material Balance calculations. The second part is based on Streamline-Streamtubes Numerical Simulation and is implemented by a commercial software developed by Texaco Exploration and Production Technology Department, named "$CO_2$ Prophet". Two examples referring to secondary and tertiary production respectively, both utilizing $CO_2$ injection, were taken by the classic textbook of Green and Willhite for "Enhanced Oil Recovery" and used to verify the credibility of the developed screening tool. The results have shown that the developed tool predicts accurately both the form of the recovery curve and its values as the observed differences between the two methodologies are of the order of 4% OOIP which is a decent match.

Although the integrated screening tool predicts successfully the two basic scenaria, real world projects involve uncertainties in many variables (e.g. reservoir heterogeneity) that the Zero-Dimensional Mapping model cannot "sense" due to its designed simplicity. However, "$CO_2$ Prophet" uses such variables as inputs, which allows the user to test the sensitivity of the whole project to any possible uncertainty. In order to investigate the software capabilities on that arena further, three case studies regarding the Dykstra-Parsons coefficient (V), the number of reservoir layers and the minimum miscibility pressure (MMP) value were conducted. The results have shown that the V coefficient has a major impact on recovery giving huge differences in recovery for the different cases studied. On the contrary, the number of layers affects the recovery a lot less. As for the MMP estimate, the results have shown that the flow pattern (miscible, immiscible) which is defined by the MMP plays a significant role in recovery and while some uncertainty in the MMP estimation is tolerable, the flow pattern must always be ensured.

# Extended Abstract

The oil and gas industry has developed over the years many powerful tools to predict and simulate the recovery processes as accurately as possible. The most famous and reliable tool are reservoir simulators which in recent years have developed so much that even very complex stratified geo models can be simulated quite accurately. However, even though detail and accuracy can be considered as a goal achieved the resources (human and financial) and the time required for the simulation to be set and run are quite high and sometimes can reach critical values. For the case of complex EOR projects, such as gas miscibility ones, setting up accurate reservoir simulation models requires a lot of detailed information, which usually is not available. The risk that the industry needs to take rises rapidly because huge resources need to be spent for an outcome that may very well be non-profitable. The need has emerged for the development of quick and cheap tools to make a first screening and decide whether the project is a potential candidate for viable-profitable oil recovery values, or no further research is required due to very low expected recovery.

The objective of this thesis is to create a methodology in two parts, one relying on basic analytical relationships and the other on fundamental simulation techniques, in a relatively easy and fast manner. The two parts will provide their results respectively and the engineer will be able to compare, interpret and decide whether the project under examination need to be run and further modeled in detail by a reservoir simulator as well or not. It is essential to point out that the methodology will serve merely as a screening tool and not as a tool for the final design of the project. For the purpose of this thesis, $CO_2$ injection as secondary and tertiary oil recovery process was tested and therefore the screening tool developed is based on such techniques and cannot be used universally for other recovery processes.

The integrated screening tool utilized in this thesis can be considered as an improvement of a combination of two such methodologies. The first one is Zero-Dimensional Mapping, a volumetric technique based on simple Material Balance calculations. The second part is based on Streamline-Streamtubes Numerical Simulation and is implemented by a commercial software developed by Texaco Exploration and Production Technology Department, named "$CO_2$ Prophet".

Two examples taken by the classic textbook of Green and Willhite for "Enhanced Oil Recovery" were tested. The first one refers to $CO_2$ injection as a secondary oil recovery process from a five-spot pattern, whereas the second one as tertiary process on an already water-flooded reservoir. Both examples were implemented on both methodologies and results were exported and compared. In general, the results have shown the following:

- The procedure for the calculation of the sweep efficiency from the chart of Claridge (1972) was automated and developed into a correlation model. The implementation is considered to be very precise since all predicted values match the ones read in the chart.
- Both the zero-dimensional mapping model and $CO_2$ Prophet agree qualitatively in the predictions of recovery. Similar s-shape curves are produced by both models. $CO_2$ Prophet is more favorable in the predictions compared to the Zero-Dimensional Mapping, giving consistently, slightly higher values of oil recovery for both examples.
- The deviation between Zero-Dimensional Mapping and $CO_2$ Prophet predictions varies from 1,44% to 7,11% with an average of 4,02% for the secondary production, while for the tertiary production the respective numbers range from 0,03% to 6,64% with an average of 4,62%.

The investigated screening tool is considered to achieve its original goal as it is a fast way to eliminate cases that do not require further examination. Further research is required in order to complete and fine tune it but the basic concept is set and with a few modifications this tool can prove quite useful for the oil and gas industry, saving valuable resources and time.

Although both the Zero-Dimensional model and "$CO_2$ Prophet" manage to predict successfully the two scenarios, the uncertainties encountered in a real project are quite a lot. The Zero-Dimensional model uses very few parameters as inputs and therefore does not manage to capture the real effect of other important variables (i.e. the Dykstra-Parsons coefficient, V, which defines the heterogeneity of the reservoir). However, "$CO_2$ Prophet" uses such variables as inputs, which allows the user to test the sensitivity of the whole project to any possible uncertainty.

In order to further investigate the dynamics of "$CO_2$ Prophet" software a series of case studies was conducted referring certain key variables of 2D problems. For this purpose, a new project, similar to the one previously examined on tertiary production, was set and solved initially exactly as indicated by the screening tool. The key variables that were tested afterwards were: the Dykstra-Parsons coefficient (V), the number of reservoir layers and the MMP estimate. For each case study three different values plus the one already tested by the initial simulation were simulated in order to enclose the whole range of possible values of this particular variable. The results showed the following:

i. The Dykstra Parsons coefficient is proved to be the most significant variable of the problem. Oil recovery is very sensitive to changes in this particular variable because V defines the heterogeneity of the reservoir, thus the degree of difficulty the fluid finds in moving through the reservoir to the production well. The test indicated that as V rises the total oil recovery drops. Naturally, the most favorable results were produced when V=0 (homogeneous reservoir). The other three, more realistic cases exhibit reasonable differences of the order of 5-10% between one another. The comparison between the two extreme cases (V=0 and V=0,9) shows huge differences ranging from 15% up to 40% proving that reservoir heterogeneity plays a major part in 2D simulations.

ii. The number of layers proved to be an important but not definitive factor, if the number is somewhat realistic. The case study showed that the number of reservoir layers plays a minor role in the recovery as the major part is taken by the V coefficient. Again, the case of single layered reservoir (V=0 by default) gives significantly higher values of recovery compared to the other tested values. Comparison between the three realistic cases shows minor differences with one another in the order of 2% for sequential curves and 5% for the 3- and 10-layers curve.

iii. The case study for the MMP estimate showed that shown that the flow pattern (miscible, partially miscible or immiscible) which is defined by the MMP plays a significant role in recovery. The differences observed are not only quantitative but also qualitative as the form of the recovery shape changes with respect to the flow pattern. Miscible flow translates into always rising recovery and partially miscible the same but with much lower rates, while immiscible flow means actually a peak in after which no further recovery is expected. Therefore, while some uncertainty in the MMP estimation is tolerable, the flow pattern must always be ensured.

## TABLE OF FIGURES

**TABLE OF TABLES**

**TABLE OF CONTENTS**

# CHAPTER 1

# Introduction

## 1.1 Problem Statement

Oil recovery processes generally can be categorized into three stages: primary, secondary, and tertiary which in early years marked the project in its life-years. The first stage, primary production, resulted from the fluid and pore compressibility existing in a reservoir (simple pressure drawdown). Secondary recovery, which is almost synonymous with waterflooding, usually was implemented with the decline of primary production. Other processes other than waterflooding is pressure maintenance, and gas injection. Tertiary recovery were implemented after secondary processes have been applied, aiming to displace residual oil after the secondary processes became non-viable economically and consisted of miscible gases, chemicals and thermal energy. The term tertiary is tending to be replaced nowadays by the term Enhanced Oil Recovery is preferred (EOR) since for some reservoirs primary and secondary recovery procedures are not helpful and tertiary techniques are the first and perhaps the only methods used throughout the life of the reservoir. EOR results principally from the injection of gases or liquid chemicals and/or the use of thermal energy. Hydrocarbon gases, carbon dioxide ($CO_2$), nitrogen, and flue gases are among the gases used in EOR processes.

Traditionally the procedure followed when EOR processes are to be designed for a target reservoir involves many steps, the most significant of which can be considered to be the reservoir simulation. Although reservoir simulators in the industry have evolved quite a lot in the recent years there are still two major problems to be taken into account: the reliability of the results and the time taken for a complete simulation. It is known that the input variables used by a reservoir simulator exhibit huge uncertainty and can only be described as "best guesses" at the time introduced in the model. Therefore, the results produced carry along these uncertainties and need to be treated with caution. Furthermore, the time needed for a full simulation is a significant factor and taking into account that numerous runs are required in order to history match the model, simulation time can be considered as a major setback. Given its drawbacks and the fact that huge economic and human resources are required in order to bring through this task, the risk involved with it rises quite high. If we further consider the fact that $CO_2$ gas is very expensive and most of the times flu-gas is used instead, it is safe to say that the necessity for a way to reduce this risk is of vital importance.

## 1.2 Scope of the Thesis

In order to overcome this problem, a new easy and fast approach is considered, prior to the reservoir simulation in order to decide whether or not it is worth proceeding with EOR methods. This methodology can be described as a "screening tool" for the proposed EOR method, which gives the engineer a quick and rough estimation of the expected efficiency and gives a first impression of what it is to be expected. Should the results be encouraging then the reservoir simulation is due in order to verify the initial predictions and move on with designing the actual EOR process selected.

This "screening tool" involves two stages.

- The first stage is based on 0-Dimensional Mapping of Real 3D Reservoir Simulations. Using empirical plots derived from 3D Simulation Results and the absolute basic properties of the reservoir and the fluids involved, this methodology works similarly to the "Tank" models implemented on many software packages and gives a rough approximation of the recovery factor.
- Secondly the commercial software named "$CO_2$ Prophet" is used. This software uses a methodology based on the 2D Streamlines-Streamtubes theory. This is a very different approximation because this theory originates from quite different inception. The advantage of both methods is simplicity and speed. All the analyses take seconds to finish and can be mapped quite fast.

For this thesis, the proposed methodology is to be tested for miscible $CO_2$ injection as either a secondary process (no waterflooding prior to it) or as a tertiary process (previously waterflood reservoir). Specifically, 2 cases taken from the classic textbook of Green and Willhite "Enhanced Oil Recovery" are to be implemented on both an excel spreadsheet using the methodology described by Stalkup and afterwards using the software "$CO_2$ Prophet" re-implement them and observe the differences that occur.

## 1.3 Structure of the Thesis

This thesis consists of (6) chapters including this introductory one. In a nutshell:

- In chapter 2, the theory behind the miscible displacement EOR processes as well as the fundamentals of Streamline Theory are presented. Furthermore, existing numerical modeling efforts of these theories are shown.
- Chapter 3 is an "in depth" description of the problems about to be processed by the book of Green and White. Furthermore, a detailed presentation of the software "$CO_2$ Prophet" is made.
- Chapter 4 deals with the analyses made for both methodologies and all problems tested and presents the emerged results.
- Chapter 5 refers to an in-depth examination of $CO_2$ Prophet's further capabilities by the use of a new project-scenario. Case studies regarding key-variables of 2D problems will be conducted and useful conclusions will be derived.
- Finally, Chapter 6 sums up all the basic conclusions derived from all the analyses done and gives some recommendation for further research on the area.

# CHAPTER 2

# Literature review on miscible displacement processes, streamline theory and numerical implementation techniques

## 2.1 Miscible Displacement Processes and MMP Modeling

### 2.1.1 Miscible Displacement Processes

This thesis deals with miscible displacement of oil through $CO_2$ injection. The $CO_2$ interacts with the oil-rock system, creating favorable conditions for oil recovery such as surface tension reduction between residual oil and reservoir rock, oil viscosity decrease and oil swelling. $CO_2$ affects the thermodynamic equilibrium of the reservoir fluids. The injected gas, initially, is not in equilibrium with the reservoir fluids and there is mass transport between the phases leading to changes in the two-phase properties. Oil displacement becomes efficient when the phase properties become "thermodynamically similar". This is the meaning of full miscibility of the phases where the phase interface stops existing and practically there is but one "movable" phase.

Various methods exist to represent the vapor/liquid phase behavior of multicomponent systems. These methods include the use of pressure versus temperature, pressure versus composition and ternary diagrams which present in a convenient manner the different regions (single-phase and multiphase) derived by experimental data or Equation of State (EOS) model calculations. However, most crude oils consist of a vast number of chemical components and the precise chemical composition is quite hard and expensive to be defined.

- Pressure – Temperature diagrams.

A p-T diagram is shown in Figure 2.1 for a fixed fluid composition. The dewpoint and bubblepoint curves intersect at the critical point (C), where properties of liquid and gas become the same (McCain 1973). All points enclosed by curve ACB consist of a liquid and a gas phase. Opposed to the single-component system, two phases can exist at a pressure or a temperature greater than the critical one. Cricondenbar the maximum pressure at which two phases may exist in equilibrium for a multicomponent system. Similarly, cricondentherm is the maximum temperature at which two phases may exist.

Assuming the system, which exists originally at Point M as a single-phase fluid, goes through an isothermal pressure reduction the following phase alteration will happen. At Point L, the system reaches the bubble-point curve and changes to a saturated liquid phase where a single bubble of vapor is formed. As pressure drops furtherly, additional vapor is created until, the system is an equal mixture of liquid and vapor (50-50% liquid-vapor at Point K). Further pressure reduction to the Point J results in vaporization of all the liquid, except for a single drop of negligible volume (dewpoint pressure). Should pressure be reduced furtherly, the system will exist solely in a vapor state.

Of course, if the fluid composition is altered, the two-phase envelope on the pressure versus temperature diagram would change position. As the number of components increases, the description gets even more complex because of the increasing number of degrees of freedom.
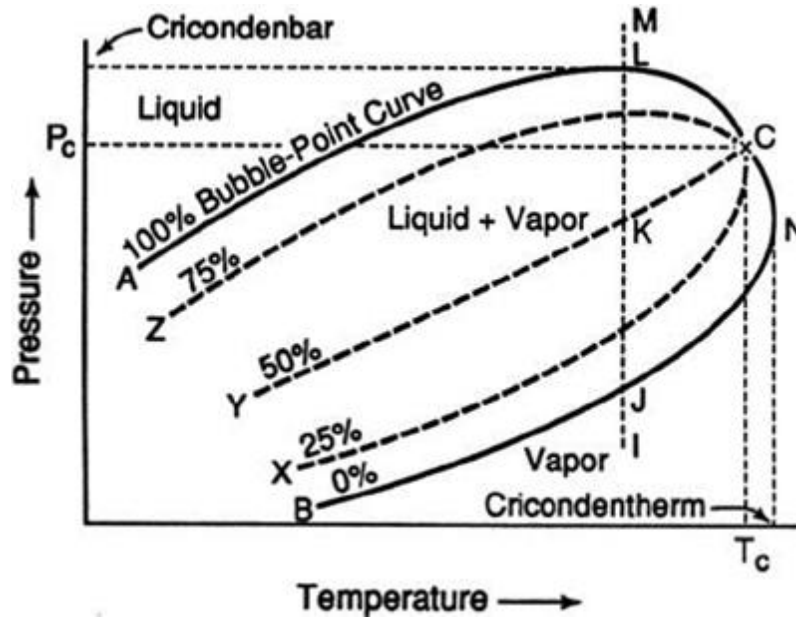
*Figure 2.1:Pressure versus Temperature plot for a fixed composition. The possible different states of matter are marked. The critical values Pc and Tc are also marked and the critical point (C) is shown on the graph too.*

- Pressure - Composition Diagrams.

Phase behavior information also can be presented on a pressure versus composition (*p-x*) diagram like the one in Figure 2.2. On the horizontal axis, the composition is conveyed as the mole fraction of the most volatile component. To demonstrate the use of the diagram, an isothermal compression of a system originally existing in the gaseous phase is described. If the pressure is increased on a system represented by Point A, no phase change occurs until the dewpoint (Point B) is reached at pressure $p_1$. At the dewpoint, an infinitesimal amount of liquid forms with a composition given by $x_1$. The composition of the vapor is still equal to the original composition, *z*. As pressure increases, more liquid forms and the compositions of the coexisting liquid and vapor phases are given by projecting the ends of the straight, horizontal line through the two-phase region of the composition axis. For example, at $p_2$, both liquid and vapor are present and the compositions are given by $x_2$ and $y_2$. At $p_3$, bubble-point (Point C) is reached. The composition of the liquid is equal to the original composition, *z*. The infinitesimal amount of vapor still present at the bubble-point has a composition given by $y_3$. Upon further compression, the system becomes single-phase liquid.

As previously indicated, the endpoints of a horizontal line inside the two-phase region define the compositions of coexisting phases. However, it is important that the amount of a phase present in a two-phase system and the composition of a phase are not mixed up. For instance, at the dewpoint, only an infinitesimal quantity of liquid is present, but it comprises finite mole fractions of the two components.

The system shown in Figure 2.2, the light component would be fully miscible in the heavy one in any concentration, at pressures greater than $p_4$ (liquid) or less than $p_0$ (vapor). Between $p_4$ and $p_0$, the system exists as single-phase for very few concentration ranges. For a binary system at a temperature above the volatile component's critical one, single-phase fluid appears over all possible compositions of the volatile component.
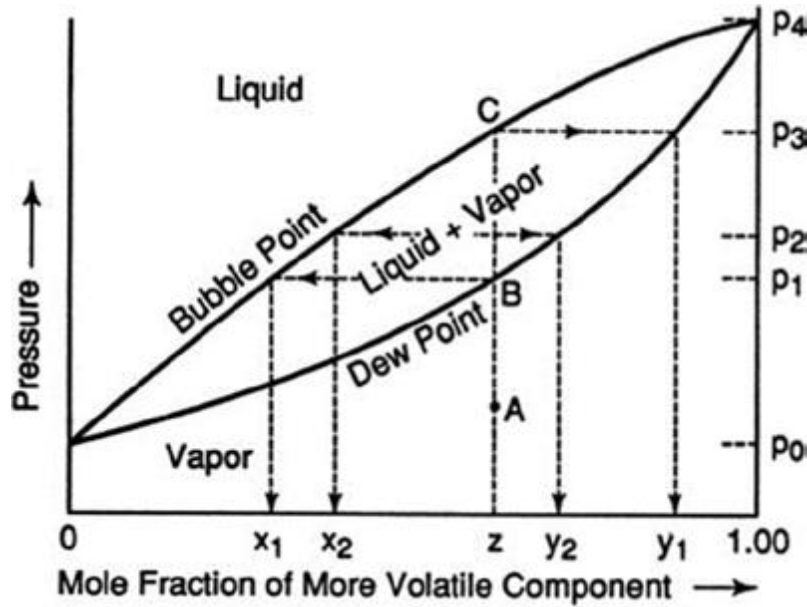
*Figure 2.2:Pressure versus Mole fraction of most volatile component. The possible different states of matter are marked.*

- Ternary Diagrams.

Ternary, or triangular, phase diagrams are used to plot the phase behavior of systems consisting of three components. For systems containing more than three components, components groups are formed, creating pseudocomponents. A widely used example is the decomposition of crude oil into $CH_4$ as volatile, $C_2-C_6$ as intermediate, and $C_{7+}$ as heavy pseudocomponents. The phase behavior on a ternary diagram is plotted at fixed pressure and temperature.

A ternary diagram for Components A, B, and C is shown in Figure 2.3 (left). Compositions are reported in weight percent (alternatively mole, or volume percentage may be used). Should all components be fully miscible, only a single-phase region would be present on the chart. The vertices represent the pure components, and the sides of the equilateral triangle are scaled to form the binary compositions of the three possible pairs. Points interior to the triangle are used to represent systems consisting of all three components/pseudocomponents.

Phase relationships can be shown on a ternary diagram, as indicated in Figure 2.3 (right). The chart displays the phase conditions at equilibrium for a 3-componenent (A, B and C) system where compositions are expressed in mole fractions. The plot is common for hydrocarbon systems where liquid-vapor equilibrium can be achieved for a handful of concentration values. Any concentration represented by points lying inside the two-phase region (which is defined by the binodal curve or 2-phase envelope) would split into two phases. Systems with concentrations represented by points outside the envelope would exist as single-phase.
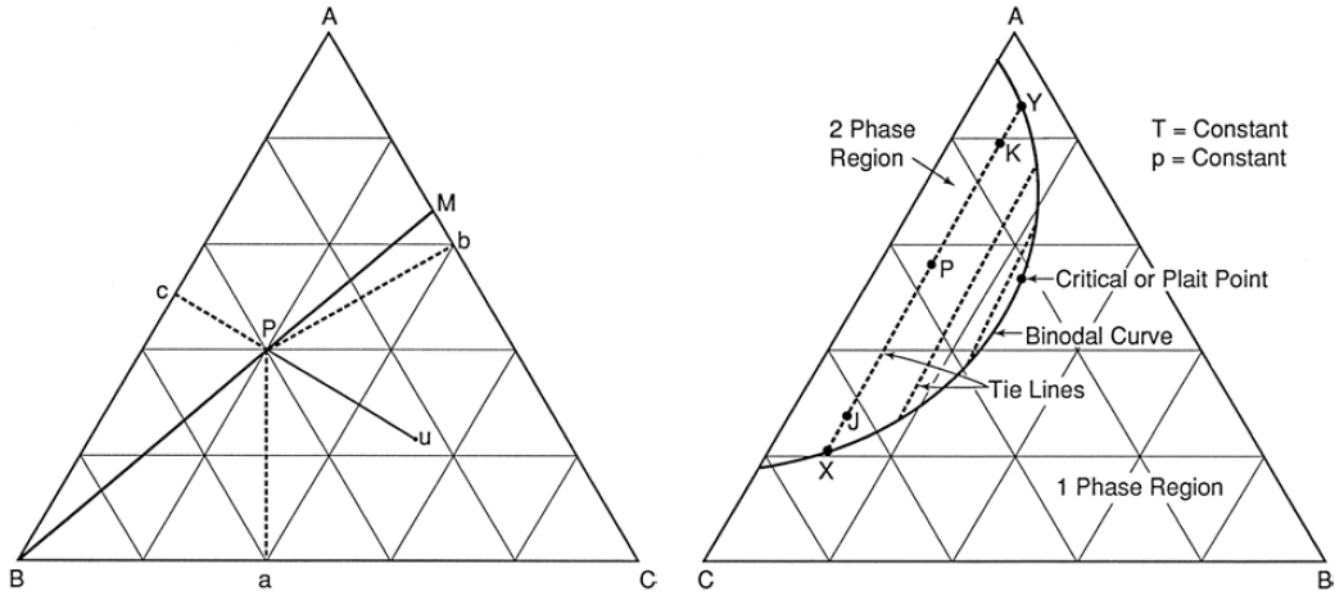
*Figure 2.3:Ternary Diagrams for constant temperature and pressure. Left –Inverse Lever Arm rule application. Right - The single and 2-phase regions are marked (right). The tie lines and the critical point (C) is shown on the graph too.*

Think of a system with an overall composition P that lies inside the two-phase envelope. If the system was a classic hydrocarbon one, then it would split into a liquid phase (X) and a vapor phase (Y), and their compositions could be determined directly from the graph. The relative amounts of the two phases can also be determined by the inverse-lever-arm rule according to which:

$$\frac{YP}{YX} = Amount\ of\ Liquid\ in\ the\ total\ amount \qquad and \qquad \frac{PX}{YX} = Amount\ of\ Vapor\ in\ the\ total\ amount$$

The lines that connect equilibrium concentrations such as XY are called tie-lines and there is an infinite number of them. However, for practical purposes, usually some of them are drawn on a chart and interpolation is used for in-between concentrations. The endpoints of the tie-lines converge at a single point, which is called the critical point, where properties of the phases become identical marking the critical concentration at the specified T and P. The tie-lines for a given system are not necessarily parallel and may shift significantly to both directions in slope as any component's quantity in the mixture changes. The critical point is not necessarily located in the midpoint of the two-phase envelope, but can be found frequently on any of its sides. Its exact location and therefore the position of the tie-lines may be such that even the slightest alteration in the mount of one phase could result in a huge change in the other phase.

In general, reservoir fluids are quite complex hydrocarbon mixtures and their components range from $C_1$ up to $C_{40+}$. Miscible displacement processes imply that, a fluid is injected into the reservoir, which is or is going to be eventually, miscible with the reservoir fluid. This will alter the composition of the total system and as a result its thermodynamic properties. Intensive thermodynamic analysis of such processes can only take place if all compositions are identified and all chemical constituents as well as all thermodynamic properties are known. Such conditions are almost impossible to meet in practice, however, should certain components be grouped in a way that the important properties of the system are preserved, complex systems can be described quite accurately. A pseudoternary diagram is a classic representation of the such a process. In Figure 2.4 a ternary diagram with pseudocomponents $C_1$, $C_2-C_6$,

and $C_{7+}$ is depicted. To define any point in the diagram, the concentrations of two pseudocomponents are needed. The two phase boundaries are described by the curves LO (saturated liquid curve) and VO (saturated vapor curve). When using pseudoternary diagrams with pseudocomponents a very important assumption is that the composition of a pseudocomponent remains unaltered throughout any phase change. For instance, the relative concentration of components that make up the $C_{7+}$ pseudocomponent must be approximately the same in the liquid phase as in the equilibrium vapor phase. If this condition is not satisfied, using a pseudoternary diagram can lead to serious miscalculations of both phase amounts and compositions.
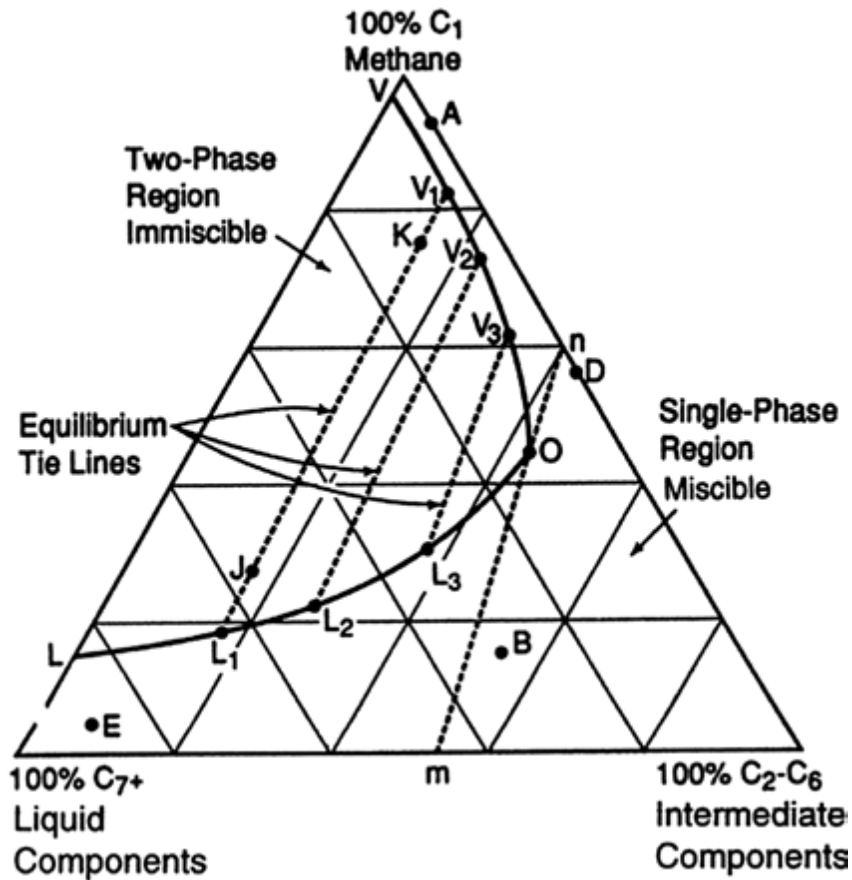


*Figure 2.4:Ternary Diagram for a mixture with pseudocomponents: Light=$C_1$, Intermediate=$C_2$–$C_6$, and Heavy= $C_{7+}$,*

Representing a system of more than three components on a ternary diagram is an approximation, however, this does not mean it lacks accuracy as can be seen by noting the concentrations for the equilibrium liquid and vapor phases given by Points $y$ and $x$ on the phase envelope of Figure 2.5. In a perfect world, a pseudocomponent, such as $C_2$ through $C_6$ should have identical relative composition both in liquid and in vapor phase, but this is not the case. The heavier components in the $C_2$ through $C_6$ pseudocomponent tended to go to the liquid phase, while the lighter moved to the vapor phase. This motion can be captured by noting the ratio of $C_2/C_6$ in the vapor and liquid phases for instance, which is quite smaller in the liquid phase than in the vapor. All the same, a pseudoternary diagram is a decent

approximation, and can be quite helpful for describing how miscibility is achieved in displacement processes. If the system's temperature or pressure is altered, the two phase envelope changes as well. At the higher pressure, the system is single phase over a broader range of possible concentrations (i.e., a higher pressure is favorable for the development of miscibility between different components).
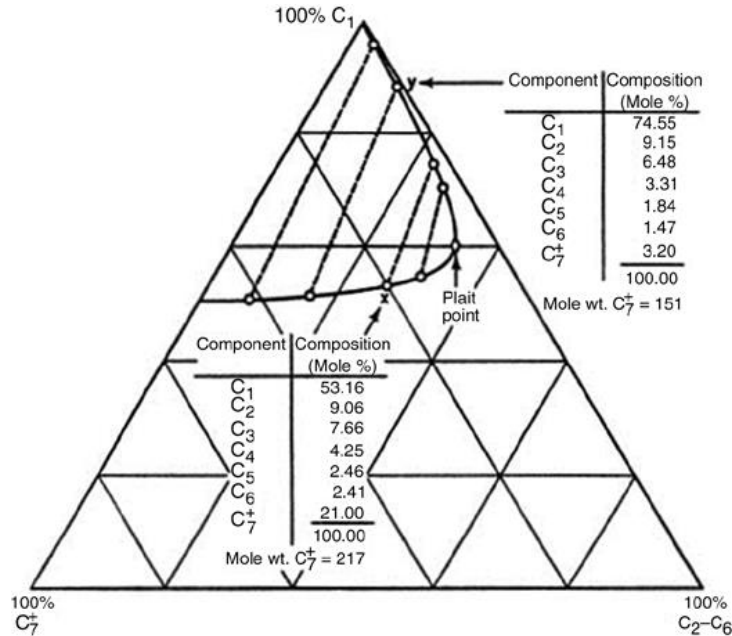


*Figure 2.5:Phase relations (mol%) of the University Block 31 field reservoir fluid at 140°F and 4,000 psia (Hutchinson and Braun 1961).*

Miscible Injection processes can be sorted into First Contact Miscible (FCM) and Multiple Contact Miscible (MCM). Both will be briefly explained below.

- First Contact Miscible (FCM)

An FCM process implies that the injected gas and the reservoir oil form a single-phase fluid immediately after their contact regardless their concentrations. This can be represented through a ternary diagram should the two fluids and any point in the straight line between them lie outside the phase envelope as shown in the Figure 2.6 Any mixture of oil and this particular gas is fully miscible at first contact.
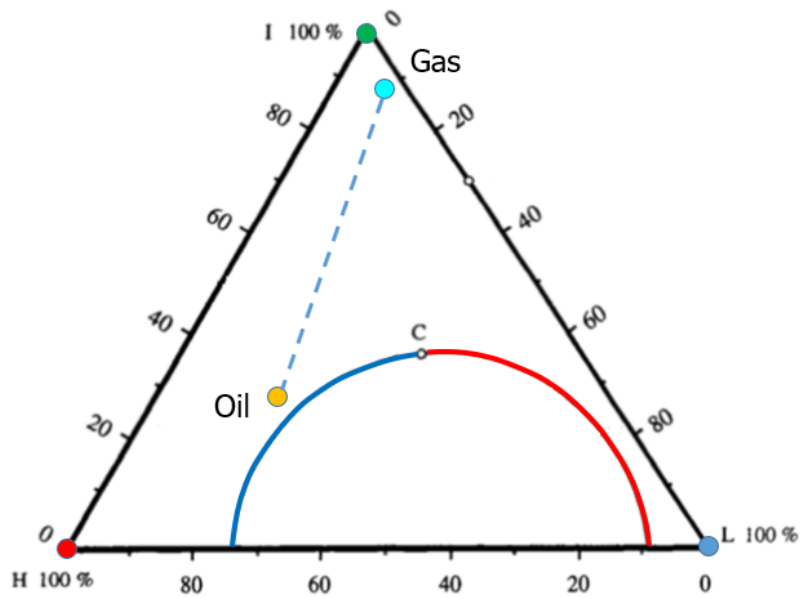
*Figure 2.6: Ternary Diagram showing two fluids that are miscible at first contact.*

A more realistic example is presented in Figure 2.7. A mixture of ethane ($C_2$) and normal heptane (n-$C_7$) is shown with different possible alternatives regarding the concentrations of the two components. In order to achieve a first-contact miscibility the point representing the mixture should lie outside the phase envelope.
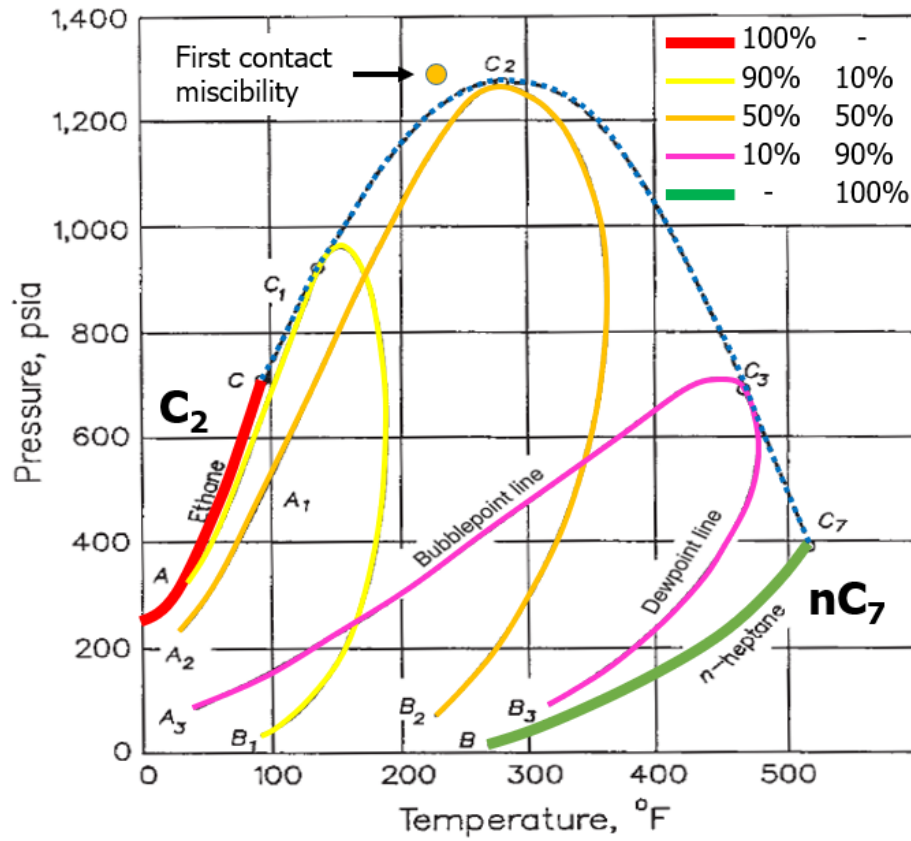
*Figure 2.7: Ternary Diagram for $C_1$ and $n$-$C_7$ mixture. FCM is achieved should the point lie outside the phase envelope.*

The FCM process requires injection of a displacement fluid that is miscible with the crude oil. Generally, such processes consist of a relatively small primary slug injection (fully miscible with the crude oil) followed by injection of a larger and cheaper secondary slug, such as water. The secondary slug should, ideally, be miscible with the primary slug and if so, phase behavior must be taken into account both upstream and downstream of the primary slug. Should the different slug materials be immiscible, then a residual saturation of the primary slug material will be trapped in the displacement process. Economic considerations are paramount for setting the slug sizes and all the necessary variables.

Figure 2.8 shows schematically a FCM displacement process involving the injection of a solvent, in this case a liquefied petroleum gas (LPG), which is miscible with the reservoir oil. If it is utilized as a secondary recovery technique, efficient displacement of the oil takes place at the leading edge of the LPG slug and there is only few residual oil or not at all. Dispersion and mixing will take place at the fluids interface and a mixing zone will form.
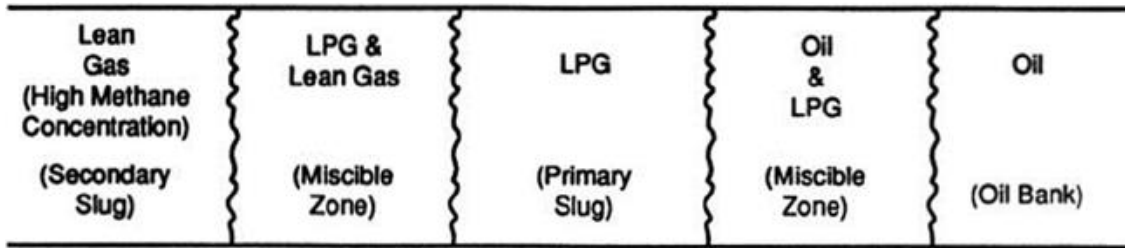
*Figure 2.8: Idealized First Contact Miscible Displacement with Lean gas and LPG as primary and secondary injection slugs.*

The general conditions of first-contact miscibility and immiscibility were marked by Clark et al. (1958) and are displayed in Figures 2.9a through 2.9c. Methane ($CH_4$) and crude oil are partially soluble in one another but, at typical reservoir conditions, they do not mix in all proportions and there is no single phase fluid. In Figure 2.9a an immiscible flood is demonstrated where $CH_4$ is the solvent and displaces crude oil. In different circumstances, heavier hydrocarbons, such as LPG or $C_4$, are completely soluble with oil at most combinations of reservoir pressure and temperature. As illustrated in Figure 2.9b, at standard conditions oil exists as a liquid and propane a gas. Should pressure and temperature increase to reservoir conditions, both propane and crude oil are liquids which will mix completely and therefore this displacement process is considered miscible. Figure 2.9c gives another example regarding $C_4$ and $C_1$. At standard conditions both components exist as vapors but at the temperature of 150°F and pressure of 2000 psia, $C_4$ is a liquid while $C_1$ is still a gas. Should they come in contact, they will form a single-phase fluid (at a gaseous state). Thus, this displacement process is a miscible displacement.
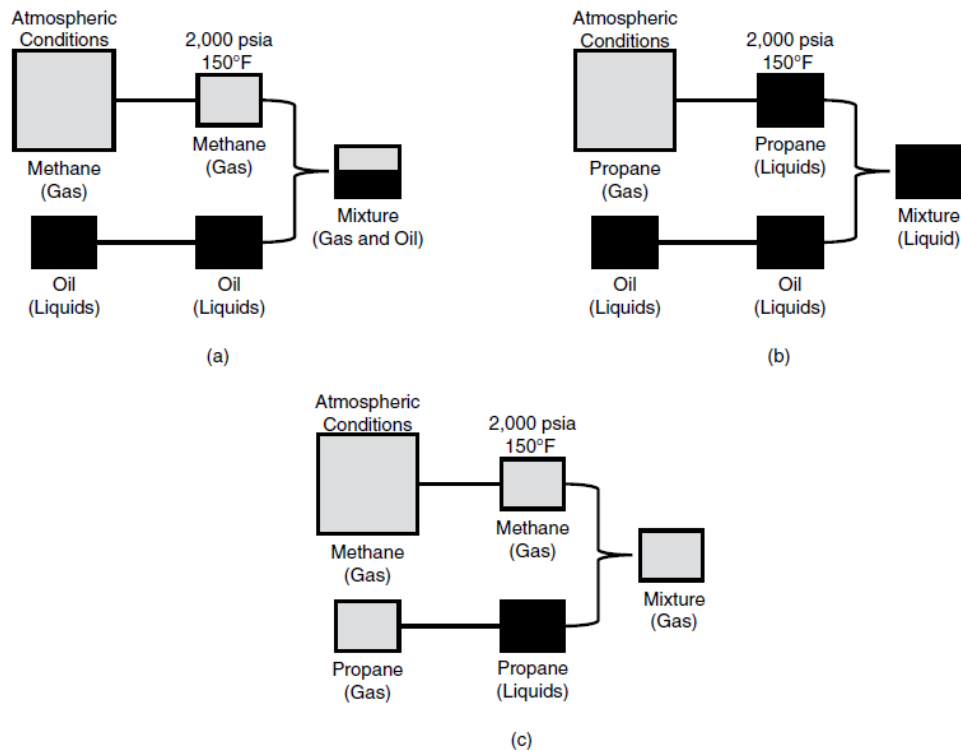


*Figure 2 9:a) Immiscible two-phase mixture of $C_1$ gas and liquid oil at common reservoir conditions b) Miscibility of $C_4$ (or LPG) liquid and oil liquid at reservoir conditions. $C_4$ (or LPG) liquid is a liquid in the presence of a liquid. c) Miscibility of $C_1$ gas and $C_4$ (or LPG) at reservoir conditions. $C_4$ (or LPG) is a gas in the presence of a gas above the critical point.*

- Multiple Contact Miscible (MCM)

The term MCM displacement processes implies that miscibility is achieved inside the reservoir through mass transfer and multiple contacts between the injected fluid and the reservoir oil which eventually results in in-situ composition changes. The MCM processes are categorized as vaporizing, condensing and condensing/vaporizing-gas (enriched-gas) displacements, and $CO_2$ displacements.

These processes work in a different way than FCM. At the beginning, at the injection front (or at low mixing ratios) the mixture remains monophasic, but as the front moves deeper in the oil-zone the mixture becomes diphasic as it enters the phase envelope and splits into an enriched gas ($G_1$) compared to the original and a lighter oil ($O_1$) compared to the reservoir oil. Equilibrium gas ($G_1$) exhibits higher mobility and moves forward. It lives at the front of the solvent slug and as it moves it contacts new oil and it splits again to a new gas $G_2$ enriched in intermediate components and oil $O_2$. This procedure repeats until finally, $G_n$ becomes first contact miscible with reservoir oil. This mechanism is called Vaporizing Gas Drive. The following figures show schematically, in a ternary diagram, the steps described above.
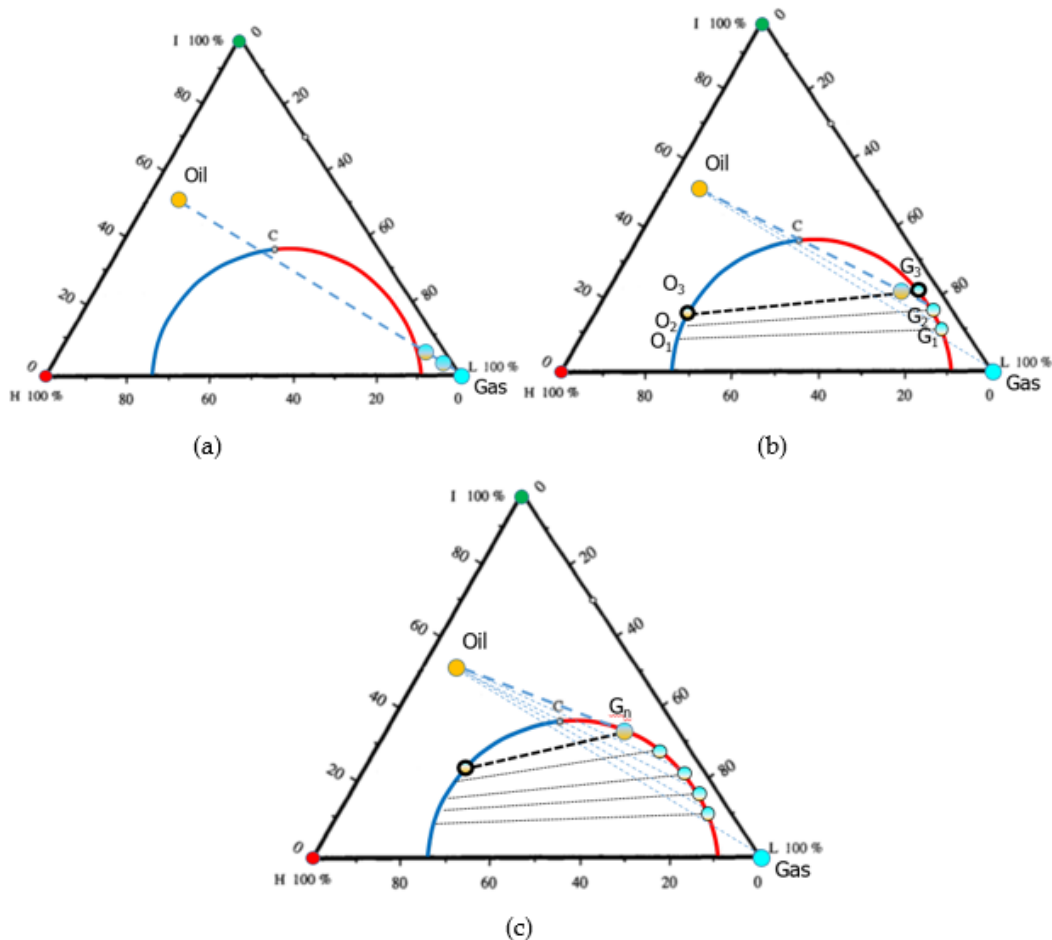


Figure 2.10: Multiple Contact miscibility process. a) Initially the mixture is single phase as the endpoints of the tie-line lie outside the phase envelope. b) The mixture enters the two-phase region and splits into a new enriched gas $G_1$ and a new oil $O_1$. As the front moves forward the reservoir oil contacts the $G_1$ gas and splits again to a $G_2$ gas and $O_2$ oil etc. c) The enriched gas $G_n$ is now FCM with the reservoir oil.
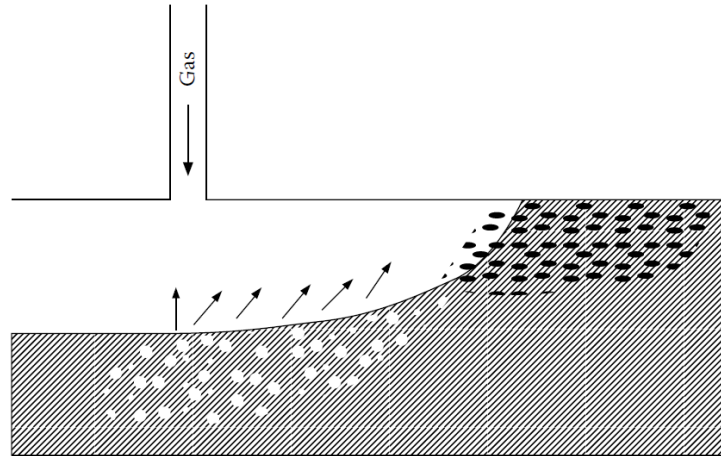
*Figure 2.11:Miscibility achieved in the advancing front through Vaporizing Gas Drive mechanism (Pedersen & Christensen, 2007)*

In the Condensing or Enriched-gas Drive process, the injected fluid generally contains larger amounts of intermediate molecular weight hydrocarbons and as a consequence is more expensive. In this mechanism, reservoir oil near the injection well is enriched in composition by contact with the injected fluid first put into the reservoir. Hydrocarbon components are condensed from the injected fluid into the oil and thus the process is called a condensing process. As the front advances, the reservoir oil encountered splits into a lighter oil and a heavier gas through a condensation mechanism. The procedure repeats until first contact miscibility is achieved like on the vaporizing gas drive mechanism. The enriched gas process typically can be operated at a lower pressure than the vaporizing process.
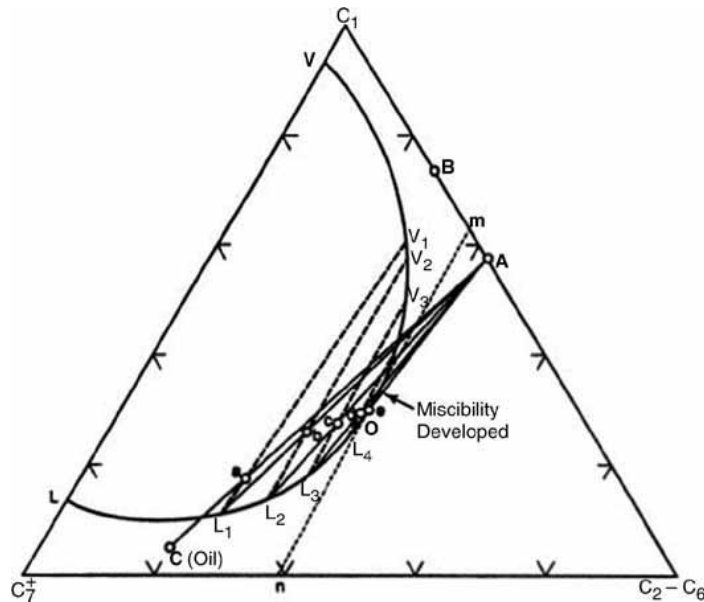


*Figure 2.12: Vaporizing-gas displacement process representation on a pseudoternary diagram.*

13
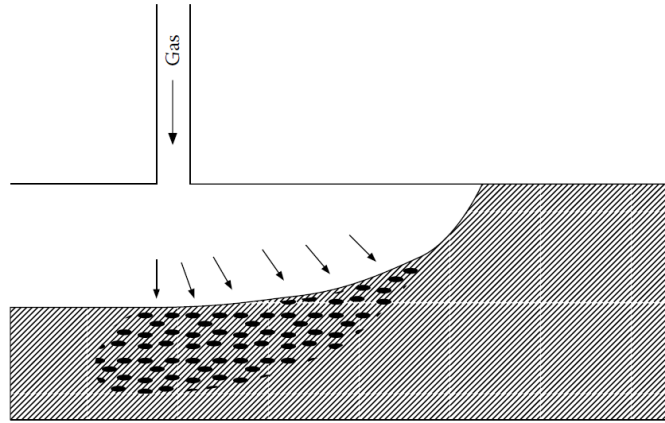
*Figure 2.13: Miscibility achieved at the injection point through Condensing Gas Drive mechanism (Pedersen & Christensen, 2007)*

It is quite possible that a combination of the two previously described mechanisms occurs. As the gas advances through the oil bank, it gets enriched with heavy components while condensing the oil simultaneously. According to Zick (1986) and Stalkup (1987) the real mechanism for multi-component mixtures is in fact the combination of the condensing gas drive at the front and the vaporizing gas drive at the injection point. It is called Condensing/Vaporizing Gas Drive and it can be visualized Figure 2.14. Figure 2.15 is a summary of the possible mechanisms taking place in MCM displacement.
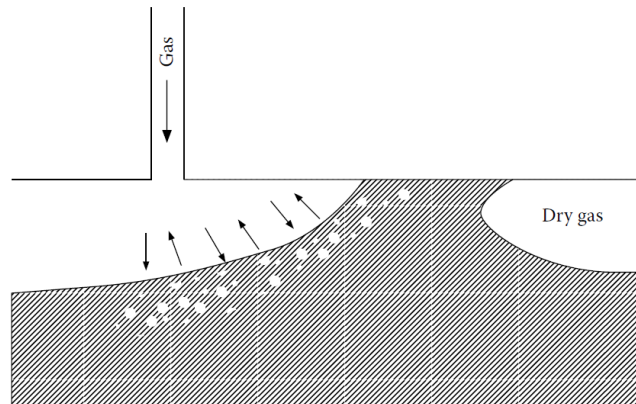


*Figure 2.14:Miscibility achieved through combination of Vaporizing and Condensing Gas Drive mechanisms in an area between the injection point and the displacement front (Pedersen & Christensen, 2007)*
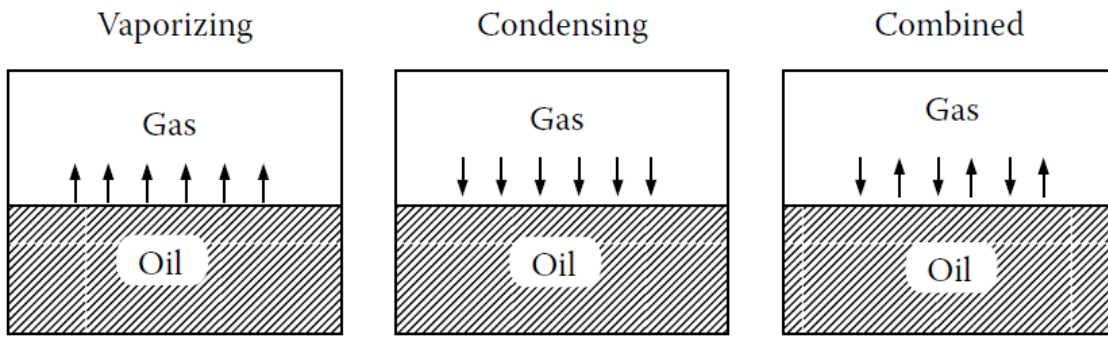
*Figure 2. 15: Possible mechanisms of MCM displacement.*

- $CO_2$ Miscible Displacement Process.

The description of the $CO_2$ miscible displacement process is actually quite similar to the high-pressure vaporizing process. At temperatures higher than 120°F, the phase behavior chart for $CO_2/(C_2-C_6)/C_{7+}$ system looks a lot like the one for $C_1/(C_2-C_6)/C_{7+}$. The important difference is that, for fixed P and T conditions, the binodal curve is much larger for the $CH_4$ system compared to the $CO_2$ system and the limiting tie-line for the $CO_2$ system tends to have a more parallel slope to the $CO_2/C_{7+}$ side than the $CH_4$ one. Therefore, lower pressures are needed to achieve miscibility between $CO_2$ and reservoir oils. This ability of $CO_2$ to generate miscibility at low pressures, is actually its primary advantage over methane. These differences between the two systems can be observed in Figure 2.16.
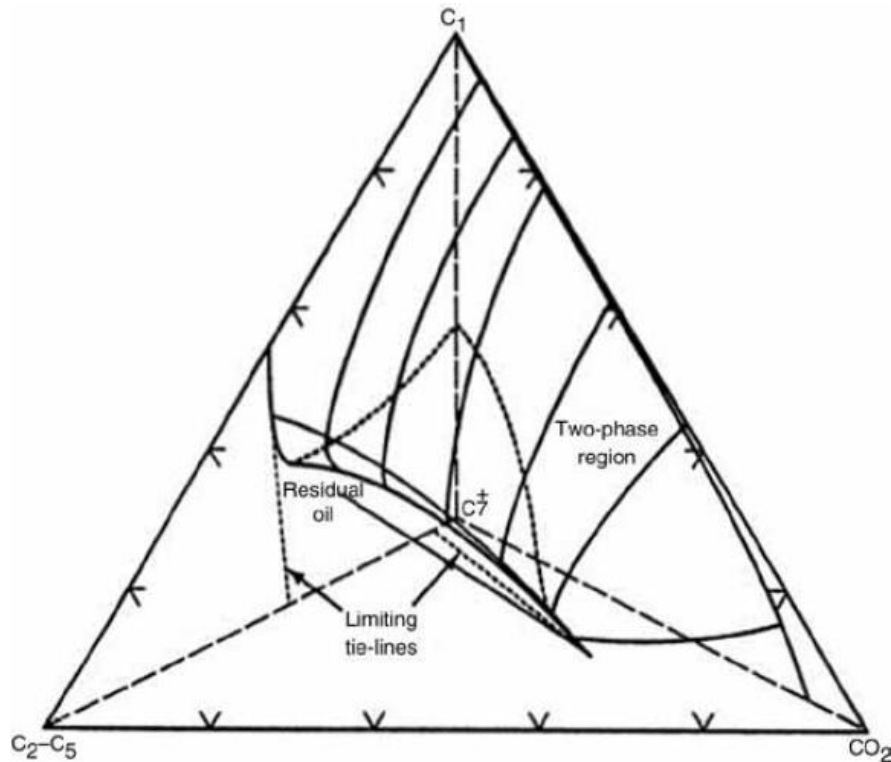


*Figure 2.16: Comparison of two-phase envelopes for CH4/hydrocarbon and CO2/hydrocarbon systems.*

If $CH_4$ were added to the $CO_2$/hydrocarbon system, the phase behavior would alter. The effect would be the increase of the miscibility pressure. That means that, for a certain oil, if $CH_4$ is present in the displacing fluid, a higher pressure is necessary to achieve miscibility. This applies for the case of other non-condensable gases, such as $O_2$ or $N_2$ and for $H_2S$ as well. Such impurities in the $CO_2$ are quite harmful for the development of miscibility. That is why, stack or flue gases are not applied directly as miscible displacement slugs at common reservoir pressures. It is wiser to use components such as $C_2$ and $C_3$ which are generally present in $CO_2$ produced from a $CO_2$ flood.

At temperatures below 120°F, $CO_2$ phase behavior leads to the formation of two liquid phases or two liquid phases and a vapor phase. Describing this phenomenon on a pseudoternary diagram is quite difficult. It has been pointed out by Metcalfe and Yarborough (1979) and Shelton and Yarborough (1977) that for $CO_2$/hydrocarbon systems, two categories of phase behavior can be identified. These are depicted in Figures 2.17a and 2.17b (Stalkup 1983a), on *p-x* diagrams. The existence of regions of two liquid phases and three phases has a major impact on the recovery mechanisms. The two different liquid phases, lead to the development of a mechanism of liquid/liquid extraction quite similar to the vaporization mechanism. Regardless the specific mechanisms, it has been proved that multiple-contact miscibility can be reached (Gardner et al. 1981) even at such low temperatures.
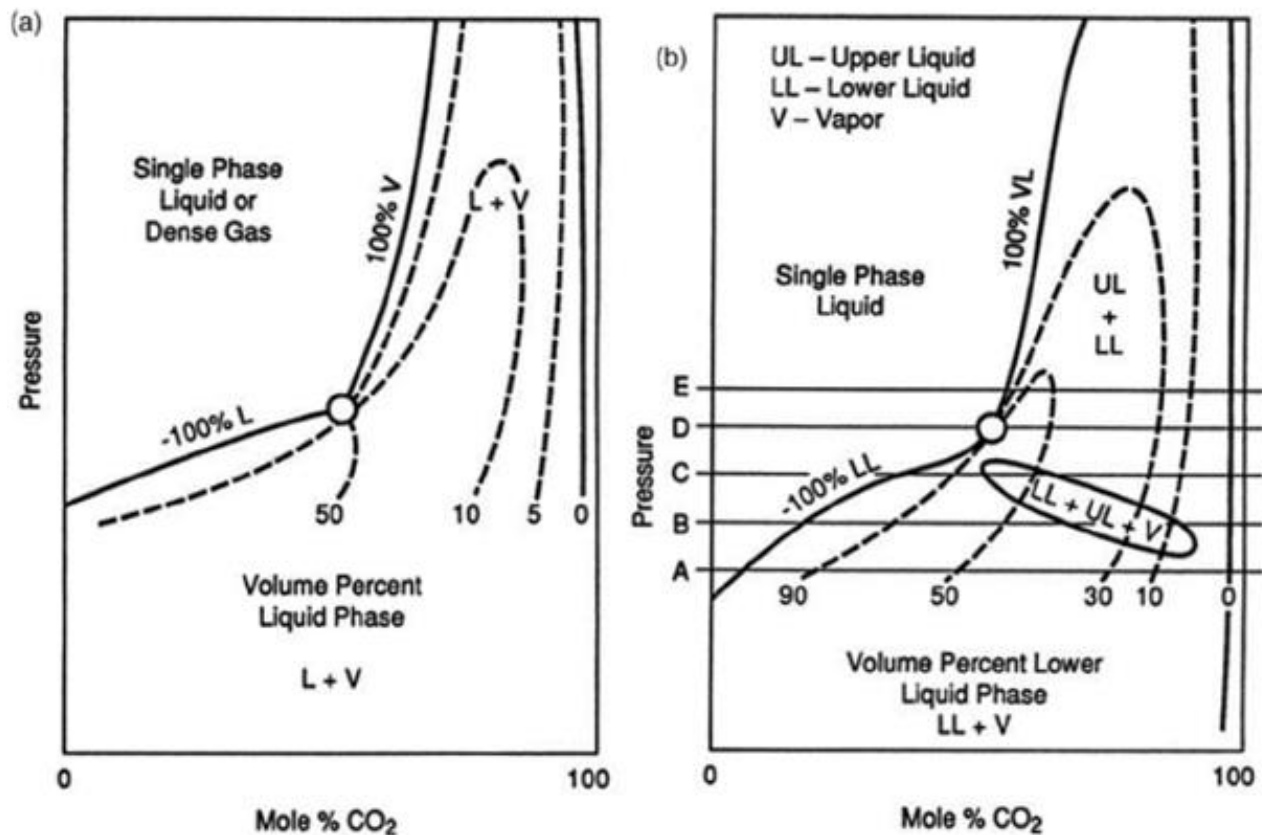


*Figure 2.17: a) CO2/hydrocarbon system phase behavior at temperatures above approximately 120°F: Type I phase behavior (Stalkup 1983a). b) CO2/hydrocarbon phase behavior at temperatures above approximately 120°F: Type II phase behavior (Stalkup 1983a).*

## 2.1.2 Minimum Miscibility Pressure (MMP)

A successful displacement depends highly on the injection pressure which must make sure that the injected gas ($CO_2$) and the reservoir oil will smoothly reach the desired pressure. It is quite clear that the minimum miscibility pressure (MMP) is a property of paramount importance for a monophasic fluid to be created from the two fluids. The prediction of the MMP can be done either experimentally, by the use of compositional (EOS) models or by the use of empirical correlations. Usually, equations of state are used correlating pressure, temperature and fluid volume in order to export all the necessary thermodynamic properties including the miscibility data. The most fundamental procedures are briefly described below.

Experimental Procedures

The most common experimental methods for MMP estimation are the Slim Tube Experiment and the Rising Bubble Experiment. Both experimental layouts can be seen in the next figure.
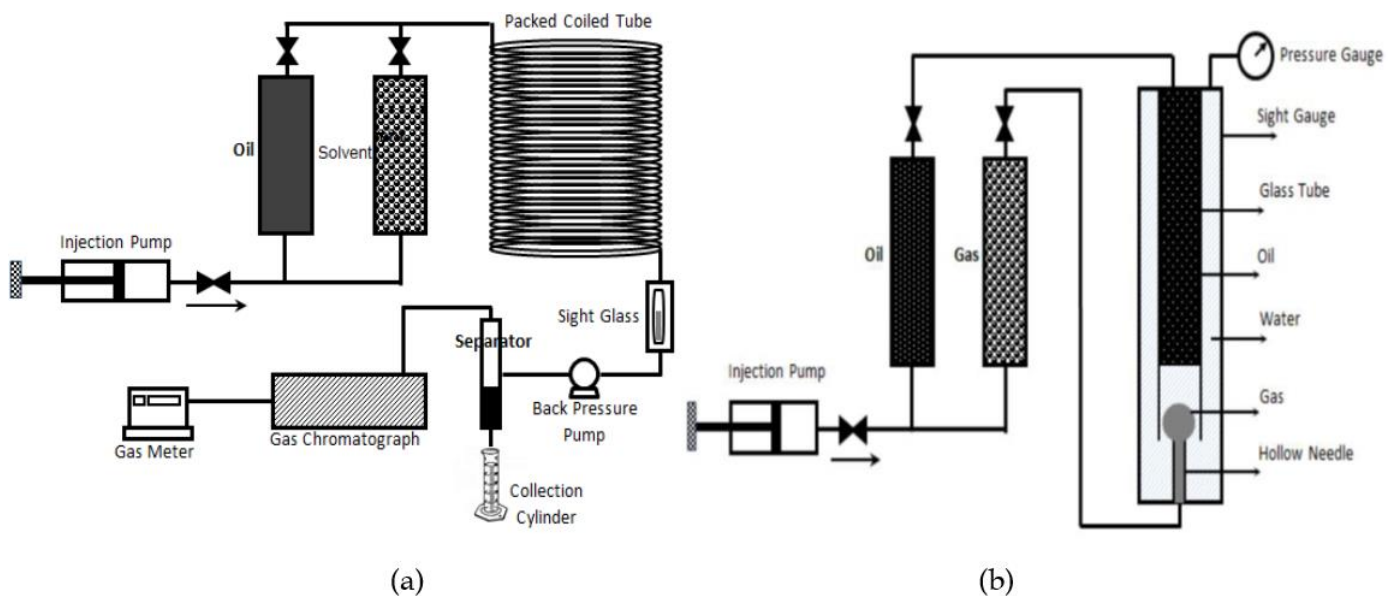


Figure 2.18: Experimental layouts for (a) Slim Tube Experiment and (b) Rising Bubble Experiment

The slim tube experiment can be used for estimating miscibility conditions such as injecting pressure and gas enrichment. On a reservoir level, however, it is not sufficient and EOS Reservoir Simulations should be used in the design. The experiment output is the Cumulative Recovery of Oil correlated to the Injected Gas Pore Volume. The experiment is conducted on many pressure values in order to construct a curve. When the displacement becomes miscible, the curve tends to level radically or smoothly. So, there are two discrete slopes and the break-point shows the MMP. The selection of the break point is quite subjective and several propositions have been made in order to standardize it. In general, the slim tube

experiment estimates better the MCM displacements but its results are highly affected by the fluids' in question phase behavior which poses as a serious issue since the reservoir conditions are quite different.

The rising bubble experiment is a faster method to estimate the MMP. In a nutshell a gas bubble is injected into a vertical system of water and oil and it is carefully observed during its journey from the bottom to the top. When it reaches the top, both fluids (oil and water) are replaced with new ones and the experiment is repeated on a different pressure value. As the bubble rises, it gets enriched with intermediate oil components simulating a vaporizing gas drive. At pressures far lower than the MMP the bubble shrinks but keeps its merely spherical shape during its ascension. In pressure values close to the MMP the bubble gets a wavy ending and at pressures above the MMP disintegrates quickly before it reaches the top. A condensing gas drive mechanism can also be simulated should already enriched gas be used. A number of 5-10 bubbles are injected for each pressure step. On pressures below the MMP every bubble exhibits the same shape shifting. At pressures equal or higher than the MMP, each injected bubble shrinks and disintegrates quicker than the last finally leading to FCM.
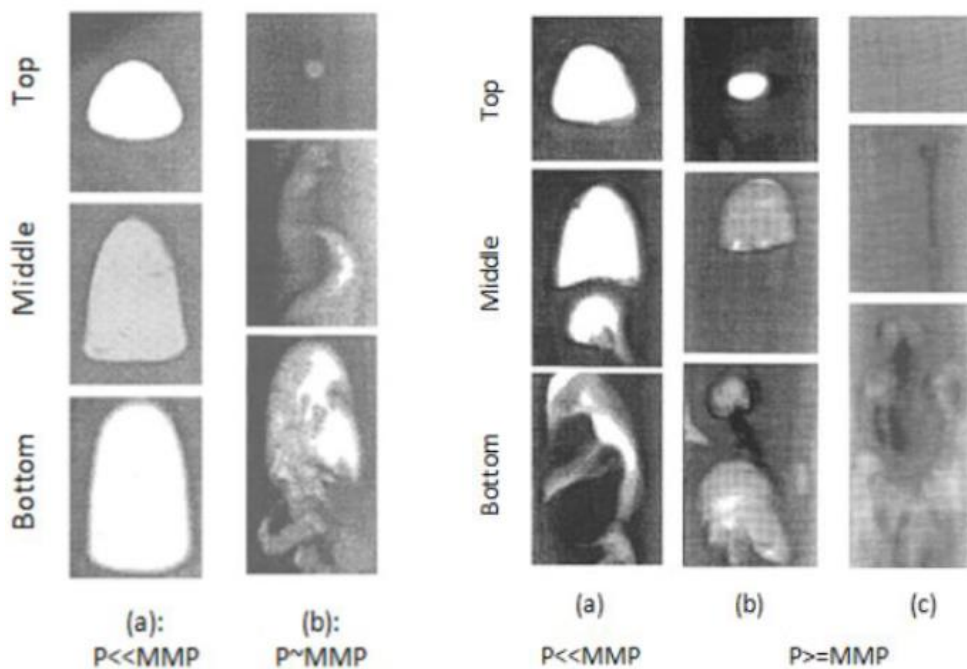


*Figure 2.19: Rising bubble experiment – Vaporizing Gas (left) Condensing Gas (right)*

Since volumetric data are not provided by the previously described experiments, several complementary experiments are carried out, known as PVT experiments. One of the most common ones is the Swelling Test. A known quantity of oil is added in a cell in reservoir temperature. Gas is injected stepwise and dilutes into the oil until the bubble-point pressure is reached and the fluid gets saturated. At each injection the volume and the saturation of the mixture is measured.
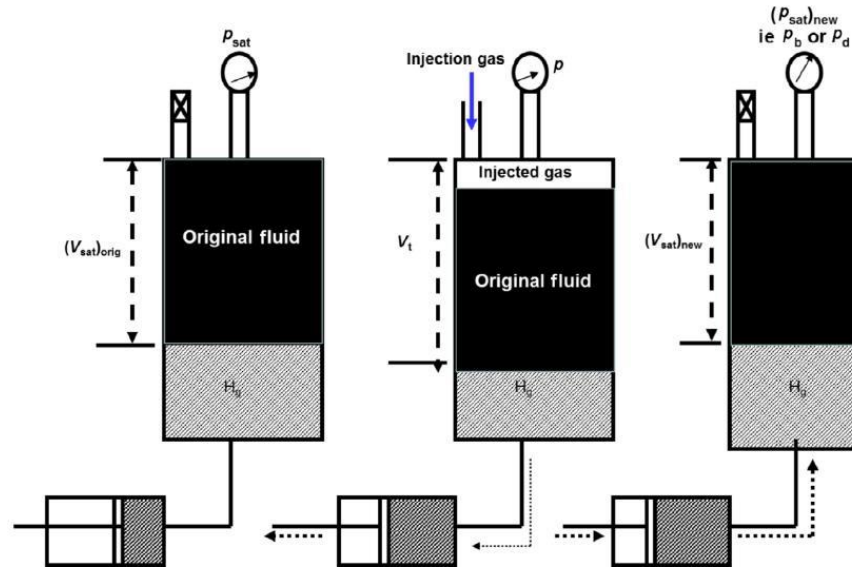
*Figure 2.20: Swelling Test*

Two other useful experiments widely used are the Forward and the Backward Multiple Contact experiment. The Forward Multiple Contact experiment simulates the conditions prevailing in a real gas injection at the front where injected gas and reservoir oil contact. As described in the vaporizing gas drive mechanism, the gas is enriched in every step and gets in contact with new reservoir oil in another cell. The variables of density, volume and composition of each phase are measured in every step of the experiment. The procedure repeats until miscibility is achieved or thermodynamic balance is reached (enriched gas above limiting tie line). On the contrary, the Backward Multiple Contact uses the same layout and principles as the Forward but what is moved to a new cell is the enriched in light components reservoir oil actually leading to the simulation of the condensing gas drive mechanism, the conditions of which are prevailing at the injection point. Again, the procedure repeats until miscibility is achieved or thermodynamic balance is reached (enriched oil on the limiting tie line). These cell-to-cell procedures (forward/backward contact experiment) provide the most accurate results as it simulates perfectly the component "swapping". This method can achieve miscibility with any of the pre-described ways (FCM, MCM) but is also very expensive.
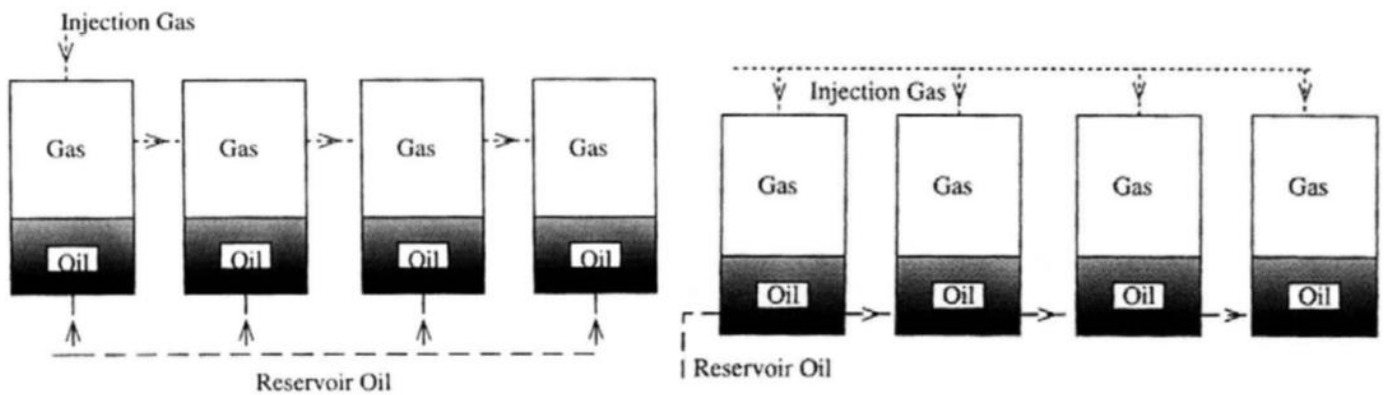


*Figure 2.21: Left- Forward MCM Experiment. Right - Backward MCM Experiment*

Another way of predicting the MMP is by the use of Equations of State (EOS). An EOS can be used to create models simulating phase behavior of all phases. Therefore, it can be used to simulate swelling and miscibility procedures with forward or backward multiple contacts. A crucial advantage of EOS methods is the numerical consistency and stability which is guaranteed. The most commonly used are the cubic EOS such as the Soave-Redlich-Kwong (SRK) and the Peng Robinson EOS. All of them are based on the same principles firstly given by the Van der Waals EOS and each one is a further improvement mostly by adding extra correction factors on various variables of the equation.

<u>Empirical Correlations</u>

Finally, there are empirical correlations for the prediction of the MMP. Most correlations used for the estimation of the MMP are derived by regressing experimental data. Usually the properties of the reservoir oil and/or the injected fluid are used as inputs. It is paramount to have in mind that these correlations provide only estimates of the real MMP and further studies should be made for the design of a real project. $CO_2$ is the most common gas used as injection gas, due to its solubility and its miscibility with reservoir oil. Diluted $CO_2$ engorges the oil and reduces its viscosity a lot making it more movable and resulting in high recovery factors. Combined with the low MMP required compared to other hydrocarbon gases and the lower cost, $CO_2$ makes the perfect candidate and therefore most of the correlations developed assume $CO_2$ injection.

There is a great number of empirical correlations but each one of them is derived by limited data and for very specific conditions. Therefore, for the same oil, the different correlations will give different estimations for the MMP and the differences are quite significant, sometimes reaching up to 1000 psia.

Holm and Josendal (1974, 1980) developed a correlation which is actually an extension of the one of Benham et al. (1960). The correlation, which is depicted in Figure 2.22, calculates the MMP given the molecular weight of the $C_{5+}$ fraction in the oil and the temperature. Mungan (1981) extended even further the Holm and Josendal (1974, 1980) correlation and included even more molecular weights of the $C_{5+}$ fraction. Mungan's correlation is also shown in Figure 2.22. Later on, Holm and Josendal (1982) proved that the $CO_2$ density plays a part as well in the development of miscibility. They correlated $CO_2$ density at the MMP value with the $C_5$ through $C_{30}$ content It is important to remember that their correlation is applicable for a displacing fluid that is pure $CO_2$.
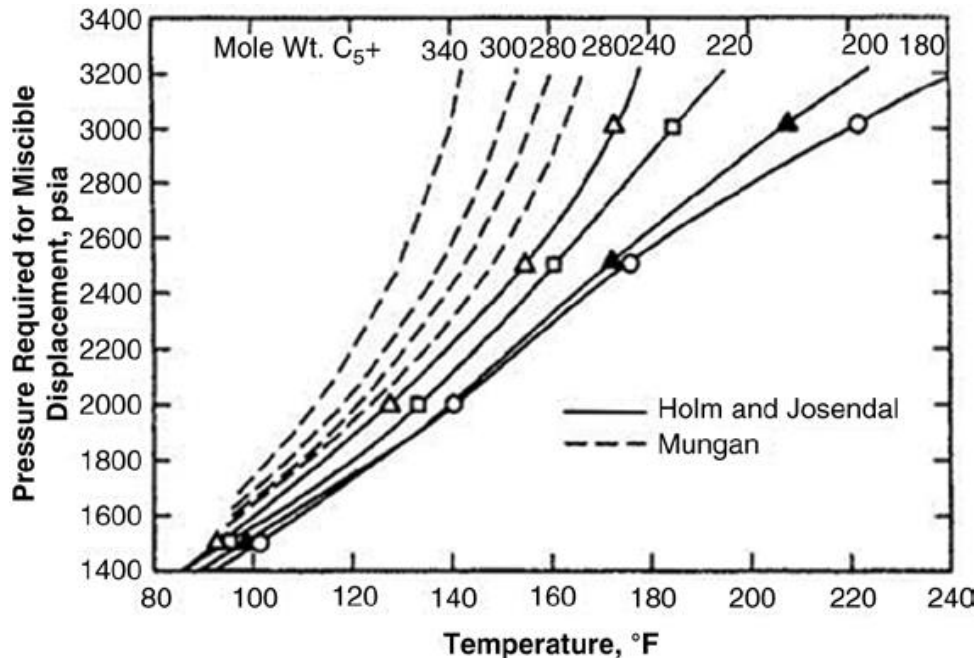
*Figure 2.22: Pressure necessary for miscible displacement in $CO_2$ flooding (Mungan 1981; Holm and Josendal 1974)*

 Yellig and Metcalfe (1980) developed an even simpler correlation, where MMP is described as a function of temperature solely, as a single curve. Should, however, the bubblepoint pressure be higher than the MMP from the curve, the bubblepoint pressure is used as the MMP. This goes for the possible formation of two phases when the MMP is below the bubblepoint pressure. Their correlation assumes a pure $CO_2$ displacing phase. Furthermore, Yellig and Metcalfe (1980) did comparisons between results for MMP values predicted with their own correlation and the one of Holm and Josendal (1974) with experimental values measured in slim tube experiments. In general, there was good agreement but, in some cases, predicted values diverged from experimental ones for 500 psia or more. Therefore, MMP estimates by empirical correlations should be used with a great deal of caution in actual design calculations.

A very important fact is that pure $CO_2$ is not always a viable solution due to the fact that it is highly expensive. As a substitute non-pure $CO_2$ such as flue gas is preferred as it can be easily found and is quite cheap also. This however poses an obstacle since most correlations refer to pure $CO_2$ as injection gas. Johnson and Pollin (1981) and Alston et al. (1985) developed correlations that account for impurities in the $CO_2$. The Alston et al. (1985) correlation applies to pure $CO_2$ streams as well as streams with impurities. It gives the MMP for CO2 as a function of reservoir temperature, the molecular weight of the heavy end ($C_{5+}$) and the molar fractions of the volatile components ($C_1$ and N2) and the intermediate components ($C_2$-$C_4$, $CO_2$ and $H_2S$). When the $CO_2$ stream is contaminated with other components, the MMP is affected. The addition of $C_1$ or $N_2$ to the $CO_2$ increases MMP, while the addition of $C_2$, $C_3$, $C_4$, or $H_2S$ reduces the MMP (Alston et al. 1985).

Alston et al. (1985) worked out a correlation which used a pseudocritical temperature of the impure $CO_2$ stream (determined with a weight-fraction mixing rule) which is subsequently used for the calculation of a correction factor for the impurities. They claim that this correction factor can be implemented in other literature MMP values based on pure $CO_2$. Furthermore, they support Yellig and Metcalfe suggestion, about using the bubble point pressure as the MMP if the predicted MMP value is below the bubblepoint.

Finally, they compared the MMP estimate obtained with their correlation to 68 experimental values. Both pure $CO_2$ and impure $CO_2$ streams were included in the dataset from both theirs and other literature experiments. The results are shown in Figure 2.23. The average error was 6.9%, with standard deviation value of 8.7%.

Sebastian et al. (1985) developed another correlation for impure $CO_2$ streams. The correlation relates MMP to the MMP for pure $CO_2$ and the pseudocritical temperature of the drive gas. It was based mainly on west Texas oils. They noted that the correlation was in general agreement with that of Alston et al. (1985).
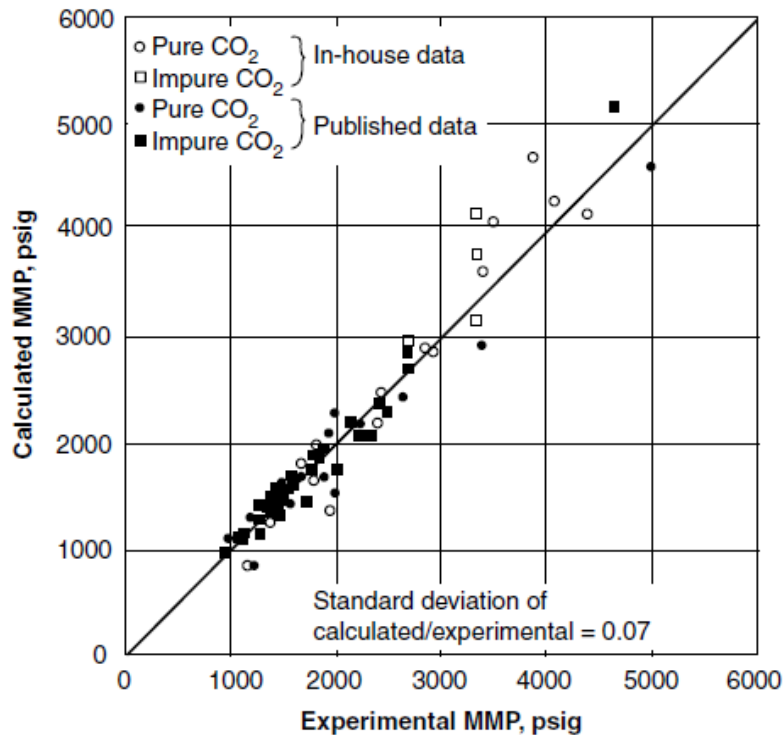


*Figure 2.23: Accuracy of correlation for predicting pure and impure CO2 MMP (Alston et al. 1985).*

## 2.1.3 Injection and Displacement Modeling

Oil recovery depends on the volume of the reservoir contacted by the injected fluid in any displacement process. A quantitative measure of this contact is the volumetric displacement (sweep) efficiency, $E_V$. Volumetric sweep is a macroscopic efficiency factor defined as the fraction of the reservoir pore volume infiltrated by the injected fluid and is, of course, a function of time. The absolute displacement efficiency in a process can be viewed conceptually as a product of the volumetric sweep, $E_V$, and the microscopic efficiency, $E_D$.

$E = E_V * E_D$ ............................................................................................................... Equation 2.1

Microscopic displacement efficiency, $E_D$, determines the outcome of a process in a great level. For crude oil, $E_D$ is reflected in the magnitude of residual oil saturation ($S_{or}$) in places contacted by the displacing fluids. Since EOR procedures generally include the injection of several fluids, the displacement efficiency of all the different slugs is important. Low values of microscopic efficiency can lead to early degeneration and breakdown of the slugs, which can sometimes translate even to project failure. Viscous and capillary forces determine both mobilization of fluids in the reservoir and phase trapping and therefore microscopic displacement efficiency, which in turn means that these forces and the relation between them play a major role in the total sweep efficiency.

Volumetric sweep efficiency can be considered conceptually as the product of the areal ($E_A$) and vertical ($E_I$) sweep efficiencies. $E_I$ is the volumetric sweep efficiency pore space invaded by the injected fluid divided by the pore space enclosed in all layers behind the location of the leading edge of the front. $E_A$ is the reservoir area swept over the total reservoir area. For a real project, in which thickness, porosity and hydrocarbon saturation vary within the reservoir area, a pattern sweep efficiency $E_P$ is used instead of $E_A$, meaning the hydrocarbon pore space enclosed behind the injected-fluid front over the total hydrocarbon pore space in the pattern or reservoir, which in fact is areal sweep efficiency corrected for variations in all the previously mentioned variables. For a displacement process, overall hydrocarbon recovery efficiency is:

$$E = E_P * E_I * E_D \hspace{4cm} \text{Equation 2.2}$$

Although the previous equations are correct in concept, application to real problems is quite difficult. In order to use them to calculate $E_V$, independent estimates of $E_A$ (or $E_P$) and $E_I$ are needed. These are quite difficult to get due to the fact that, in 3D systems, areal and vertical sweep efficiencies are not independent. In practice, $E_V$ is usually defined by applying appropriate correlations or 3D systems-based mathematical models.

$E_A$ and $E_I$ are affected strongly by the mobility ratio in and type of displacement process (miscible or immiscible). Mobility of a fluid phase flowing in a porous medium is expressed by the Darcy equation as:

$$U_i = (\mu_i / k_i)(dp/dx) \hspace{4cm} \text{Equation 2.3}$$

- $U_i$ is the superficial velocity of the phase.
- $\mu$ is the viscosity of the phase.
- $k_i$ is the permeability of the phase:
  single-phase flow$\rightarrow k_i$ = absolute permeability of the porous medium.
  multiphase flow$\rightarrow$ $k_i$ = effective permeability of the flowing phase =$f(S_{phase})$
- $dp/dx$ is the infinitesimal pressure drop between two points.

When modelling displacement processes, a significant variable is the mobility ratio, *M*, of the displacing and displaced fluid phases:

$$M = \lambda_D / \lambda_d \hspace{4cm} \text{Equation 2.4}$$

- $\lambda_D = k_D / \mu_D$, mobility of the displacing fluid phase
- $\lambda_d = k_d / \mu_d$, mobility of the displaced fluid phase.

The mobility ratio M is dimensionless. It is a variable of paramount importance for all displacement processes as it influences both vertical and areal sweep. As *M* increases for a given volume of injected

fluid, sweep decreases. What is more, M defines whether or not the displacement process will be stable. The flow becomes unstable when M> 1.0 (viscous fingering). M values >1.0 are usually called unfavorable while M values < 1.0 favorable.

M can be defined in several ways and is a function of the flow conditions in a particular process. For instance, when a specific solvent is displacing another one with which it is fully miscible and we have single-phase flow, the mobility ratio is the viscosities ratio because the permeability to each solvent is the absolute porous-medium permeability.

$$M = \mu_d / \mu_D \hspace{6cm} \text{Equation 2.5}$$

Typically, at least two phases are flowing both ahead of and behind a front and phase saturations are changing with time and location. Therefore, the use of total mobilities $\lambda_{tD}$, which is the sum of the mobilities of all phases flowing behind the displacement front measured at the average saturation behind the front, is a good approximation:

$$Mt = (\lambda_{tD})_{SD} / (\lambda_{td})_{Sd} \hspace{5cm} \text{Equation 2.6}$$

Stalkup (1983) proposed this definition for characterizing mobility ratio between an oil bank and the solvent displacing it when mobile water is present. Furthermore, he claims that in several processes, that involve for example multiple slug injection, there will be more than one displacement front. Flow behavior of any displacement front is influenced by the fluid' mobilities all around the front not only directly ahead of it. In this case, there is not a unique definition of the mobility ratio which will lead to accurate prediction of the sweep efficiency. Concluding, due to the various definitions of mobility ratio, caution must be taken when empirical correlations based on mobility ratio.

As previously pointed out, defining volumetric sweep as a product of areal and vertical sweep efficiencies comes in quite handy as it allows the application of correlations based on separate studies of the two. The most important parameters affecting both areal and vertical efficiencies will be briefly mentioned below.

Areal Sweep Efficiency

Areal displacement efficiency is affected by four main factors:

- Well pattern (5-spot, line drive etc.)
- Reservoir permeability heterogeneity (e.g. fractures, permeability anisotropy, flow barriers)
- Mobility ratio (as M decreases, sweep efficiency increases)
- Flow regime dominance of viscous or gravity forces (Capillary number $N_C$ and Bond number $N_B$)

Since for this thesis miscibility between fluids and the 5-spot pattern are widely used, these topics will be furtherly discussed. Figure 2.24 shows fluid fronts at distinct points in a flood for two values of mobility ratio. The results rely on photographs taken, in a scaled model, during miscible displacements two differently colored liquids.
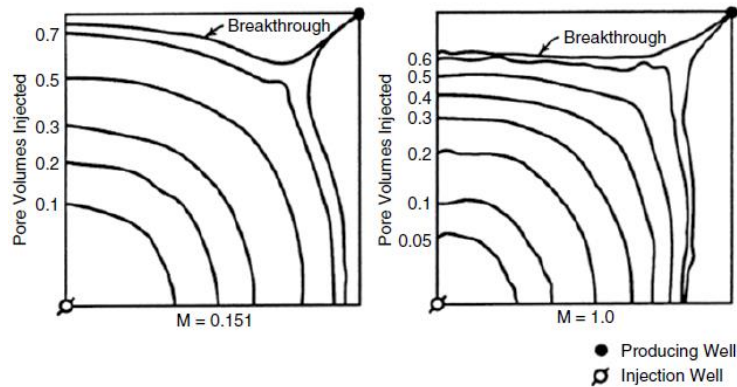
*Figure 2.24: Miscible displacement in 1/4 of a 5-spot pattern at mobility ratios< 1.0 (Habermann 1960).*
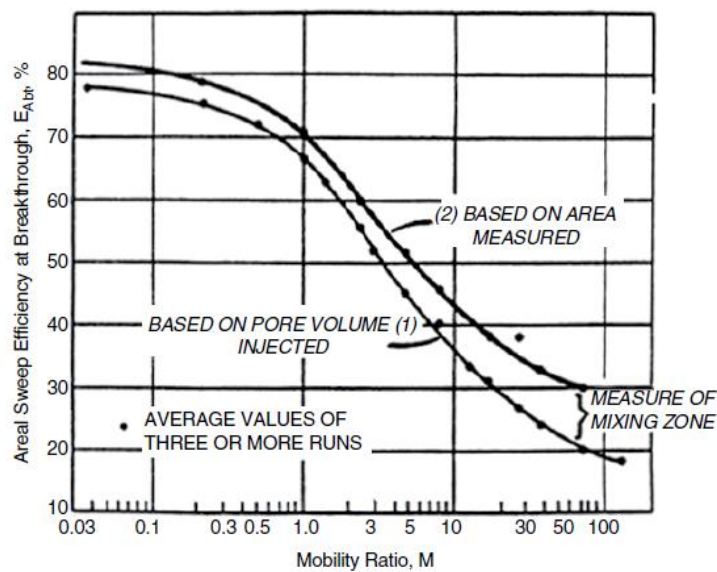


*Figure 2.25: $E_{As}$ at breakthrough as a function of mobility ratio during miscible displacement at a 5-spot pattern (Habermann 1960).*

Figure 2.25 is a chart that shows the sweep efficiency as a function of mobility ratio for two cases, one calculated based on the measured area and another based on the pore volume of injected fluid. The divergence of the two curves is an indicator of the mixing that took place at the interface. It is quite clear that $E_A$ at breakthrough is strongly affected by M. For M = 1.0, areal sweep is approximately 70% and at somewhat smaller mobility ratios it increases. Should M increase, $E_A$ decreases very abruptly for two main reasons:

- Viscous fingering
- Geometry contributes to the early breakthrough.

The biggest flow velocity is along the center line connecting the wells (injectors and producers) because of the geometry and therefore, fluid that flows along this particular line will break through first in a homogeneous reservoir. When M exhibits values larger than unity, the injected fluid displaces the reservoir fluid because it has a higher mobility. Since the biggest flow is along the centerline path, the resistance is already the lowest encountered compared to the other flow-lines. Additionally, a larger slug

of injected fluid flows through this line, leading to further reduction of the resistance. In the end that means that as the value of M increases, breakthrough happens sooner.

Claridge (1972) worked out an improvement of the areal sweep correlation for a five-spot pattern. He saw that the sweep efficiencies reported by Caudle and Witte (1959), which were based on unscaled models, were too high compared with other scaled-model results. However, their reported sweep efficiencies agreed with the fractional area inside a curve drawn through the tips of the viscous fingers in photographs of displacements taken in more properly scaled models. Claridge assumed that the X-ray shadowgraph work of Caudle and Witte predicted "the fraction of total pattern area invaded by fingers at breakthrough and subsequent levels of throughput." Claridge (1972) developed a correlation by combining the Caudle and Witte (1959) data with the model of viscous fingering derived by Koval (1963). The correlation is shown in Figure 2.27. The recovery factor is obtained in displaceable PVs of oil produced as a function of displaceable PVs of fluid injected, $F_i$, and mobility ratio, M.
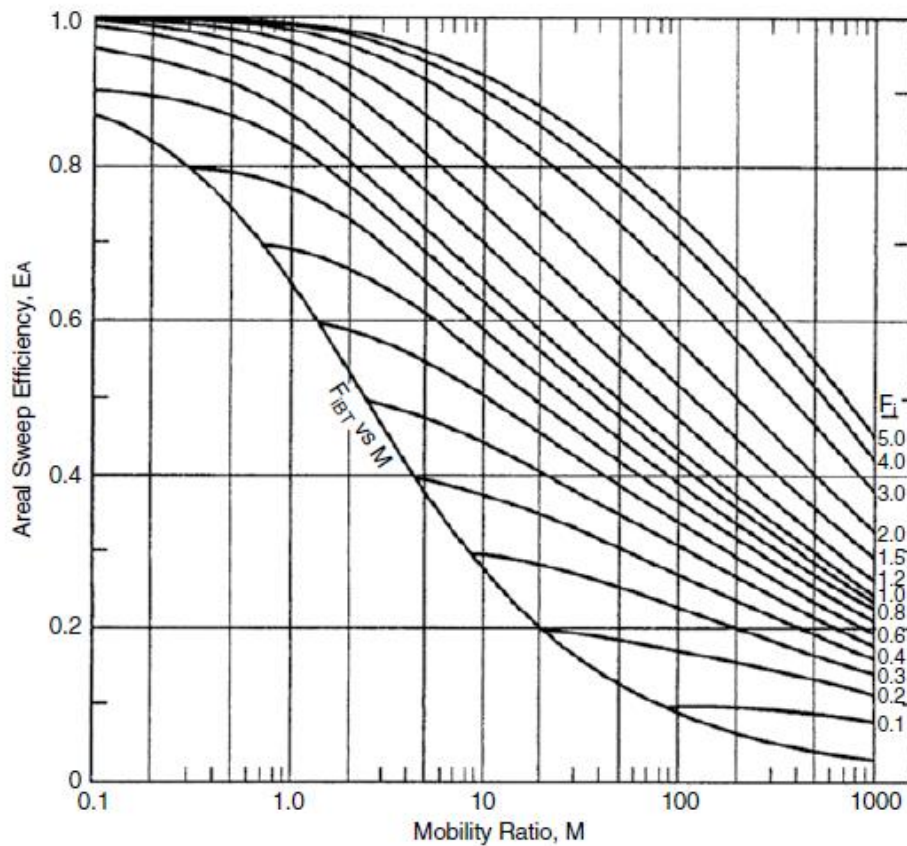


*Figure 2.26: Claridge correlation for areal sweep efficiency (Claridge 1972).*

Vertical sweep efficiency

Vertical displacement efficiency is primarily affected by four parameters which are:

- Differences in density (Gravity Segregation)
- Mobility ratio
- Vertical-horizontal permeability variation
- Capillary forces.

When large density differences between injected and reservoir fluids exist an important component of fluid flow is forced in the vertical direction. This phenomenon is called gravity segregation. When the reservoir/displaced fluid is denser than the injected/displacing one, the injected/displacing fluid overrides the reservoir/displaced fluid (Figure 2.27a). Gravity override can be observed in several processes such as steam displacement, solvent flooding, $CO_2$ flooding, and in-situ combustion. On the other hand, when the injected/displacing fluid is denser than the reservoir/displaced fluid, e.g. waterflood (Figure 2.27b), early breakthrough of the injected fluid occurs and vertical sweep efficiency is reduced.
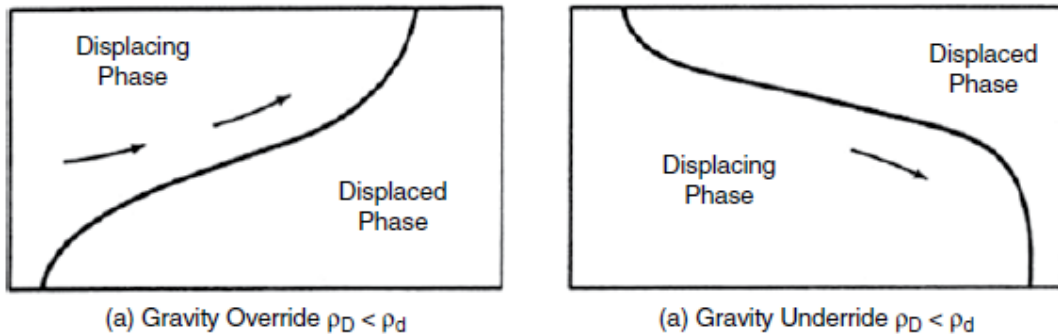


*Figure 2.27: Gravity Segregation in displacement processes*

Vertical variation in permeability in reservoirs is quite regular. Figure 2.29 shows a vertical cross section a reservoir subdivided into layers of different permeabilities and thicknesses. This is a simplified geologic model as permeability generally varies over a significant thickness. As a consequence, vertical sweep efficiency at breakthrough is reduced due to the not equal flowrates in the different reservoir layers. Note that this is an idealization since unity mobility ratio was assumed and no gravity segregation.
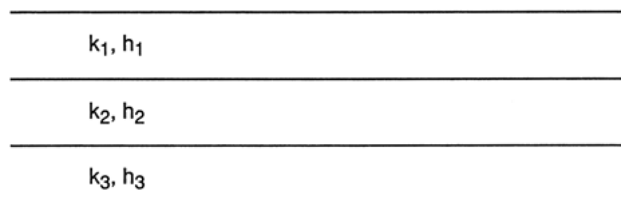


*Figure 2.28: Vertical variation in permeability - layered reservoirs*

Simple models can be used to quantify the effects of reservoir heterogeneity and permeability variation on vertical sweep efficiency. A key assumption is that the reservoir layers do not communicate and gravity segregation is negligible. A model with these characteristics was developed by Dykstra and

Parsons. It refers to piston-like displacement in a linear reservoir flooded at constant pressure drop (Willhite 1986; Stalkup 1983; Dykstra and Parsons 1950). Dykstra and Parsons introduced the concept of permeability variation V, also known as the Dykstra-Parsons coefficient, designed to describe the degree of heterogeneity within the reservoir.

$$V = k_{50\%} - k_{84,1\%} / k_{50\%} \hspace{4cm} \text{Equation 2.7}$$

The permeability (k) values are retrieved in logarithmic scale. Values for this coefficient range between zero (0) for a completely homogeneous system and one (1) for a completely heterogeneous system. For most cases, V varies between 0.5 and 0.9 indicating that a geologic formation is moderately to highly heterogeneous.

In a nutshell the Dykstra Parsons method, which is used extensively for recovery calculations in non-communicating layers:

- Values of oil relative permeability at connate water saturation ($k_{ro,max}$) , water and/or gas relative permeability at breakthrough, and the viscosities of all involved fluids need to be known.
- Permeabilities are tabulated in decreasing order of magnitude and for each entry, the % percentage of total number of permeability values exceeding it is calculated.
- A log-log plot of the permeabilities versus the total number of permeability values exceeding each entry is constructed.
- The Dykstra-Parsons coefficient V is calculated.
- Compute the Mobility Ratio M
- Read the values of recovery ER as a fraction of the pore space for different WOR values from already existing tables.

3D volumetric displacement efficiency may be determined by numerical simulation. This approach requires the formulation of differential equations that mathematically represent the physical displacement process and of course their solution through numerical-analysis techniques implemented by a computer. Because of the complexity of the equations and the calculation procedures, significant effort often is required to obtain a solution algorithm but should that barrier be overleaped a large number of cases can be computed and the effect of different parameters can be examined. The previously mentioned assumption of noncommunicating vertical reservoir layers is a quite common method of approaching a 3D reservoir simulation performance. The 3D results are derived from the combination of all the 2D evaluated results. The layers may be described in different ways (reservoir geology, permeability groups etc.).

## 2.2 Streamlines - Streamtubes Theory

### 2.2.1 Overview

Streamline simulation is a considerable alternative to cell-based (finite elements/differences) grid techniques in reservoir simulation. Streamlines are in fact snapshots of the flow field and produce data such as drainage or irrigation areas connected with the different wells (producers/injectors) and flow rate allocation between injector-producer pairs that are difficult to derived by other simulation techniques.

Streamline-based flow simulation is quite different from common cell-based simulation techniques because phase saturations and components are transported along a flow-based grid defined by the streamlines and are not moved from cell-to-cell. This actually makes streamline simulation ideal for solving large, heterogeneous models if key assumptions are made regarding the physical system about to be simulated.

The computational speed and simplicity of the method classifies it as a very powerful approach which can compete with traditional simulation approaches. It can be used for several tasks such as:

- Sensitivity runs.
- Quantification of the impact of upscaling (geo-modeling scale - simulation scale).
- Visualization of the flow field.
- Reliability in full-field simulations (otherwise sector models would have to be used).
- Evaluate multiple production scenarios and input parameters in short time.
- Evaluation of injector/producer efficiency.
- Reduce turnaround time in history matching.

The main objective is to describe how injected reservoir volumes (water or/and gas usually) displace the reservoir fluid volumes given the following:

- ❖ Well locations
- ❖ Well rates
- ❖ Reservoir geometry
- ❖ Geological description

The major assumption in streamline simulation is that the system be close to incompressibility. This decouples saturations from the underlying pressure field and allows each streamline to be treated independently from the streamlines next to it.

Streamlines have been in the petroleum literature since the late 1930's and have received repeated attention as a way to predict the fluids' motion numerically. In the early 1990s, as advances in geological modeling techniques were producing models too large for finite differences to simulate in an acceptable time frame streamlines were revived and since then huge advances were made that extended streamlines to 3D and made them applicable to real field cases.

## 2.2.2 Mathematics of the Streamline Method

The streamline method is an IMPES-type formulation. The pressures are solved for implicitly whereas the fluids' saturations are solved for explicitly along streamlines. Pressure, $P$, for multiphase incompressible flow without capillary or diffusion effects is described by Equation 2.8. The total velocity is derived from the 3D solution to the pressure equation and application of Darcy's law.

$$\nabla \cdot \sum_{j=1}^{n_p} \frac{\overrightarrow{\overrightarrow{k}} k_{rj}}{\mu_j} \left( \nabla \cdot P + \rho_j \overrightarrow{g} D \right) = 0,$$

Equation 2.8

- o   $D$ = depth below the datum level
- o   $g$ = gravitational acceleration constant
- o   $k$ = the permeability tensor
- o   $kr_j$ = relative permeability
- o   $\mu_j$ = viscosity
- o   $\rho_j$ = phase density of phase j.

The explicit material balance equation for each incompressible phase $j$ is then given by Equation 2.9 whose variables are explained below.

$$\phi \frac{\partial S_j}{\partial t} + \overrightarrow{u}_t \cdot \nabla f_j + \nabla \cdot \overrightarrow{G}_j = 0.$$

Equation 2.9

- o   $f_j$ = phase fractional flow
- o   $G$ = phase velocity (gravity segregation)
- o   $U$ = total velocity

Each phase fractional flow, $f_j$, is given by Equation 2.11. Phase velocity resulting from gravity segregation because density differences of the phases is given by Equation 2.12.

$$f_j = \frac{k_{rj}}{\mu_j} \frac{1}{\sum_{j=1}^{n_p} k_{rj} \Big|_{\mu_j}},$$

Equation 2.10

$$\overrightarrow{G}_j = \overrightarrow{\overrightarrow{k}} \cdot g f_j \nabla D \sum_{i=1}^{n_p} k_{ri}(\rho_i - \rho_j)/\mu_i.$$

Equation 2.11

The difference between streamline simulation and finite-differences is the way the explicit material balance equations (Equations 2.9, 2.10 and 2.11) are solved. In streamline simulation the material balance equations are solved along streamlines, whereas in finite differences, the material balance equations are solved between gridblocks.

In finite-differences, Equation 2.9 is discretized and solved on the underlying grid on which the pressure field is computed. The solution is governed by the grid Courant-Friedrichs-Lewy (CFL) condition, which can lead to prohibitively small timestep sizes, especially for models with high permeability variation or high local flow velocities, or both. With streamlines, this grid CFL condition is avoided completely by solving Equation 2.9 along each streamline using a time-of-flight (TOF) coordinate transform.

Streamlines are traced from injectors to producers based on the underlying total velocity field. As each streamline is traced the TOF is calculated along the streamline, which is defined by Equation 2.12

$$\tau = \int_0^{s} \frac{\phi(\delta)}{\left| \overrightarrow{u}_t(\delta) \right|} d\delta.$$

<div align="right">Equation 2.12</div>

A better way of expressing Equation 2.9 is by using Equation 2.8 and transforming it to:

$$\frac{\partial S_j}{\partial t} + \frac{\partial f_j}{\partial \tau} + \frac{1}{\phi} \nabla \cdot \overrightarrow{G}_j = 0.$$

<div align="right">Equation 2.13</div>

In Equation 2.13, the gravity term is not aligned along a streamline direction which in turn means that the equation can be split into two discrete parts giving two 1D equations:

- The convective part of the material-balance equation along streamlines, given by Equation 2.14

$$\frac{\partial S_j^c}{\partial t} + \frac{\partial f_j}{\partial \tau} = 0,$$

<div align="right">Equation 2.14</div>

- The part referring to by phase-density differences, which is solved along gravity lines, given by Equation 2.15.

$$\frac{\partial S_j^g}{\partial t} + \frac{1}{\phi} \nabla \cdot \overrightarrow{G}_j = 0.$$

<div align="right">Equation 2.15</div>

Both Equations 2.14 and 2.15 represent 1D equations that are solved using standard finite-difference numerical techniques. Of course, there are still CFL conditions that restrict timestep sizes, but these limits are local to each streamline or gravity line, which make the problem much simpler and are insignificant compared to the ones existing for 3D finite difference simulations.

## 2.2.3 Time-stepping and Computational efficiency of streamlines

In field-scale displacements, the streamline paths change with time because of the changing fluid distributions and the changing well conditions. As a result, the total velocity field is periodically updated, and new streamlines are recomputed to reflect the nonlinear nature of the displacement. To move the 3D saturation distribution forward in time between successive streamline distributions from time $T_i$ to $T_{i+1} = T_i + dT_i$, the basic algorithm is

- Given initial conditions (i.e., pressures and saturations for each active cell in the system) and well conditions, the pressure is solved implicitly for each cell using Equation 2.8.
- Since the pressures are known, the total velocity for every cell interface can be calculated using Darcy's Law. The total velocity is then used to trace streamlines (Pollock's algorithm).
- The 1D mass conservation equations are solved along each streamline, independently of each other as demonstrated in Equation 2.14. The initial conditions are found by a mapping from the underlying 3D grid onto each streamline. The mass-transport problem is marched forward in time along each streamline for a pre-specified global timestep $dT_i$, and then the solution is mapped back onto the 3D grid. Gravity is considered by including a vertical segregation step along gravity lines after movement along all streamlines, using Equation 2.15.

It is a quite simple approach, however important details must be considered, such as:

- The algorithm is similar to an IMPES approach, because the pressure is solved implicitly for a new time level n+1 using saturations at level *n*. The saturations at time n are given by mapping back solutions from each streamline onto the 3D grid at the previous timestep. The implicit nature of the pressure solution is the reason why there is no limitation on the timestep to reach n+1. However, compressible systems that exhibit numerical convergence problems, might limit the actual size of the timestep, exactly the same way as in finite difference simulation.
- Pollock's algorithm, used for streamline tracing, assumes Cartesian (orthogonal) cells. Any other shape of cells requires an isoparametric transformation for tracing streamlines.
- For incompressible systems, each streamline will start at injection wells and end at production wells. For compressible systems though, streamlines can start or end anywhere in the system, because any gridblock in the system might behave as a source (volume expansion) or a sink (volume contraction).
- Initial launching of streamlines from wells can be analogous to the total flux at the wells, though this will, most likely, leave many cells in the system without a streamline passing through them. For missed cells, tracing begins at the center of the missed cell and then traced backward until a source is encountered. Should a cell not have a streamline passing through it, it impossible to assign an updated saturation back to that cell.
- In practice, it impossible to have all streamlines carrying the same flux and simultaneously assign at least one streamline per cell. Therefore, streamlines do not carry the same flux.
- For incompressible systems the flux along each streamline is constant, while for compressible ones it is not.
- The tracing of streamlines using the TOF variable produces a highly irregular 1D grid along each streamline. To numerically solve the 1D problem efficiently, the 1D grid must be regularized, solved using an implicit approach, or regridded in some way to allow for a more efficient solution.
- The tracing of the streamlines relies on an accurate solution of the velocity field. Excessive distortions of the grid (nonorthogonal) or a pressure solution that has not been solved to a small enough tolerance can cause problems in tracing streamline paths.

One advantage of streamline simulation over more traditional approaches is its innate efficiency, both in computational speed and memory terms. In particular, streamline-based simulation can exhibit an almost linear scaling in run times as a function of active cells in the model.

Memory efficiency is a result of two key aspects of the formula:

- Streamline simulation is an IMPES method (involving only the implicit solution of pressure)
- Tracing of streamlines and solution of the relevant transport problem along each streamline is done sequentially. Only one streamline needs to be kept in memory at any given time.

Computational speed, on the other hand, is achieved because the transport problem is decoupled from the 3D grid and instead solved along each streamline. Because transport along streamlines is 1D, they can be solved efficiently. Because the number of streamlines increases linearly with the number of active cells, and streamlines only need to be updated infrequently, the computational time exhibits a near-linear scaling with increasing number of gridblocks.

The number of global timesteps is related to how often the flow field (streamlines) requires updating and changing flow paths depend on:

- Heterogeneity
- Mobility changes
- Gravity
- Changing well conditions

In several practical problems, the changing well rates cause the biggest impact on a changing flow field and therefore are the limiting factor for global timestep sizes. Grouping well events into semi-yearly or yearly intervals and assuming that no change in the streamlines over each period is quite reasonable (30-40 year histories are successfully and routinely simulated with 1-year timesteps).

Streamlines produce new data not available with conventional simulators. A major advantage is that because streamlines start at a source and end in a sink, it is possible to determine which injectors are (or which part of an aquifer is) supporting a particular producer, and exactly by how much. A high water cut in a producing well can be traced back to specific injection wells or boundaries with water influx. Thinking vice versa, it is possible to determine just how much volume from a particular injection well is contributing to the producers it is supporting which is significantly valuable information on balance patterns or water injection optimization problems.

Streamlines can also identify the reservoir volume associated with any well in the system, because a block traversed by a streamline attached to a particular well will belong to that well's drainage volume. It is therefore possible to divide the reservoir into dynamically defined drainage zones attached to wells. Properties normally associated with reservoir volumes can now be expressed on a per-well basis, such as oil in place, water in place, and average pressure, just to mention a few. The most successful uses of new data produced by streamlines are in the area of waterflood management and reservoir surveillance, and in the area of history matching.

# CHAPTER 3

# Screening Tool Development: Zero-Dimensional Mapping Model and "CO$_2$ Prophet" Software

## 3.1 Zero (0)-Dimensional Mapping of Real 3D Reservoir Simulations

A number of procedures are available for calculation of performance of a miscible displacement process. These range from simple calculations that may be considered as rough estimates to complex numerical simulations that require large computers. Zero-Dimensional Mapping is a category of methods making relatively simple calculations that can be performed by hand. Most of these are based on results from physical models. The calculations are considered as rough estimates of performance and even though they illustrate the effects of different variables on process performance, they generally are not sufficient for final design calculations. The calculations focus on ultimate recovery and recovery as a function of solvent (and other drive fluids) injected and the rates of injection and recovery are considered as well. The methods are illustrated for single-layer reservoirs, but can be extended to multilayered ones.

Some basic definitions need to be presented due to their wide use throughout this thesis. In general, results from an appropriately scaled physical model can be used in a straightforward manner to determine oil production as a function of displaceable pore volumes (PVs) of miscible solvent injected. Displaceable pore volumes of injected fluid, $V_{pd}$, is defined as:

$$V_{pd} = \frac{V_{si}}{V_p \cdot (1 - S_{orm} - S_{cw})} \quad\text{-------------------------------------------------------}\quad \text{Equation 3.1}$$

- $V_{si}$ = Volume of solvent injected
- $V_p$ = Pore volumes in the pattern area,
- $S_{orm}$ = Residual oil saturation at the end of the miscible displacement
- $S_{cw}$ = Irreducible water saturation.

Claridge (1972) developed a set of curves giving displacement efficiency as a function of *M* and PVs injected for gravity effects assumed negligible. His correlation was based on the physical model results of Caudle and Witte (1959) and the viscous fingering model of Koval (1963). Claridge's correlation is used widely for both examples about to be presented and therefore it should be carefully examined and understood beforehand. As seen in the diagram the sweep displacement efficiency E$_{As}$ is given as a function of *M* and PVs of solvent injected. As expected, the larger the slug injected for the same M value, the better the sweep efficiency. Also, it is quite clear that for a mobility ratio equal or as close as possible to unity, the curves are all maximized indicating the favorability discussed earlier. Of course, the horizontal axis is logarithmic in order to capture all possible values of M.
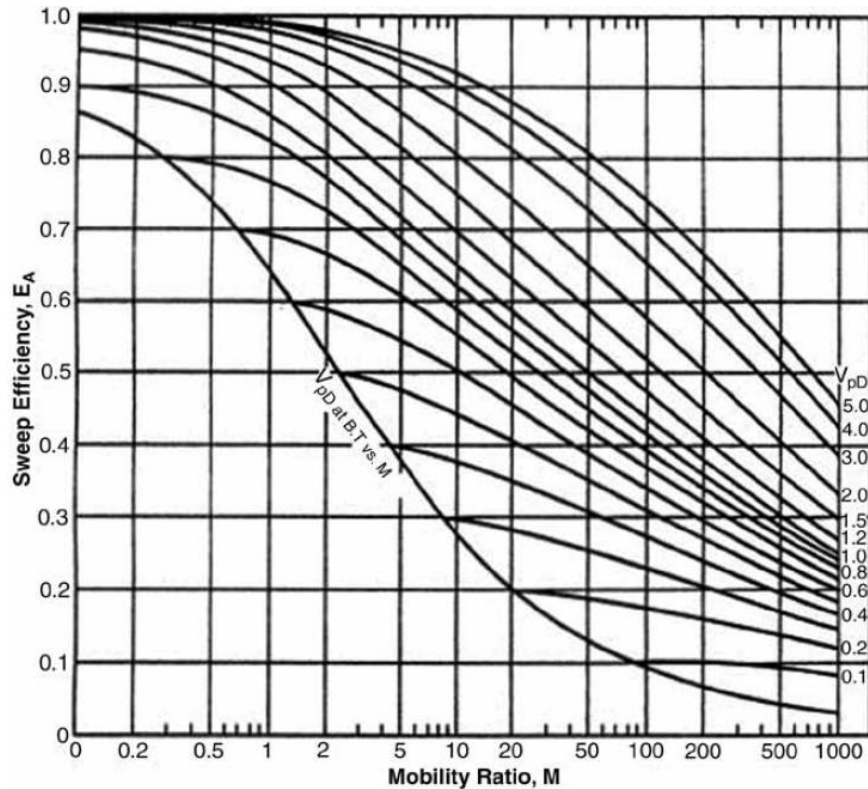
*Figure 3.1: Claridge correlation for Areal Sweep Efficiency $E_{As}$ versus Mobility Ratio M and displaceable reservoir pore volumes $V_{pd}$*

Two examples from the book of Green and Willwhite will be presented below, as these two will be examined further in the thesis. The first refers to a miscible $CO_2$ flood as a secondary production technique and the second to a miscible $CO_2$ flood but as a tertiary production technique in an already waterflooded reservoir. For both examples, the average reservoir pressure is assumed to be above the minimum miscibility pressure (MMP) in order for the fluids to be fully miscible. Also, in both cases about to be presented, the mobility ratio (M) is first calculated and values of production as functions of injection are read directly from the selected correlation. Most of the available correlations assume gravity effects to be negligible indicating that viscous forces prevail. The different studies are in good agreement for mobility ratios in the vicinity of unity. At large M values, however, significant differences appear, reflecting differences in scaling.

### 3.1.1 Secondary Production - CO$_2$ Flood

The first problem states the following:

Assume that a large slug of $CO_2$ is to be used to displace oil miscibly in a secondary recovery process. A 5-spot pattern is to be used. The objective is to calculate oil recovery as a function of solvent injected with the Claridge (1972) correlation. Table 3.1 lists data for the problem. Gravity effects are assumed to be negligible and continuous solvent injection is assumed due to the large size of the gas slug. The reservoir is completely liquid filled; i.e., there is no initial gas saturation requiring liquid fill-up.

| | |
|---|---|
| Pattern area A (acres) | 20 |
| Thickness h (ft) | 20 |
| Porosity φ | 0.18 |
| Permeability k (md) | 120 |
| Initial oil saturation ($S_{oi}$) | 0.75 |
| Connate water saturation $S_{ow}$ | 0.25 |
| Residual oil saturation (ROS) at the end of miscible displacement, $S_{orm}$ | 0.05 |
| Oil viscosity at $T_{res}$, $\mu_o$ (cp) | 1.5 |
| CO$_2$ viscosity at $T_{res}$, $\mu_s$ (cp) | 0.06 |
| Oil formation volume factor, $B_o$ | 1.15 |
| Reservoir temperature $T_{res}$ | 120 |
| Average reservoir pressure , $P_{res}$ | 2500 |

*Table 3.1: Data required for the solution of the secondary CO$_2$ flood problem*

The procedure followed is:

- Calculate the OOIP using the volumetric method. Caution needs to be taken in the units' transformations.

$$N = A \cdot h \cdot \varphi \cdot S_{oi} \cdot \frac{1}{B_o} \rightarrow \text{N= 364000 stb.}$$

- Calculate the displaceable reservoir volume of injected solvent $V_{pds}$

$$V_{pds} = \frac{V_{si}}{A \cdot h \cdot \varphi \cdot (1 - S_{orm} - S_{cw})} \rightarrow V_{pds} = V_{si}/391000 \text{ bbl.}$$

- Calculate the mobility ratio, M. Since the permeability is the absolute porous-medium permeability for all fluids, as mentioned in Chapter 2, the mobility ratio is:

$$M = \mu_o/\mu_s \rightarrow \text{M=25}$$

- Read the areal sweep efficiency, $E_{As}$, vs. displaceable PVs injected, $V_{pD}$, from Figure 3.1 (Claridge 1972). For a single-layer reservoir, $E_{As}$ is equivalent to volumetric sweep efficiency. The dimensionless PVs injected could also be expressed in terms of hydrocarbon pore volumes injected as:

$$V_{\text{hcpv}} = V_{pds} \cdot \frac{(1 - S_{orm} - S_{cw})}{1 - S_{cw}} \quad \text{................................................................} \quad \text{Equation 3.2}$$

This expression is very helpful for the implementation of the problem on the "CO$_2$ Prophet" software which will be discussed in the next chapter.

- Repeat the procedure with various $V_{pds}$ values.

Results are shown in Table 3.2 and Figure 3.2. At the very unfavorable mobility ratio, breakthrough of solvent occurs relatively early, at 0.18 displaceable PV injected. The process becomes less efficient as the injection continues, as indicated by the change in slope of the recovery curve in Figure 3.2. The same general approach can be used with results from physical models other than the Claridge correlation.

| $V_{pDs}$ | Volume Injected, $V_{Si}$ (RB) | $E_{As}$ | $N_p$ (STB) | $N_p/N$ |
|---|---|---|---|---|
| 0.185 | 72,300 | 0.185 | 62,900 | 0.173 |
| 0.20 | 78,200 | 0.197 | 67,000 | 0.184 |
| 0.30 | 117,300 | 0.270 | 91,800 | 0.252 |
| 0.40 | 156,400 | 0.345 | 117,300 | 0.322 |
| 0.50 | 195,500 | 0.395 | 134,300 | 0.369 |
| 0.60 | 234,600 | 0.440 | 149,600 | 0.411 |
| 0.70 | 273,700 | 0.480 | 163,200 | 0.448 |
| 0.80 | 312,800 | 0.515 | 175,100 | 0.481 |
| 0.90 | 351,900 | 0.540 | 183,600 | 0.504 |
| 1.00 | 391,000 | 0.570 | 193,800 | 0.532 |
| 1.20 | 469,200 | 0.615 | 209,100 | 0.574 |
| 1.50 | 586,500 | 0.670 | 227,800 | 0.626 |
| 2.0 | 782,000 | 0.725 | 246,500 | 0.677 |
| 3.0 | 1,173,000 | 0.800 | 272,000 | 0.747 |
| 4.0 | 1,564,000 | 0.845 | 287,300 | 0.789 |
| 5.0 | 1,955,000 | 0.870 | 295,800 | 0.813 |

*Table 3.2: Results for oil recovery from secondary production*
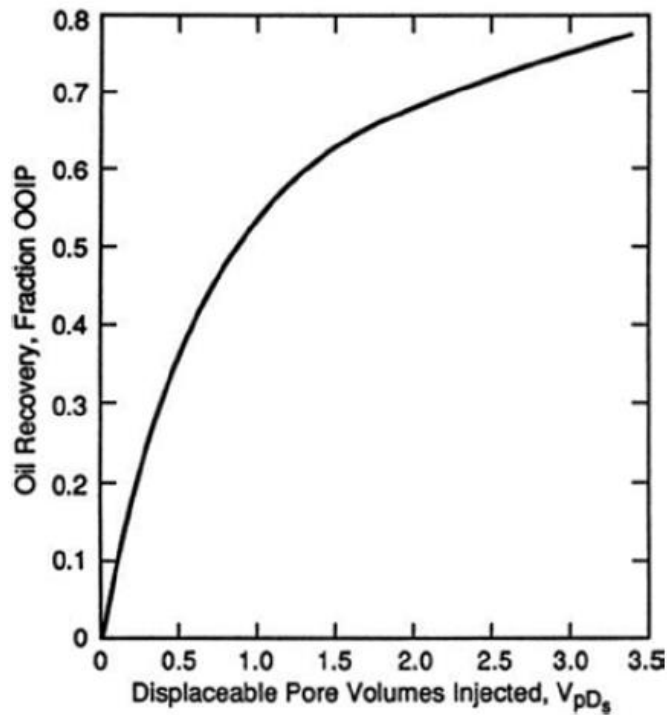


*Figure 3.2: Calculated oil recovery versus Displaceable Pore Volumes Injected V$_{pds}$*

Initially, the concept of recovering 17.3% by injecting only 18% of solvent in pore volumes, is very encouraging. However, it is important to have in mind that the reservoir has not even be waterflooded, but has only been depleted down to a pressure above the bubble point. This means that the high recovery values are to be expected due to the fact that the reservoir's energy is still quite high and supports production.

### 3.1.2 Tertiary Production – CO$_2$ Flood (Waterflooded Reservoir)

Before describing the second problem some introductory facts need to be stated. In a miscible displacement conducted as a tertiary recovery process, the oil resource target is assumed to exist in two different saturation conditions. In the part of the reservoir previously swept by water or other secondary recovery fluid, oil is at a residual saturation. In the remaining part of the reservoir, oil saturation is relatively high and may exist at a saturation of $(1.0 - S_{cw})$. The mobility ratio in a miscible displacement is typically more unfavorable than the value in a waterflood. Thus, sweep efficiency will be poorer in a tertiary miscible process than in the preceding secondary waterflood. The swept zone in the miscible process thus may reasonably be assumed to exist initially at ROS. Stalkup (1983a) proposed a procedure for making a rough performance calculation for a tertiary miscible displacement in which solvent injection is continuous. The process is shown schematically in Figure 3.3, where piston-like displacement is assumed. Fractional-flow behavior and mixing of miscible fluids would cause fluid interfaces to be "smeared;" thus, the piston-like displacement is an idealization.
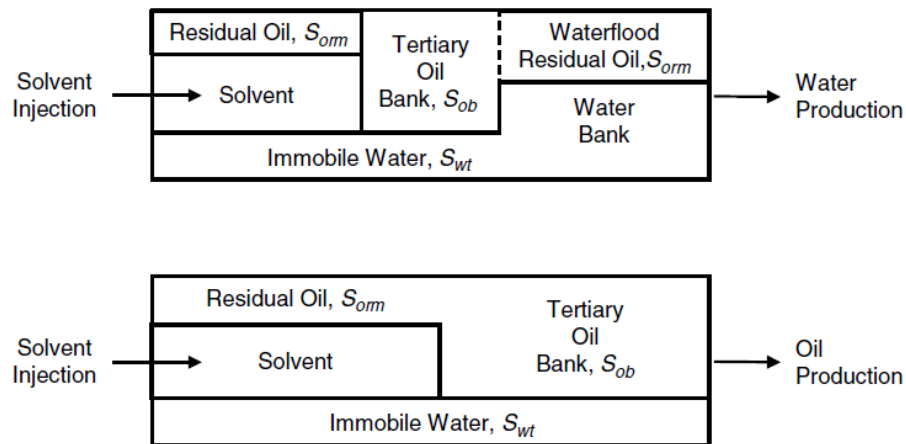


*Figure 3.3: Tertiary Production - CO$_2$ Injection process*

In this procedure the following assumptions and equations are applied.

i. Residual oil from the prior waterflood is banked up into a tertiary oil bank by injected miscible solvent. At the leading edge of the oil bank, waterflood residual oil is mobilized and water is displaced with a sharp front.
ii. The tertiary oil bank is displaced by solvent with a sharp front. There may be an ROS, $S_{orm}$, after the solvent displacement. The water saturation through the oil and solvent banks is assumed to be a constant value, $S_{wt}$. The saturation would, in fact, vary across these banks, and the average value could be estimated from frontal-advance theory.
iii. The mobility ratio governing sweepout is the ratio of mobility in the solvent-invaded region to that in the region of water flow ahead of the tertiary oil bank.
iv. Sweepout correlations used for the oil bank and solvent are the same.
v. A pseudodisplaceable PV injected is calculated that includes the oil bank:

$$V_{pdob} = V_{pds} + \Delta V_{pdob} \dotfill \text{Equation 3.3}$$

where $V_{pDob}$ = pseudodisplaceable PVs injected and accounts for solvent plus the oil bank, $V_{pDs}$ = displaceable PVs of solvent injected with $S_{wi}$ replaced by $S_{wt}$ and $\Delta V_{pDob}$ = incremental contribution to the pseudodisplaceable PVs from the oil bank. The quantity $\Delta V_{pDob}$ is determined by calculating the number of PVs occupied by the oil bank:

$$\Delta V_{pdob} = \frac{oil\ displaced\ by\ the\ solvent\ bank}{displaceable\ PV\ in\ the\ oil\ bank} = \frac{E_{vs} \cdot V_p \cdot (S_{orw} - S_{orm})}{V_p \cdot (1 - S_{wt} - S_{orw})} = Evs \cdot \frac{S_{orw} - S_{orm}}{S_{ob} - S_{orw}} \quad\text{Equation 3.4}$$

- o $E_{Vs}$ = volumetric sweep efficiency of the solvent,
- o $S_{orw}$ = waterflood ROS,
- o $S_{orm}$ = ROS in zone invaded by solvent,
- o $S_{ob}$ = oil saturation in the oil bank,
- o $S_{wt}$ = water saturation in the oil and solvent banks,
- o $V_p$ = reservoir PV.

The saturations are indicated in Figure 3.3. The saturation, $S_{orw}$, can be determined from the relative permeability curves. Oil-bank saturation, $S_{ob}$, can be estimated from frontal-advance theory and the Welge-tangent method (Stalkup 1983a) or as a simplification, $S_{ob}$ can be assumed equal to $(1 - S_{wr})$, a value that is somewhat too large.

vi. Oil recovery is given by :

$$N_p = [V_p \cdot E_{vs} \cdot (S_{orw} - S_{orm}) - V_p \cdot (E_{vob} - E_{vs}) \cdot (S_{ob} - S_{orw})] \cdot \frac{1}{B_o} \quad\text{Equation 3.5}$$

where $E_{Vob}$ = volumetric sweep efficiency of the oil bank.

That being said, the second problem statement is the following: Assume that a large slug of a solvent is to be used to displace oil miscibly in a tertiary recovery process. The unit has previously been waterflooded to $S_{orw}$. Table 3.3 lists all the necessary data. There are no gravity effects or vertical heterogeneities. The objective again is to calculate oil recovery as a function of PVs of solvent injected.

| | |
|---|---|
| Pattern area A (acres) | 20 |
| Thickness h (ft) | 20 |
| Porosity φ | 0.18 |
| Permeability k (md) | 120 |
| Initial oil saturation ($S_{oi}$) | 0.75 |
| Connate water saturation $S_{ow}$ | 0.25 |
| Residual oil saturation at the end of miscible displacement, $S_{orm}$ | 0.05 |
| Oil viscosity at $T_{res,}$ $\mu_o$ (cp) | 1.5 |
| $CO_2$ viscosity at $T_{res,}$ $\mu_s$ (cp) | 0.06 |
| Oil formation volume factor, $B_o$ | 1.15 |
| Reservoir temperature $T_{res}$ | 120 |
| Average reservoir pressure, $P_{res}$ | 2500 |
| Waterflood residual oil saturation, $S_{orw}$ | 0.30 |
| Oil-bank saturation, $S_{ob}$ | 0.75 |
| Water saturation in oil-bank, $S_{wt}$ | 0.25 |
| Water viscosity, $\mu_w$ | 0.70 |
| Water relative permeability at waterflood ROS, $k_{rw}$ | 0.20 |
| Solvent relative permeability at waterflood ROS, $k_{rs}$ | 0.80 |

*Table 3.3: Data required for tertiary production with CO$_2$ injection problem*

The following procedure is used until $V_{pDs}$ reaches the maximum desired value:

1. The displaceable volume $V_{pDs}$ is set.
2. Calculate $\Delta V_{pDob}$ and $V_{pDob}$ are calculated be Equations 3.3 and 3.2 respectively
3. Sweep Efficiencies $E_{As}$ and $E_{Aob}$ are found by the Claridge correlation. Areal sweep in the Claridge correlation is equal to volumetric sweep.
4. The recovered amount $N_p$ is calculated with Equation 3.4.
5. Return to Step 1 and repeat with a new $V_{pds}$ value.

The results are presented in terms of fractional recovery, $N_p/N$ in Table 3.4 and Figure 3.4, where $N$ in this case is the oil in place at the start of the tertiary recovery project. The fractional recovery also could be expressed relative to OOIP. The recovery at 2.0 displaceable PV of solvent injected is calculated to be 14.6% OOIP. In a tertiary project, oil-bank breakthrough occurs after a certain amount of solvent is injected ($\approx$33,200 RB in the example). Also, if solvent injection is continuous, as in this example, the solvent/oil produced ratio is large, which adversely affects the economics of the project. Stalkup (1983a) discusses the fact that the procedure is a rough approximation. The overall average mobility and controlling mobility ratio change as the displacement proceeds. The waterflooded area is relatively large in the early part of the process, and consequently, the water mobility has a large effect. The size of the oil bank and the relative importance of the oil-bank mobility increase with continued injection.

| $V_{pDs}$ | $\Delta V_{pDob}$ | $V_{pDob}$ | $E_{As}$ | $E_{Aob}$ | Volume Solvent Injected, $V_{si}$ (RB) | $N_p$ | $N_p/N$ |
|---|---|---|---|---|---|---|---|
| 0.07 | 0.039 | 0.109 | 0.07 | 0.109 | 27,400 | 0 | 0 |
| 0.087 | 0.048 | 0.135 | 0.087 | 0.135 | 34,000 | 0 | 0* |
| 0.10 | 0.056 | 0.156 | 0.100 | 0.156 | 39,100 | 120 | — |
| 0.20 | 0.111 | 0.311 | 0.190 | 0.270 | 78,200 | 5,600 | 0.038 |
| 0.30 | 0.167 | 0.467 | 0.260 | 0.340 | 117,300 | 14,100 | 0.097 |
| 0.40 | 0.222 | 0.622 | 0.315 | 0.405 | 156,400 | 18,600 | 0.128 |
| 0.50 | 0.278 | 0.778 | 0.360 | 0.450 | 195,900 | 24,000 | 0.165 |
| 0.60 | 0.333 | 0.933 | 0.397 | 0.495 | 234,600 | 26,800 | 0.184 |
| 0.70 | 0.389 | 1.089 | 0.425 | 0.520 | 273,700 | 30,800 | 0.211 |
| 0.80 | 0.444 | 1.244 | 0.460 | 0.560 | 312,800 | 34,000 | 0.233 |
| 0.90 | 0.500 | 1.400 | 0.485 | 0.590 | 351,900 | 35,900 | 0.246 |
| 1.00 | 0.556 | 1.556 | 0.510 | 0.605 | 391,000 | 41,200 | 0.283 |
| 1.20 | 0.667 | 1.867 | 0.550 | 0.650 | 469,200 | 44,900 | 0.308 |
| 1.50 | 0.833 | 2.333 | 0.600 | 0.690 | 586,500 | 53,200 | 0.365 |
| 2.0 | 1.111 | 3.111 | 0.665 | 0.750 | 782,000 | 62,200 | 0.427 |
| 3.0 | 1.667 | 4.667 | 0.740 | 0.810 | 1,173,000 | 74,600 | 0.512 |
| 4.0 | 2.222 | 6.222 | 0.785 | 0.825 | 1,564,000 | 86,600 | 0.594 |

*Oil bank breakthrough.

*Table 3.4: Tertiary production with CO2 Injection - Results*
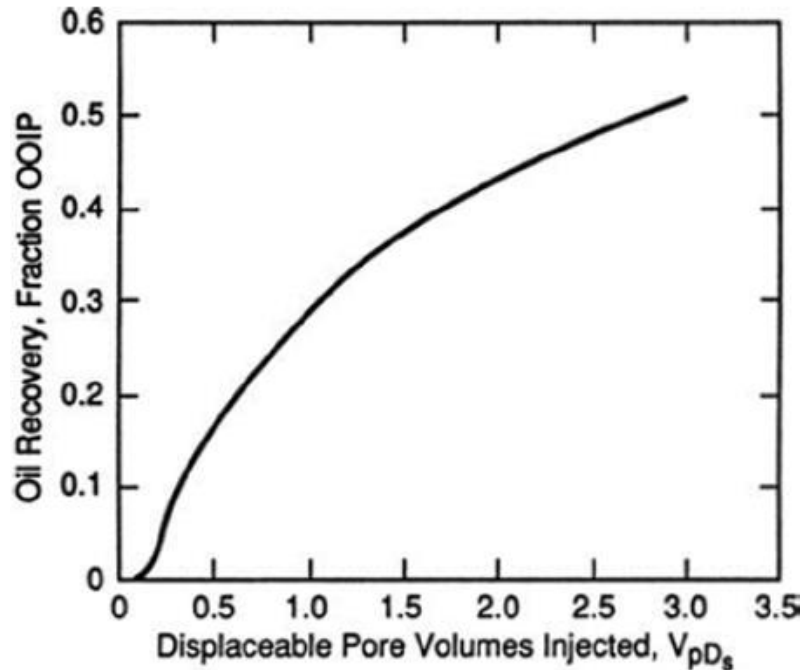
*Figure 3. 4: Tertiary production with CO2 Injection - Oil Recovery vs $V_{pDs}$*

## 3.2 "CO₂ Prophet" – Water and CO₂ Flood Prediction Software

### 3.2.1 General Overview

CO₂ Prophet was developed as a better alternative to the U.S. Department of Energy's CO₂ miscible flood predictive model, CO2PM, by Texaco Exploration and Production Technology Department (EPTD). It is a screening tool which falls between crude empirical correlations and sophisticated numerical simulators and was designed to identify how key variables influence CO₂ project performance and economics prior to performing detailed numerical simulation.

The software was originally developed in 1994 and is therefore run only in DOS systems. Due to the fact that such computer systems can no longer be found in the market, the need for a DOS-emulator software is due. For this thesis the DOS-Box Emulator is used. Once the drive is mounted on the emulator, the project is set on the software interface. When all data are imported, an execution command (Do It) produces a text file which contains the project created in the correct code-form.

CO₂ Prophet performs two principal operations. It first generates streamlines for fluid flow between injection and production wells and then does displacement and recovery calculations along the streamtubes. The streamlines form the flow boundaries for the streamtubes. A finite difference routine is used for the displacement calculations over time. A special advantage of the streamtubes method is the avoidance of grid orientation effects. The effect of areal sweep efficiency is handled by incorporating streamlines and streamtubes, which implies that it is a 2-D approach. Doing calculations along the streamtubes also eliminates the need for using an empirical correlation for areal sweep efficiency. A mixing parameter approach, the same to that proposed by Todd and Longstaff, is used for simulation of the miscible CO₂ process. Mixing parameter models simulate the mixing and viscous fingering which

occur in miscible displacements by adjusting solvent and oil viscosities ultimately altering the fractional flow of solvent and oil. More on that matter will be said in the following paragraphs.

The software can handle an unlimited number of well (injectors and producers) patterns. However, streamtubes for common flooding patterns have already been embedded and do not have to be generated. The flow calculations are performed along the previously generated streamtubes. Pregenerated streamtubes exist for the following patterns:

- 5 Spot
- Special West Texas 7 Spot
- Inverted 9 Spot
- Line Drive
- 4 Spot (Inverted 7 Spot)
- Isolated 2 Spot

The streamlines for all patterns were created by assuming same rate for all production wells. If these existing patterns are not sufficient, the user can also generate a custom pattern (or reservoir) which includes up to 10 injection wells and 10 production wells. If it is necessary to run a case in which the producers have different rates, streamlines should be regenerated by running the custom pattern case.

Regarding the types of recovery, CO2 Prophet is versatile and many types of recovery process can be simulated. The model can simulate the following:

- Waterflood
- Straight miscible CO$_2$ flood
- Miscible CO$_2$ WAG
- Immiscible CO$_2$ flood

Up to four periods of recovery can be simulated sequentially. For instance, a waterflood, followed by straight CO$_2$, followed by CO$_2$ WAG, followed by water injection can be simulated. The saturation distributions at the end of each period are retained as the starting saturation distributions for the next period. For example, the saturation distribution at the beginning a typical CO$_2$ flood is not uniform but rather is what resulted at the end of the prior waterflood.

Other important parameters are the following:

- The reservoir model can include up to 10 layers (the default is 5 layers).
- There is no crossflow between the layers.
- The effect of gravity is not incorporated.
- The injection and production rates are balanced. There are 3 components in this model: solvent (gas), water, and oil. The terms gas and solvent are used interchangeably.

## 3.2.2 Input Parameters

The interface is shown in the figure below and is pretty easy to handle. It consists of several pull down menus and panels for the entry of data. All input parameters are going to be discussed in the following section in order to gain a full-scale view of the software capabilities.

*Figure 3.5: CO$_2$ Prophet Software - Interface*

Each pull down tab will be examined sequentially. The first tab named "Prophet" is merely a general information tab about the software. The second tab, "File", serves as a kind of server from which the user can save projects or load already existing projects. To retrieve previously saved input files, READ is selected under the FILE menu. To save a modified file under the same or a new name, SAVE is selected. Files saved and stored with a SAV extension, as shown on the picture below. It is of paramount importance that all the projects are saved on the same file-location-path where the software is.
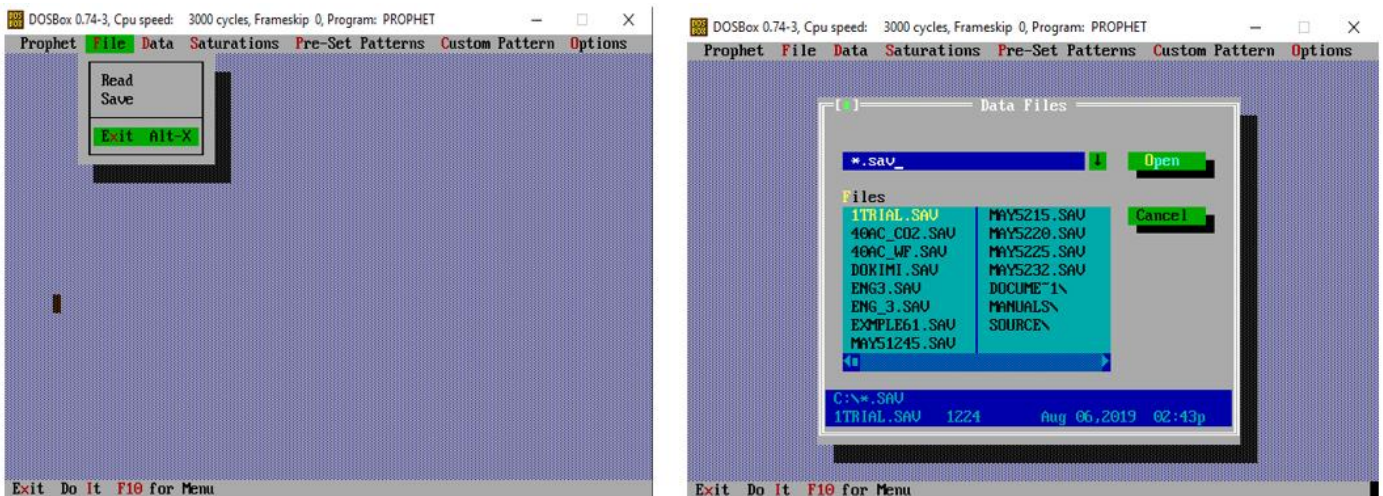


*Figure 3.6: CO$_2$ Prophet Software - File Tab - Read and Save Commands*

## DATA TAB

Next on the line, the "Data" panel can be found. The data panel consists of three (3) different tabs in which the user imports data. Those tabs are:

- Reservoir Data
- Data Specifying the Original Oil In Place (OOIP)
- Data for the Calculation of the Original Oil in Place (OOIP)

RESERVOIR DATA

Regarding the Reservoir tab, the data required by the software is shown in the figure below (with the existing default values of the software).
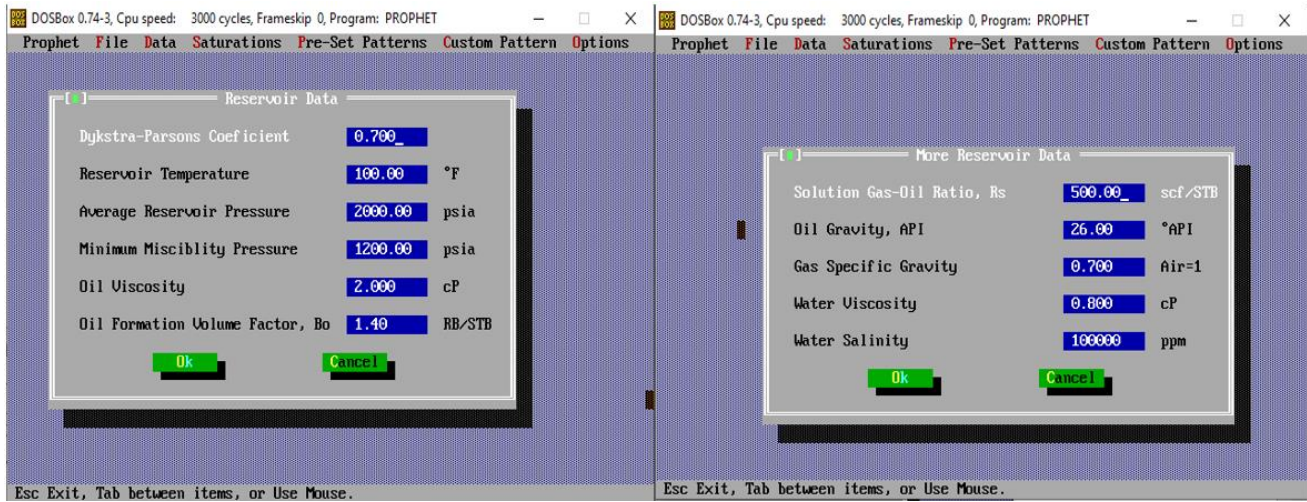


*Figure 3.7:CO₂ Prophet Software - Data Tab - Reservoir*

Each one of these parameters are commented below. The parameters which are especially important and should be as accurate as possible are the Dykstra-Parsons coefficient, the oil viscosity, the water viscosity, the reservoir temperature, the average reservoir pressure and the minimum miscibility pressure (MMP).

The Dykstra-Parsons Coefficient is the most important of the input parameters and can have an extremely large impact on recovery. It essentially describes the difficulty the fluids find in moving throughout the reservoir. The Dykstra-Parsons coefficient is used to calculate the permeability variation between the layers in the model. The calculation of layer permeabilities is done internally in the program. For the Dykstra-Parsons coefficient to have a large influence on recovery, 3 or more layers should be selected. When the Dykstra-Parsons coefficient is large, increasing the number of layers between 1 to about 5 has a significant impact on recovery. Increasing the number of layers past 5 generally has only a small effect. The number of layers is selected in the advanced options menu. The default is 5. The Dykstra-Parsons coefficient is a common measure of reservoir heterogeneity. There is a large variation in reservoir permeability with a large Dykstra-Parsons coefficient. The recovery is greatest in the highest permeability layer. The default value is 0.7 indicating an average of heterogeneity reservoir.

The Reservoir Temperature is only used to calculate $CO_2$ viscosity. After testing the credibility of this internal calculation by cross-referencing with existing tables for $CO_2$ viscosity values as a function of temperature and pressure, the numbers given by the software can be trusted. The default is 100°F.

The Average Reservoir Pressure value is used to determine the $CO_2$ viscosity and combined with the Minimum Miscibility Pressure (MMP) determine whether the flood will be completely miscible, partially miscible, or totally immiscible. For a totally miscible flood the MMP must be set below the ¾ of the average reservoir pressure, whereas for an immiscible one the MMP must be higher than the average reservoir pressure. Any intermediate condition results in a partially miscible flood. The default for the Average Reservoir Pressure is 2000 psia while for the MMP the respected value is 1200 psia.

The Oil Viscosity value, in centipoise (cP), is used in the fluid mobility calculations. The default is 2.0 cp. The same applies for the Water Viscosity parameter, with a default value at 0.80 cp.

The Oil Formation Volume Factor (Bo) is used to compute oil recovery in surface units. The default is 1.4 RB/STB. Solution Gas-Oil Ratio (Rs) is used to calculate gas produced on the surface. The default is 500 Scf/STB.

For the Oil Gravity, API and Gas Specific Gravity (Sg) values, the default is 26.0 $^{\circ}$ for the API and 0.70 for the Sg. Finally, for the Water Salinity, imported in ppm the default is 10,000 ppm.

ORIGINAL OIL IN PLACE

Regarding the OOIP, the user can either specify the exact quantity of reserves existing in the reservoir via the "Specify OOIP" option or give the necessary data (Area, Thickness and Porosity) for the calculation of it through the option (Calculate OOIP). It is recommended to use the latter, due to the fact that if given only the number of OOIP the program internally will choose values for Area, Thickness and Porosity internally, which might be well beyond realistic. If the value of the original oil in place is not accurate, the volumetric production will not be accurate. However, the production in terms of hydrocarbon pore volumes will still be accurate.

**SATURATIONS TAB**

Relative Permeability Relationships

This section describes the relative permeability equations which are used in the software as well as the default model parameter values. The relative permeability curves are approximated by analytical equations. In this model there are three flowing phases: water, oil, and gas. The only gas phase that is permitted in the model is the solvent phase, as a hydrocarbon gas does not exist in the model because there is no point in talking about miscible gas flood in an already saturated reservoir. The relative permeability equations used for simulating both miscible and immiscible flow are built from two-phase flow equations.

"CO$_2$ Prophet" uses a 3-Phase relative permeability model similar to the Stones model. In a nutshell the 3-Phase system (water, oil and gas) is split into two 2-Phase systems of water-oil and oil-gas respectively. For these two systems the relative permeability curves of each phase are generated. Therefore, in the end there are two oil relative permeability curves which are combined through a relationship in order to produce the final oil relative permeability. This is done by the program internally and the user basically has to construct the relative permeability curves for the two 2-Phase systems solely.

Default values (from the 1984 NPC study) are provided for all variables used in the base two phase flow equations. However, it is strongly recommended that better representative values be used wherever available. The important parameters are the endpoint relative permeabilities and the residual saturations. The exponents for the curves are not that important. The input parameters are entered in the equations which appear in the input screens available under the "SATURATIONS" heading. They can be entered for all the equations by selection of Do It All, or values for just a single equation can be entered by selecting the desired equation. The equation parameters are sometimes found in more than one equation, and they are entered in the first equation where they appear. The variables which can be entered for each equation are shown in bold and underline face. The parameters which can be entered for each equation are also listed in each equation panel.
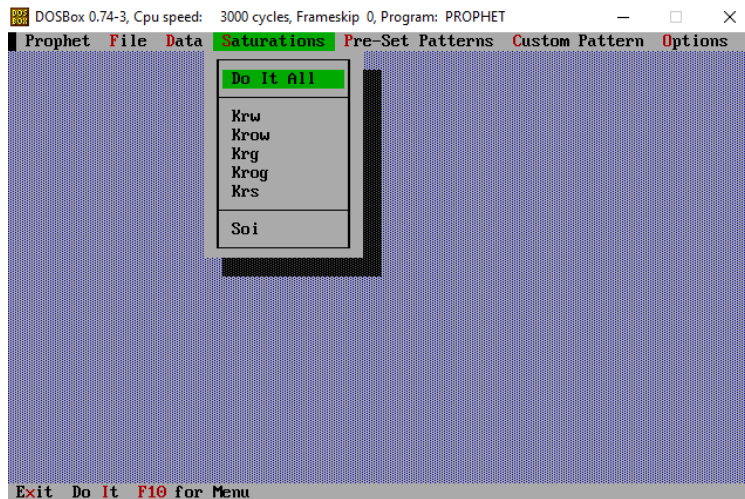
*Figure 3.8: CO$_2$ Prophet Software - Saturations Tab*

Below each one of the existing relative permeability equations used in the model will be described.

1) The equation for the two-base water relative permeability, K$_{rw}$, is

$$K_{r,w} = K_{wro} \cdot \left(\frac{S_w - S_{wir}}{1 - S_{wir} - S_{orw}}\right)^{Expw} \qquad \text{Equation 3.6}$$

where:

- $K_{r,w}$: Relative Permeability of Water
- $S_w$: Water saturation
- Expw: Water equation exponent. The default is 2.0
- $S_{wir}$: Irreducible water saturation. The default is 0.2 which is also the same as Swc.
- $S_{orw}$: Residual oil to waterflood. The default is 0.37.
- $K_{wro}$: Endpoint (maximum) relative permeability of water at the residual oil saturation. The default is 0.30.

The entry panel for Krw is:
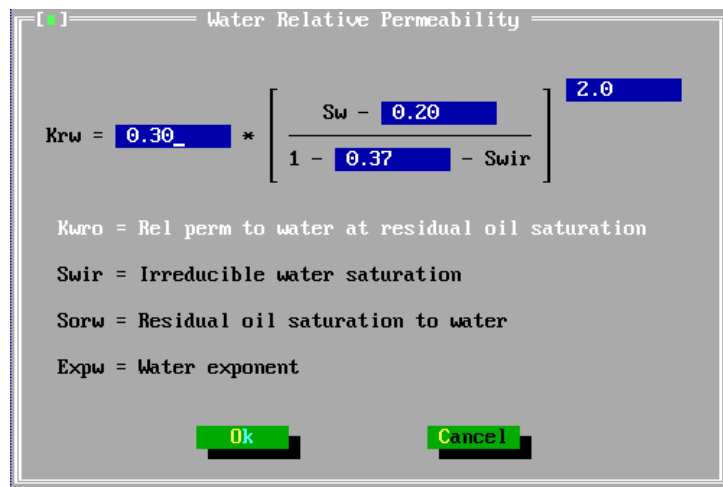


*Figure 3.9:CO$_2$ Prophet Software - Water Relative Permeability K$_{rw}$*

47

2) The equation for the two-phase oil relative permeability in the presence of water, $K_{row}$, is

$$K_{r,ow} = K_{r,ocw} \cdot \left(\frac{1-S_w-S_{wor}}{1-S_{wc}-S_{orw}}\right)^{Expow}$$   ......................................................Equation 3.7

where:

- $K_{r,ow}$: Relative Permeability of Oil
- $S_w$: Water saturation
- Expow: Oil equation exponent. The default is 2.0.
- $S_{wc}$: Connate water saturation. The default is 0.2.
- $S_{orw}$: Residual oil to waterflood. The default is 0.37.
- $K_{r,ocw}$: Endpoint (maximum) relative permeability of oil at the irreducible water saturation. The default is 0.40.

The entry panel for $K_{row}$ is:
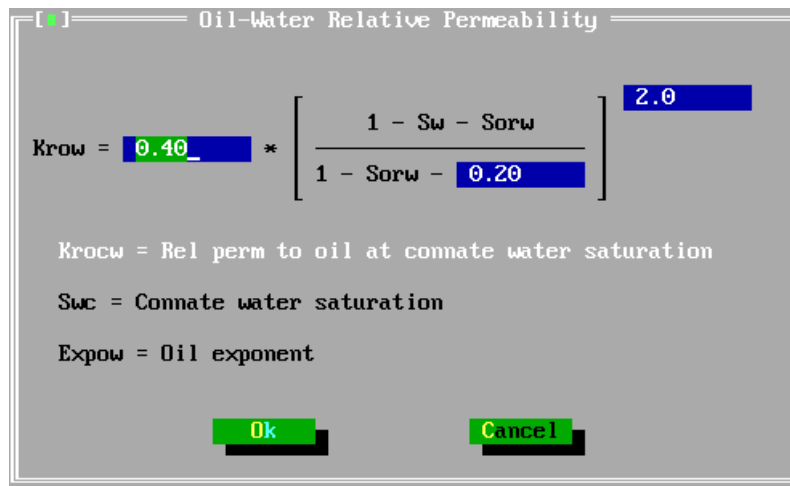


*Figure 3.10: CO₂ Prophet Software - Oil Relative Permeability K_row (Oil-Water System)*

3) The equation for the two-phase gas relative permeability in the presence of oil, $K_{rg}$, is

$$K_{r,g} = K_{r,gcw} \cdot \left(\frac{S_g-S_{gr}}{1-S_{wc}-S_{gr}}\right)^{Expg}$$   .............................................Equation 3.8

where:

- $K_{r,g}$: Relative permeability of gas
- $S_g$: Gas saturation
- Expg: Gas equation exponent. The default is 2.0.
- $S_{wc}$:  Connate water saturation. The default is 0.2
- $S_{gr}$: Residual gas saturation to an oilflood. The default is 0.37 which is the value for Sorw.
- $K_{r,gcw}$: Endpoint (maximum) relative permeability of gas at the connate water saturation. The default is 0.40.

The entry panel for the Krg is:
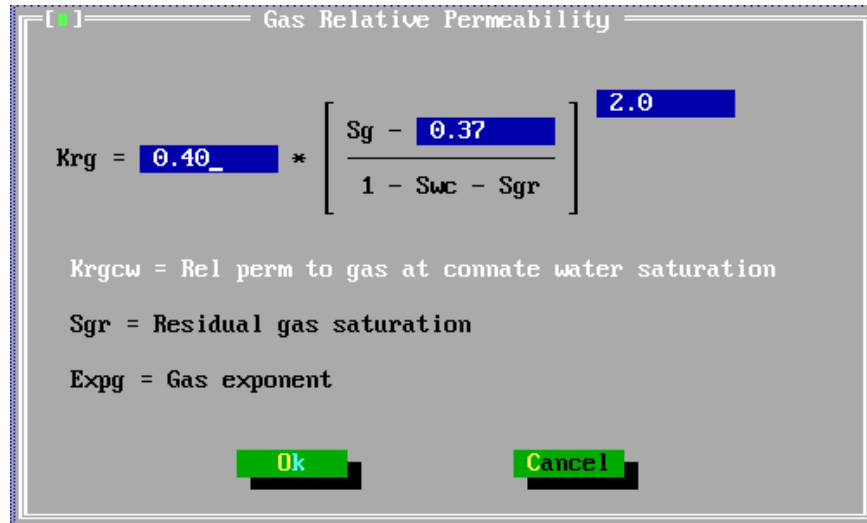
*Figure 3.11:CO₂ Prophet Software - Gas Relative Permeability $K_{rg}$*

4) The equation for the two-phase oil relative permeability in the presence of gas, $K_{r,og}$, is

$$K_{r,og} = K_{r,ocw} \cdot (\frac{1-S_{wc}-S_{org}-S_g}{1-S_{wc}-S_{ogr}})Expog \quad\quad\quad\quad\quad\quad\text{Equation 3.9}$$

where:

- $K_{r,og}$: Relative permeability of oil
- Expog: Oil equation exponent.  The default is 2.0
- S_org: Residual oil to a gas flood.  The default is 0.37 which is also the value for Sorw
- $K_{r,ocw}$: Endpoint (maximum) relative permeability of oil at irreducible water saturation. The default is 0.4.

The panel for the $K_{r,og}$ equation is:
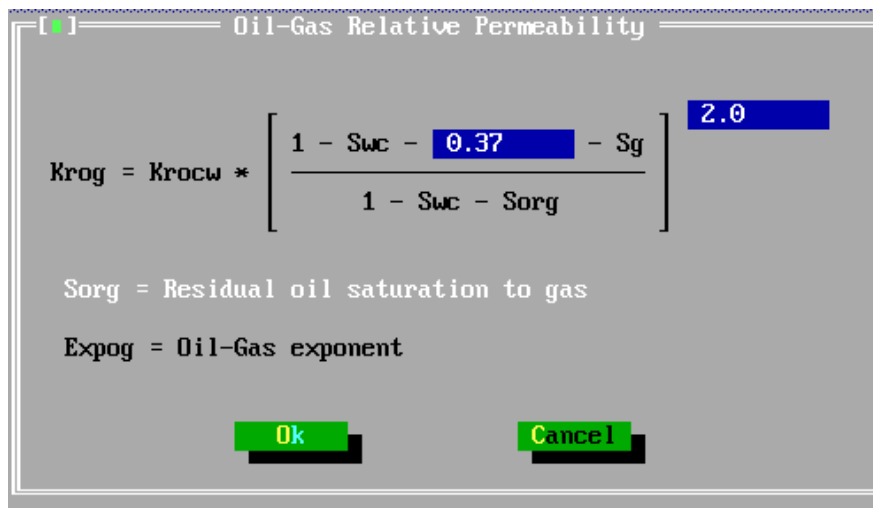


*Figure 3.12: CO₂ Prophet Software -Oil Relative Permeability $K_{rog}$ (Gas-Oil System)*

5) There is also an equation for the solvent relative permeability, $K_{r,s}$, if it is desired to use an equation different from that of the gas relative permeability. This could have an effect for immiscible floods only. Since for this thesis, only miscible floods will be tested it makes no sense to use different curves for gas and solvent. The solvent relative permeability $K_{r,s}$ is defined as:

$$K_{r,s} = K_{r,smax} \cdot \left(\frac{S_g - S_{sr}}{1 - S_{wir} - S_{sr} - S_{orm}}\right)^{Exps}$$ ................................................................ Equation 3.10

where

- $K_{r,s}$: Relative permeability of solvent
- Exps: Solvent equation exponent.  The default value is Expg which is 2.0.
- $S_{sr}$: Residual gas (i.e., solvent) saturation.  The default value is Sgr which is 0.37.
- Sorm: Residual oil saturation to solvent. The default value is 0.001.
- $K_{r,smax}$: Endpoint (maximum) relative permeability of solvent at the irreducible water saturation. The default value is the same as $K_{r,ogcw}$, which is 0.4.

The default values, which are derived from the gas relative permeability, are automatically used. The only value which can be changed in this panel is the residual oil saturation to a miscible flood, Sorm.  However, changes in the other defaults can be entered under the advanced options menu.

The entry panel for Krs is the following:
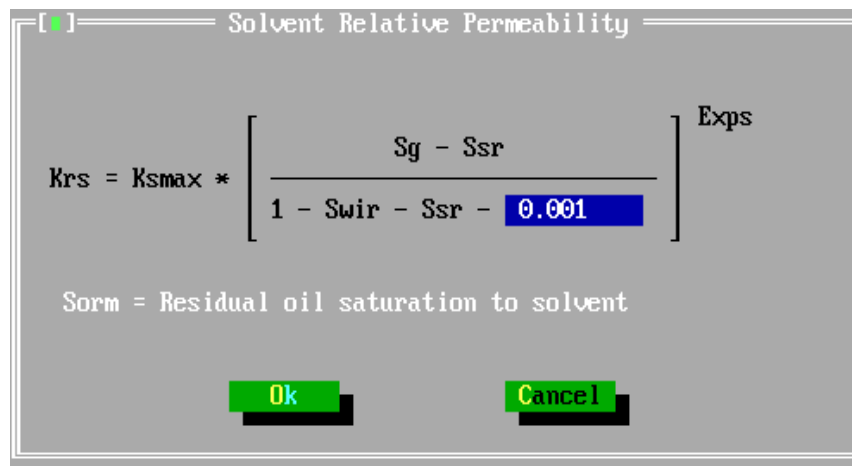


*Figure 3.13: CO$_2$ Prophet Software - Solvent Relative Permeability K$_{rs}$*

<u>Three-Phase Miscible and Immiscible Equations</u>

One of the main ways that miscible and immiscible flow are differentiated is by the use of different relative permeability equations. The two cases of miscible and immiscible flow are examined below.

    I.    Immiscible Flow.

The water relative permeability is a function of water saturation only. The gas (or solvent) relative permeability in immiscible flow is a function of the gas (i.e., solvent) saturation only. The oil relative permeability, $K_{r,o}$, is given by the modified Stone method:

$$K_{r,o} = \frac{1}{K_{r,ow}} \cdot (A - K_{r,g} - K_{r,w})$$
<div align="right">Equation 3.11</div>

where:

$$A = \left(\frac{K_{r,ow}}{K_{r,ocw}} + K_{r,w}\right) \cdot \left(\frac{K_{r,og}}{K_{r,ocw}} + K_{r,g}\right)$$
<div align="right">Equation 3.12</div>

This definition means in fact that out of the three phases present, gas and water depend only in their own saturation while the oil relative permeability is a function of the other two and therefore depends on them. The A factor acts as a weighted average, based on maximum phase permeabilities, for the contribution of the two other phases in the oil relative permeability.

    II.    Miscible Flow.

In miscible flow there are actually only two phases, water and a miscible phase composed of solvent and oil. The water relative permeability is the same as in immiscible flow and remains a function of only the water saturation. However, the miscible phase relative permeability, which is denoted $K_{r,m}$, must be computed since it is not measured. There is no definitive way to compute or handle the miscible phase relative permeability, and three options are given to user. The option for calculation of $K_{r,m}$ is selected under the advanced options menu. The miscible phase relative permeability, $K_{rm}$, can be selected as

- a saturation weighted average of $K_{r,ow}$ and $K_{r,s}$:

$$K_{r,m} = \left(\frac{S_o - S_{orm}}{1 - S_w - S_{orm}}\right) \cdot K_{r,ow} + \left(\frac{S_g}{1 - S_w - S_{orm}}\right) \cdot K_{r,s}$$
<div align="right">Equation 3.13</div>

- an average of $K_{r,ow}$ and $K_{r,g}$:

$$K_{r,m} = 0,5 \cdot (K_{r,ow} + K_{r,g})$$
<div align="right">Equation 3.14</div>

- or equal to $K_{r,ow}$:

$$K_{r,m} = K_{r,ow}$$
<div align="right">Equation 3.15</div>

The third option which sets $K_{r,m}$ equal to $K_{r,ow}$, the oil phase relative permeability, is the default. This is the standard formulation in mixing parameter models. However, the first option which makes $K_{r,m}$ a saturation weighted average is physically more realistic. In addition, the saturation weighted formulation produces results closest to those of a compositional simulator when $K_{r,g}$ parameters are used for $K_{r,s}$.

The solvent and oil can be treated separately even though they are miscible. This can be done by assigning to the solvent and oil the correct fractions of the miscible phase relative permeability. The correct fractions are based on saturation. Under miscible conditions, the gas and oil relative permeability are

$$K_{r,gm} = \left(\frac{S_g}{1-S_w-S_{orm}}\right) \cdot K_{r,m} \quad\text{................................................................................Equation 3.16}$$

$$K_{r,gm} = \left(\frac{S_o-S_{orm}}{1-S_w-S_{orm}}\right) \cdot K_{r,m} \quad\text{................................................................................Equation 3.17}$$

For example, if the solvent saturation is 25% of the flowing miscible phase saturation, then 25% of the miscible phase relative permeability is assigned to the solvent and 75% is assigned to the oil.

III.     Combined Miscible and Immiscible Flow.

The equations actually used in the model can handle miscible, immiscible, and partially miscible flow. The equation for the effective relative permeability of oil, $K_{r,o,eff}$, is

$$K_{r,o,eff} = (1-a) \cdot K_{r,o} + a \cdot \left(\frac{S_o-S_{orm}}{1-S_w-S_{orm}}\right) \quad\text{............................................Equation 3.18}$$

The equation for the effective permeability of the solvent (i.e., gas), $K_{r,g,eff}$, is

$$K_{r,g,eff} = (1-a) \cdot K_{r,g} + a \cdot \left(\frac{S_g}{1-S_w-S_{orm}}\right) \cdot K_{r,m} \quad\text{................................Equation 3.19}$$

If a condition of partial miscibility exists and the reservoir pressure, P, is less than the MMP but greater than 0.75 times the MMP, then

$$a = \frac{P-0,75\cdot MMP}{0,25\cdot MMP} \quad\text{...............................................................................Equation 3.20}$$

If complete miscibility exists and the reservoir pressure is greater than the MMP, then $\alpha$ = 1.0 and if complete immiscibility exists and the reservoir pressure is less than 0.75 times the MMP, then $\alpha$ = 0.0. This is actually an interpolation scheme as the reality in these intermediate situations is quite difficult to model.

Furthermore, the oil saturation, Soi, at the start of the first injection period is required. The entire pattern or reservoir is initialized uniformly to this saturation. The water saturation does not have to be at the connate level. This in particular is going to pose quite the challenge for the "assumptions" made in the next part of the thesis.

## PRESET PATTERNS TAB

At this menu, the user is called to select one of the existing patterns that were discussed previously. A key assumption that is made by the software is that the streamlines for all patterns were created by assuming the same rate for all production wells. For this thesis only the 5-Spot Pattern will be examined and partially some Line-Drive tests will be conducted. After selecting the pattern, the user is required to provide the software with the type of injecting fluids and injection rates. The rates and injection characteristics must be specified for each injection period. Up to 4 periods can be used. Specifically, for each injection period the following injection rate information is needed:

- Rate of water in bbls/day (this would be 0.0 if only CO$_2$ were being injected).
- Rate of CO$_2$ in MMScf/day (this would be 0.0 if only water were being injected).



*Figure 3.14: CO2 Prophet Software - Pre-Set Patterns Tab- Patterns*

The absolute permeability of the reservoir is of vital importance in finite element models, in streamline models it is not that significant due to the fact that it is related to pressure which is not considered in streamline models. The definitive variables are the amounts injected not the changing pressures. Therefore, reservoir permeability is not a direct input but must be considered during the entry of injection rates. The model will accept any rate no matter how large; consequently, the rates entered in the model should reflect reservoir permeability and any relative permeability effects anticipated during the injection of CO$_2$ or during WAG. Also required is the Water/CO$_2$ injection ratio for periods in which both water and CO$_2$ are being injected. This number is related to the WAG ratio. It is the amount of water relative to gas when the gas is 1.0. The meaning of the Water/CO$_2$ injection ratio number depends on whether a time or volume basis is selected. If a time basis is selected and this number is 2, then 67% of the time water is injected and 33% of the time CO$_2$ is injected at the specified rates. If a volume basis is selected and this number is 2, then 67% (on a reservoir volume basis) of the total fluid injected is water and 33% is CO$_2$. The last information which needs to be specified is the hydrocarbon pore volume (or volumes) injected. During a period when a single fluid is being injected, this is simply the hydrocarbon pore volumes of that fluid. During a WAG injection, this number is the hydrocarbon pore volumes of CO$_2$ injected. The injected water is not included in this number during a WAG period.
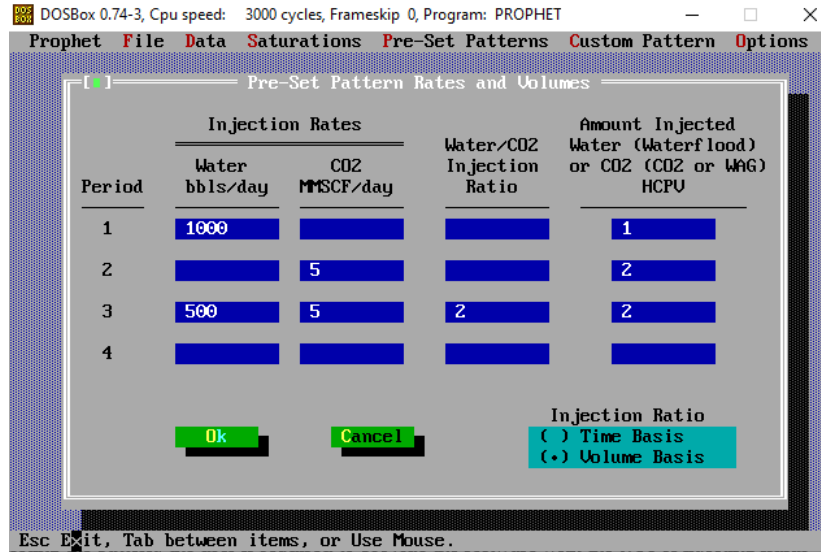
*Figure 3.15: CO2 Prophet Software - Pre-Set Patterns Tab - Rates and Volumes*

## CUSTOM PATTERN MENU

If these existing patterns are not applicable, the user can also generate a custom pattern (or reservoir) which includes up to 10 injection wells and 10 production wells. If it is necessary to run a case in which the producers have different rates, streamlines should be regenerated by running the custom pattern case. To do a custom pattern, the pattern boundaries, well locations, injection rates, and production rates all need to be defined. When doing a custom pattern, the option "plot streamlines" should be enabled the first time so that the correctness of the streamlines can be verified. Both the boundaries and well locations are specified with X,Y coordinates on a grid. After all data are filled the custom pattern can be simulated. For this thesis no such concept will be used.

## OPTIONS TAB

Finally, the "Options" menu is discussed. Several items of data are included under the Options menu. They are:

- Project Title
- Report Frequency: Monthly, quarterly, semi-annually or annually are the possible options.
- Plot Streamlines: When the custom pattern is chosen, another option is available. If plot streamlines is chosen, then the streamlines are plotted to the screen. A screen capture utility can be used to capture the streamlines.
- Advanced Options:
    - Number of Layers
    - Miscible Relative Permeability $K_{r,m}$
    - Mixing Parameter, Omega
    - Solvent Relative Permeability $K_{r,s}$

As said previously, at least 3 layers should be used for the Dykstra-Parsons coefficient to be effective and increasing the number of layers has a significant effect on recovery when the number of layers is between 1 and 5. However, increasing the number of layers past 5 generally has only a small effect on production.

Regarding the mixing parameter, Omega, it determines the effective viscosity of the solvent and oil. If the mixing parameter is set to 0.0, then there is no mixing and the solvent and oil viscosities are equal to their individual immiscible values. If the mixing parameter is set to 1.0, then there is complete mixing, and the oil and solvent viscosities are made equal. The default value for Omega is 0.666 and can be changed in the advanced options menu.

CO2 Prophet is started by typing PROPHET at the DOS prompt. Once all the data are imported, CO2 Prophet can be executed by selecting Do It from the bottom menu. Alternatively, CO2 Prophet can be executed by editing the file Indata so that it has the desired input variables and then typing CO2 at the DOS prompt.

### 3.2.3   Output Parameters

CO2 Prophet creates several output files. These are ASCII files which can be accessed with a txt reading app such as Notepad and can be imported into spreadsheets and graphics programs. The files include:

- OUTPUT: a file of production data supplied in terms of hydrocarbon pore volumes (HCPV). Four columns (all in terms of HCPV) are provided; they are: Injected total, Oil produced, CO$_2$ produced, Water produced.
- LABELOUT:   a complete output file. This file includes a summary of the input data, cumulative injection and production data, and incremental injection and production data. The data is organized by time rather than by hydrocarbon pore volumes.
- DIGITOUT: an ASCII file specifically for import into any spreadsheet. This file includes the same production information as LABELOUT except that it is in a series of columns with headings.
- INDATA: an ASCII input file actually used in running the program. This file is generated by the input portion of CO2 Prophet.

Whenever CO2 Prophet is executed, files with these same names are generated. If any of these output files are to be saved, they need to be renamed or moved to another disk location. Otherwise, they will be overwritten. Two other files are created when CO2 Prophet is executed. These are INFO.RUN which provides additional information about a run such as the run times and ERROR.IN which provides error information in case a run failed. Of the previously mentioned output files, the most significant one is undoubtedly the DIGITOUT file containing all the desired results. In the following paragraph an overview of this file will be given describing each parameter contained in it thoroughly in order to understand exactly what are the results and how are they produced.

In order to describe and go through the produced results one by one, a quick example simulating a regular waterflood is going to be presented. All input values are the default ones both for reservoir data and for the relative permeabilities. The Soi value is chosen to be 0.80 and the connate water saturation equal to 0.20, indicating a "virgin" reservoir filled with oil and water at the connate level. The area is 10 acres and the thickness 10 feet. The porosity value is chosen to be 0.20. A regular waterflood is to be simulated with an injection rate of 1000 bbl/day of water up until 2 times the hydrocarbon pore volume of the reservoir has been injected. The program is executed and the DIGITOUT file produced is shown below. The second picture is actually a continuation of the first but is presented separately for spacial reasons.
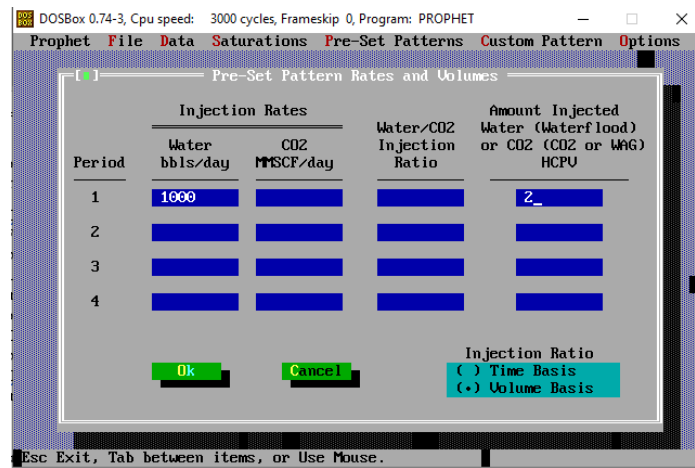
*Figure 3.16: Prophet CO₂ Software Example - Injection Rate Input Data*

| TIME<br>YRS | RECOVERY<br>%OOIP | CUM<br>OIL | PRODUCED<br>WATER | FLUIDS<br>SOLVENT | HCPV<br>TOTAL | CUM INJECTED<br>WATER_M | SOLVENT_MM | OIL<br>MSTB | WATER<br>MSTB | HC_GAS<br>MMSCF | SOLVENT<br>MMSCF | CUM_GOR<br>MSCF/STB | CUM_WOR<br>STB/STB |
|---|---|---|---|---|---|---|---|---|---|---|---|---|---|
| 0.000 | 0.00 | 0.0000 | 0.0000 | 0.0000 | 0.0000 | 0.0 | 0.0 | 0.0 | 0.0 | 0.0 | 0.0 | .000E+00 | .000E+00 |
| 0.083 | 20.15 | 0.2015 | 0.0453 | 0.0000 | 0.2468 | 30.4 | 0.0 | 17.9 | 5.6 | 8.9 | 0.0 | .500E+00 | .313E+00 |
| 0.167 | 28.51 | 0.2851 | 0.2084 | 0.0000 | 0.4935 | 60.9 | 0.0 | 25.3 | 25.7 | 12.6 | 0.0 | .500E+00 | .102E+01 |
| 0.250 | 33.16 | 0.3316 | 0.4087 | 0.0000 | 0.7403 | 91.3 | 0.0 | 29.4 | 50.4 | 14.7 | 0.0 | .500E+00 | .171E+01 |
| 0.333 | 36.28 | 0.3628 | 0.6243 | 0.0000 | 0.9870 | 121.7 | 0.0 | 32.2 | 77.0 | 16.1 | 0.0 | .500E+00 | .239E+01 |
| 0.416 | 38.36 | 0.3836 | 0.8502 | 0.0000 | 1.2338 | 152.1 | 0.0 | 34.0 | 104.8 | 17.0 | 0.0 | .500E+00 | .308E+01 |
| 0.500 | 39.99 | 0.3999 | 1.0806 | 0.0000 | 1.4805 | 182.6 | 0.0 | 35.5 | 133.2 | 17.7 | 0.0 | .500E+00 | .376E+01 |
| 0.583 | 41.34 | 0.4134 | 1.3139 | 0.0000 | 1.7273 | 213.0 | 0.0 | 36.7 | 162.0 | 18.3 | 0.0 | .500E+00 | .442E+01 |
| 0.666 | 42.51 | 0.4251 | 1.5489 | 0.0000 | 1.9740 | 243.4 | 0.0 | 37.7 | 191.0 | 18.8 | 0.0 | .500E+00 | .507E+01 |
| 0.675 | 42.62 | 0.4262 | 1.5738 | 0.0000 | 2.0000 | 246.6 | 0.0 | 37.8 | 194.1 | 18.9 | 0.0 | .500E+00 | .514E+01 |

| INC_ER<br>%OOIP | INC<br>OIL | PRODUCED<br>WATER | FLUIDS<br>SOLVENT | HCPV<br>TOTAL | OIL<br>MSTB | WATER<br>MSTB | HC_GAS<br>MMSCF | SOLVENT<br>MMSCF | INC_GOR<br>MSCF/STB | INC_WOR<br>STB/STB |
|---|---|---|---|---|---|---|---|---|---|---|
| 0.00 | 0.0000 | 0.0000 | 0.0000 | 0.0000 | 0.0 | 0.0 | 0.0 | 0.0 | .000E+00 | .000E+00 |
| 20.15 | 0.2015 | 0.0453 | 0.0000 | 0.2468 | 17.9 | 5.6 | 8.9 | 0.0 | .500E+00 | .313E+00 |
| 8.36 | 0.0836 | 0.1631 | 0.0000 | 0.2468 | 7.4 | 20.1 | 3.7 | 0.0 | .500E+00 | .271E+01 |
| 4.65 | 0.0465 | 0.2002 | 0.0000 | 0.2468 | 4.1 | 24.7 | 2.1 | 0.0 | .500E+00 | .599E+01 |
| 3.11 | 0.0311 | 0.2156 | 0.0000 | 0.2468 | 2.8 | 26.6 | 1.4 | 0.0 | .500E+00 | .963E+01 |
| 2.08 | 0.0208 | 0.2259 | 0.0000 | 0.2468 | 1.8 | 27.9 | 0.9 | 0.0 | .500E+00 | .151E+02 |
| 1.63 | 0.0163 | 0.2305 | 0.0000 | 0.2468 | 1.4 | 28.4 | 0.7 | 0.0 | .500E+00 | .197E+02 |
| 1.35 | 0.0135 | 0.2333 | 0.0000 | 0.2468 | 1.2 | 28.8 | 0.6 | 0.0 | .500E+00 | .240E+02 |
| 1.17 | 0.0117 | 0.2351 | 0.0000 | 0.2468 | 1.0 | 29.0 | 0.5 | 0.0 | .500E+00 | .280E+02 |
| 0.11 | 0.0011 | 0.0249 | 0.0000 | 0.0260 | 0.1 | 3.1 | 0.0 | 0.0 | .500E+00 | .318E+02 |

*Figure 3.17: Prophet CO2 Example - Output*

The output data is organized in time steps. In this particular example the report frequency is set to be monthly, therefore each step implies one-month time. So, for start, by the first column which sets the time step, it takes a little more than 9 months in order to inject 2 hydrocarbon pore volumes into the reservoir.

The second column is recovery factor at each time step which here indicates that the final recovery is of the order of 42%. The three following columns are the cumulative produced fluids (oil water and solvent respectively) in each step expressed in hydrocarbon pore volumes (HCPV), followed by the total amount of HCPV produced. The oil fraction is the same as the first column, just in a different expression. The water fraction is rising faster as the months go by which makes sense since water is replacing oil in the reservoir and as a result the water cut increases as time moves forward. The column regarding the solvent fraction stays at 0 value in this example as there is no solvent present. As expected, the final column at the end of production gives a number of 2,0 HCPV produced which is actually the number of HCPV that were injected inside the reservoir.

The two (2) following columns show the total quantity of injected fluids. All of them are given in standard conditions indicating that the B$_{o/w/g}$ values are to be used for the transformation from standard to reservoir conditions. As expected, the solvent column is zero due to the fact that this is a regular waterflood example. In order to provide the monthly production, the software uses as a "month unit" the division of 365 days of the year divided by 12. So, one month equals to approximately 30.42 days. That being said, the total water injection would be 30.4 Mbbls. The B$_w$ value is calculated internally and is: B$_w$=1.0067, which is a reasonable value.

The value for the B$_g$ can be computed by any gas-properties calculator found online. Given the values of pressure, temperature and Z-factor (which emerges to be 0.30647 for CO$_2$ under these thermodynamic conditions) the value is: B$_g$ =0.00043334.

In order to test the validity of this number, should the oil, water, hydrocarbon and solvent gas be expressed in the same reservoir units and summed they should add up to the injected quantity of water also expressed in reservoir units. So, expressed in millions of reservoir barrels:

Injected Water * B$_w$ = Produced Oil * B$_o$ + Produced Water* B$_w$ + Produced Gas (HC+Solvent) * B$_g$

246.6*1.0067 = 37.8*1.4 + 194.1*1.0067 + (18.9*10$^3$/5.615) * 0.00043334

=52.92+195.4+1.4586

248.3=249.78

The equation is not perfect due to the rounding of the fractions but it obviously converges verifying the initial claim.

The next four (4) columns are the produced fluids at the separator that is why we can observe the hydrocarbon gas column having non-zero values. To examine the whole point of these columns we will need the Bg value so we will get to that later on. The cumulative GOR column is set at 0.500 Mscf/bbl equal to the given input value of 500 scf/bbl. The cumulative WOR column results from the division of the Water (Mstb) and Oil (Mstb) columns.

The following columns show the same data but incrementally. The incremental recovery is obviously declining by the same "rhythm" as was shown in the total recovery columns. In the incremental produced water column, we can verify the rising water cut values with time, whereas the solvent column is of course zero. In the incremental total HCPV a steady amount is observed which makes absolute sense since at each step the same amount of water is injected so the exact total amount should be produced. About the last four columns the things said about the cumulative variables apply here as well.

In order to understand the software fully, another example of sole CO$_2$ injection is going to be considered. All the used data are the same as in the first example. The only difference is the fluid injected being CO$_2$ instead of water. Figure 3.18 shows the rate of injection being set at 2 million standard cubic feet per day up until the 3 HCPV have been injected. The results are show in Figure 3.19.

As expected, all the columns regarding produced water are zero due to the fact that the water is already at connate level and no water is being injected throughout the production and therefore no water is produced whatsoever. In one month time, the injected CO$_2$ is approximately 60.9 MMscf. The GOR columns emerge from the summation of the HC gas and Solvent columns divided with the Oil production column.

*Figure 3.18: CO₂ Software Example 2 - Injection Rate Input Data*



*Figure 3.19: CO₂ Prophet Software Example 2 - Output*

The huge advantage of $CO_2$ Prophet over any reservoir simulator is the simplicity and the speed of its calculations. In a matter of minutes, a simplified scenario can be set and run and the results can be interpreted just as fast giving a quick overview of the problem. It surely cannot be used as a prediction tool but the role of a screening tool fits perfectly to it and can save huge amounts of both time and money for the industry.

# CHAPTER 4

# Numerical Simulation Results- Screening Tool Reliability Tests

The previously described examples on Paragraph 3.1 will be used as guides in order to setup the screening tool. The screening tool consists of two parts:

- Zero-Dimensional Mapping Model
- $CO_2$ Prophet – Streamline Simulation Model

For the first part, the methodology described in paragraph 3.1 will be implemented on Microsoft Excel in order to be easy for any user to change parameters and modify conditions. The second part is a very quick streamline simulation commenced by $CO_2$ Prophet Software.

Regarding the implementation of the Stalkup-Claridge Methodology for the 0-Dimensional Mapping, the whole concept is relatively straight-forward. The only tricky part is the value of the sweep efficiency retrieved by the diagram of Claridge (1972). A consistent model needs to be produced in order to automate the task of "eyeballing" the value from the diagram. The Claridge chart was firstly imported and digitized in AutoCAD. The plot curves were digitized to many points with X,Y coordinates. The X coordinate is a logarithmic value of mobility ratio and the Y coordinate is the areal sweep efficiency value, for a specific displaceable volume $V_{pds}$. The points were imported on an Excel spreadsheet and a 4th degree polynomial trendline was assigned to each line using the excel regression tool. The mobility ratio and displaceable volume values are normalized in order to deal with more manageable numbers. In Claridge's diagram the mobility ratio ranges from 0.1 up to 1000 and the displaceable volume values range from 0.05 up to 5. Therefore the normalization limits are from $\log(0.1)=-1$ to $\log(1000)=3$ for the mobility ratio and from $\log(0.05)=0.699$ to $\log(5)=1.301$ for the $V_{pd}$. The initial coefficients produced and used for the construction of all 4th degree polynomials are:

$$A_i = a \cdot x^4 + b \cdot x^3 + c \cdot x^2 + d \cdot x + e$$

|   | $A_4$ | $A_3$ | $A_2$ | $A_1$ | $A_0$ |
|---|-------|-------|-------|-------|-------|
| a | -27.340 | 35.966 | 12.610 | -29.549 | 8.289 |
| b | 37.300 | -53.368 | -14.493 | 45.161 | -14.691 |
| c | 0.599 | 0.560 | -0.481 | -1.579 | 1.389 |
| d | -16.265 | 26.037 | 2.428 | -21.093 | 8.904 |
| e | 5.682 | -9.807 | 0.159 | 6.917 | -2.880 |

*Table 4.1 : Initial Coefficients produced by the Claridge Diagram Implementation*

Each final coefficient is produced by a 4th degree polynomial constructed by the original coefficients of the initial regression and the normalized value of the displaceable volume $V_{pds}$ as an independent variable. Lastly, the final 4th degree polynomial is designed where the normalized mobility ratio is used as an independent variable combined with the coefficients $A_i$ constructed before and the sweep efficiency is given by:

$$E_{As} = A_4 \cdot x^4 + A_3 \cdot x^3 + A_2 \cdot x^2 + A_1 \cdot x + A_0$$

# 4.1 Secondary Production - $CO_2$ Injection

## 4.1.1 Stalkup-Claridge Model Implementation on Microsoft Excel (Zero-Dimensional Mapping)

The first example of Green and Willwhite, regarding $CO_2$ injection as a secondary production technique is to be examined. The steps followed are going to be straight forward as presented in Chapter 3. The procedure will be revised in a bullet way and then presented in an Excel spreadsheet tabulated form.

In a nutshell:

- The OOIP is calculated using the volumetric method.
- The displaceable reservoir volume of injected solvent $V_{pds}$ is calculated.
- The Mobility Ratio M is calculated and since the permeability is the absolute porous-medium permeability for all fluids, the mobility ratio is the fluids viscosity ratio $\mu_o/\mu_s$.
- The areal sweep efficiency, $E_{As}$, is calculated using the Claridge's Implementation Model. The normalized Mobility Ratio and $V_{pds}$ as well as the initial polynomial coefficients are used in order to reach the final solution. Note that for a single-layer reservoir, $E_{As}$ is equivalent to volumetric sweep efficiency.
- Repeat the procedure with different $V_{pds}$.

The following tables consist of the used data and the implementation of the procedure described above:

| DATA | | | | | | | | | | | |
|---|---|---|---|---|---|---|---|---|---|---|---|
| $A(ft^2)$ | $h(ft)$ | $\varphi$ | $k(md)$ | $S_{wc}$ | $S_{oi}$ | $S_{orm}$ | $\mu_o(cP)$ | $\mu_s(cP)$ | $B_o$ | $T_{res}(F)$ | $P_{res}$ (psia) |
| 873000 | 20 | 0.18 | 120 | 0.25 | 0.75 | 0.05 | 1.5 | 0.06 | 1.15 | 120 | 2500 |

*Table 4. 2: Secondary Production - Initial Input Data*

| Initial Volumetric Calculations - Mobility Ratio Calculation | | | | |
|---|---|---|---|---|
| N(OOIP in ft³) | Displaceable Volume $V_{pd}$ | Mobility Ratio M | log(M) | Normalized log(M) |
| 365031.55 | 391800.53 | 25 | 1.39794 | 0.5995 |

*Table 4. 3: Secondary Production - Initial Volumetric Calculations and Mobility Ratio*

| | | | Sweep Efficiency Calculations - Claridge Model | | | | | |
|---|---|---|---|---|---|---|---|---|
| $V_{pDs}$ | $\log(V_{pDs})$ | Norm $V_{pDs}$ | $A_4$ | $A_3$ | $A_2$ | $A_1$ | $A_0$ | $E_{As}$ |
| 0.2 | -0.6990 | 0.3010 | 1.6331 | -3.0785 | 0.5546 | 1.4132 | -0.4068 | **0.187** |
| 0.3 | -0.5229 | 0.3891 | 1.0148 | -1.9107 | 0.4663 | 0.4535 | 0.1189 | **0.278** |
| 0.4 | -0.3979 | 0.4515 | 0.7573 | -1.3539 | 0.3472 | -0.0004 | 0.4154 | **0.346** |
| 0.5 | -0.3010 | 0.5000 | 0.6530 | -1.0714 | 0.2292 | -0.2264 | 0.6005 | **0.401** |
| 0.6 | -0.2218 | 0.5396 | 0.6223 | -0.9299 | 0.1211 | -0.3347 | 0.7232 | **0.446** |
| 0.7 | -0.1549 | 0.5731 | 0.6289 | -0.8668 | 0.0248 | -0.3773 | 0.8075 | **0.485** |
| 0.8 | -0.0969 | 0.6021 | 0.6544 | -0.8490 | -0.0597 | -0.3819 | 0.8668 | **0.518** |
| 0.9 | -0.0458 | 0.6276 | 0.6890 | -0.8581 | -0.1332 | -0.3638 | 0.9092 | **0.547** |
| 1.0 | 0.0000 | 0.6505 | 0.7268 | -0.8829 | -0.1968 | -0.3325 | 0.9398 | **0.573** |
| 1.2 | 0.0792 | 0.6901 | 0.8006 | -0.9543 | -0.2979 | -0.2512 | 0.9775 | **0.633** |
| 1.5 | 0.1761 | 0.7386 | 0.8880 | -1.0701 | -0.3971 | -0.1214 | 1.0012 | **0.686** |
| 2.0 | 0.3010 | 0.8010 | 0.9526 | -1.2134 | -0.4625 | 0.0534 | 1.0050 | **0.749** |
| 3.0 | 0.4771 | 0.8891 | 0.8253 | -1.2486 | -0.3693 | 0.1904 | 0.9884 | **0.822** |
| 4.0 | 0.6021 | 0.9515 | 0.4697 | -1.0187 | -0.1155 | 0.1004 | 0.9879 | **0.860** |
| 5.0 | 0.6990 | 1.0000 | -0.0244 | -0.6116 | 0.2224 | -0.1433 | 1.0104 | **0.879** |

*Table 4. 4: Secondary Production - Sweep Efficiency Calculation*
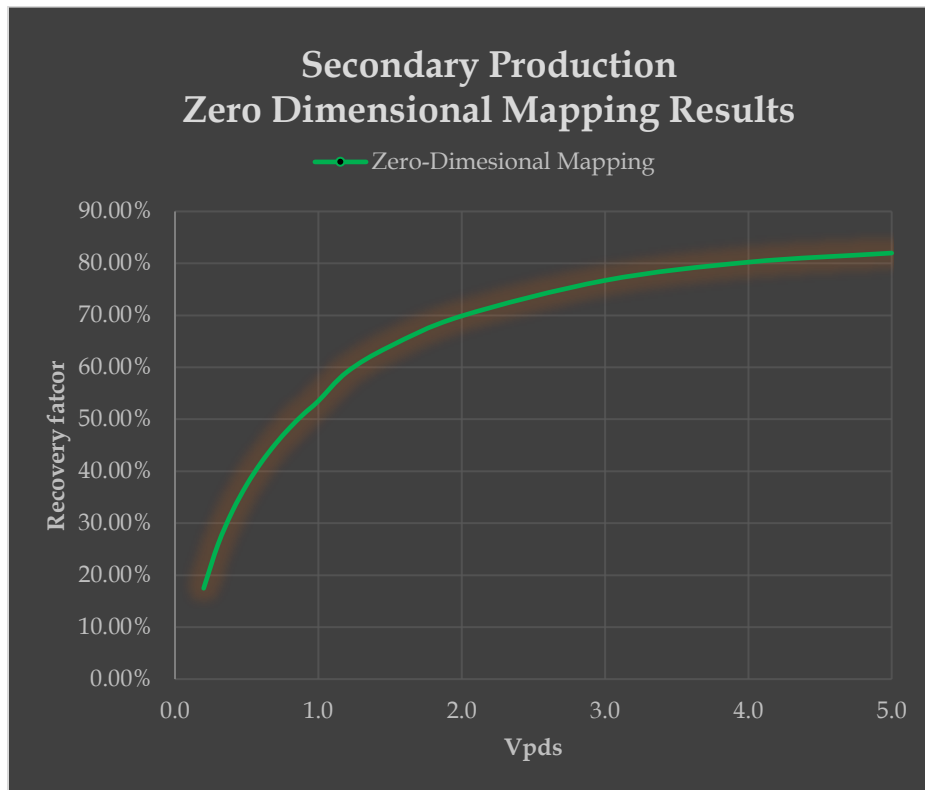


| | Oil Recovery Calculations | | |
|---|---|---|---|
| $V_{pDs}$ | $E_{As}$ | $N_p$ | RF |
| 0.2 | 0.187 | 63827.27 | **17.49%** |
| 0.3 | 0.278 | 94631.70 | **25.92%** |
| 0.4 | 0.346 | 117896.47 | **32.30%** |
| 0.5 | 0.401 | 136522.87 | **37.40%** |
| 0.6 | 0.446 | 151979.54 | **41.63%** |
| 0.7 | 0.485 | 165123.49 | **45.24%** |
| 0.8 | 0.518 | 176502.06 | **48.35%** |
| 0.9 | 0.547 | 186487.45 | **51.09%** |
| 1.0 | 0.573 | 195344.94 | **53.51%** |
| 1.2 | 0.633 | 215786.00 | **59.11%** |
| 1.5 | 0.686 | 245464.71 | **64.04%** |
| 2.0 | 0.749 | 280611.68 | **69.88%** |
| 3.0 | 0.822 | 322081.23 | **76.73%** |
| 4.0 | 0.860 | 351483.79 | **80.24%** |
| 5.0 | 0.879 | 374150.07 | **82.00%** |

*Figure 4.1: Secondary Production - Oil Recovery (Zero-Dimensional Mapping)*

A comparative study below shows the difference in percentage which comes out to be significantly small. This is to be expected as the same methodology was followed and only precision details and subjective interpretation (decimals $E_{As}$ values) explain this small difference between the results which maximizes at 3%. Due to that fact, no comparative plot is designed since the differences are not observable.

| Green & Willwhite | Zero-Dimensional Mapping | Difference (%) |
|---|---|---|
| 18.40% | 17.49% | 0.91% |
| 25.20% | 25.92% | 0.72% |
| 32.20% | 32.30% | 0.10% |
| 36.90% | 37.40% | 0.50% |
| 41.10% | 41.63% | 0.53% |
| 44.80% | 45.24% | 0.44% |
| 48.10% | 48.35% | 0.25% |
| 50.40% | 51.09% | 0.69% |
| 53.20% | 53.51% | 0.31% |
| 57.40% | 59.11% | 1.71% |
| 62.60% | 64.04% | 1.44% |
| 67.70% | 69.88% | 2.18% |
| 74.70% | 76.73% | 2.03% |
| 78.90% | 80.24% | 1.34% |
| 81.30% | 82.00% | 0.70% |

*Table 4.5: Secondary Production Comparative Study - Green Willwhite vs Zero-Dimensional Mapping Model Results*

## 4.1.2 CO$_2$ Prophet – Streamline Simulation

The concept is to use CO$_2$ Prophet to re-implement the example and make comparisons between this and the zero-dimensional model. In order to set the example, the same input data are used as introduced by Table 4.2. Due to the fact that the solvent viscosity is computed internally by the program, an internet research was conducted and several calculators were used in order to verify the value of CO$_2$ at reservoir conditions (T=120 F and P=2500 psia). All calculators and table properties agree with the example's given value of $\mu_s$=0.06 cP with values diverging in the worst case scenario 5% and therefore the assumption that the software uses a decent solvent viscosity value can be considered valid.
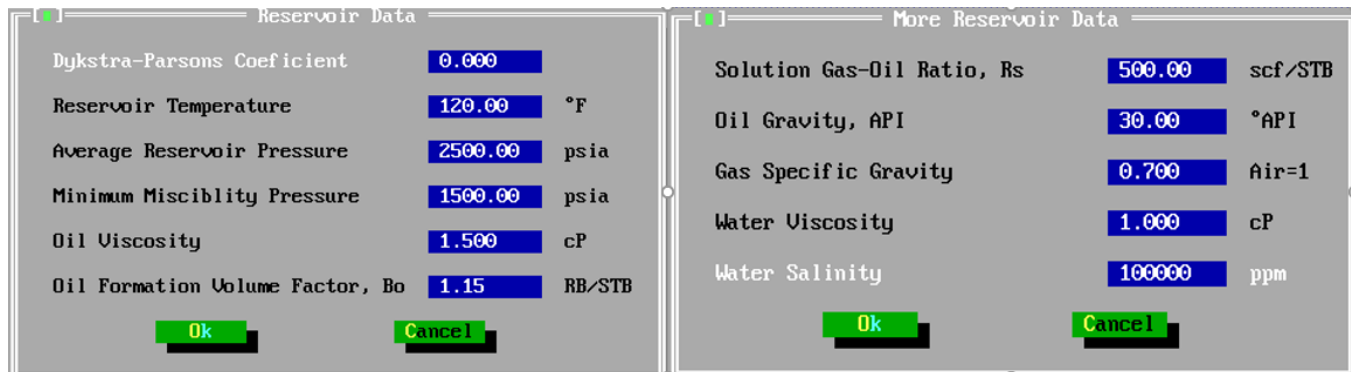


*Figure 4.2: Reservoir Data for Secondary Production- CO$_2$ injection*

The data used for the reservoir tab can be seen in Figure 4.1. The Dykstra-Parsons coefficient is set to zero since the example refers to a single layer reservoir and therefore no permeability variation exists. Since no data exist for the minimum miscibility pressure (MMP) a value below 75% of the average reservoir pressure is chosen in order to ensure full miscibility which is assumed by the example itself. Furthermore, since the specific gravity, water salinity, oil API gravity and GOR values are completely unknown reasonable values are chosen as inputs. These variables however do not interfere with the results of interest and do not pose a critical point of reference. The same goes for the water viscosity which since it is already at connate level is immovable and its viscosity does not play a significant role. A value of 1 cP is selected.

Regarding the Saturations tab, since no relative permeability data are available the permeability curves are chosen to be kept at their default values, since no better guesses can be made. The only variables set is the initial oil saturation $S_{oi}=0.75$ and the connate water saturation set at $S_{wc}=0.25$. All input data can be seen at Figure 4.2.



*Figure 4.3: Saturations Data - Secondary Production CO2 Injection*

On the Patterns and Rates tab, initially a 5-spot Pattern is chosen. On the Amounts and Rates menu, the volumes are chosen to be injected on a Volume Basis implying that each injection lasts up until the volume defined by the last column. In order to be consistent with the example and the previous implementation on the zero-dimensional model, for each $V_{pds}$ value defined in Table 4.7 an injected volume in hydrocarbon PV units ($V_{ph}$) is computed which is inserted as input in the model using Equation 3.1 Specifically:

| $V_{pDs}$ | 0.20 | 0.30 | 0.40 | 0.50 | 0.60 | 0.70 | 0.80 | 0.90 | 1.0 | 1.20 | 1.50 | 2.0 | 3.0 | 4.0 | 5.0 |
|-----------|------|------|------|------|------|------|------|------|-----|------|------|-----|-----|-----|-----|
| $V_{ph}$ | 0.186 | 0.28 | 0.373 | 0.466 | 0.56 | 0.653 | 0.746 | 0.84 | 0.933 | 1.12 | 1.40 | 1.866 | 2.80 | 3.73 | 4.67 |

*Table 4.6: $CO_2$ amount injected in Hydrocarbon Pore Volumes*

Therefore, 15 simulations are run each one differing only in the final injected volume of $CO_2$. The value chosen for the injection rate per day is not of great importance since the only difference it will make will be for the total time needed to complete the injection. A relatively low amount of 1 MMscf/day is chosen in order to keep track of the project status more often. From the DIGITOUT output file produced only the final value of the second column is of interest. Finally, the project is set extract monthly reports. The mixing parameter omega is set at default value 0.666 and the $K_{r,m}$ is set equal to $K_{r,ow}$ having no effect whatsoever on the results since full miscibility is assumed. The values are exported in an Excel spreadsheet and the final results presented below in tabulated and diagrammatic form.



| $V_{pDs}$ | $CO_2$ Prophet RF |
|-----------|-------------------|
| 0.2 | 16.05% |
| 0.3 | 27.81% |
| 0.4 | 36.02% |
| 0.5 | 42.16% |
| 0.6 | 46.68% |
| 0.7 | 49.85% |
| 0.8 | 53.19% |
| 0.9 | 56.14% |
| 1.0 | 58.25% |
| 1.2 | 61.73% |
| 1.5 | 66.34% |
| 2.0 | 72.60% |
| 3.0 | 80.13% |
| 4.0 | 86.36% |
| 5.0 | 89.11% |
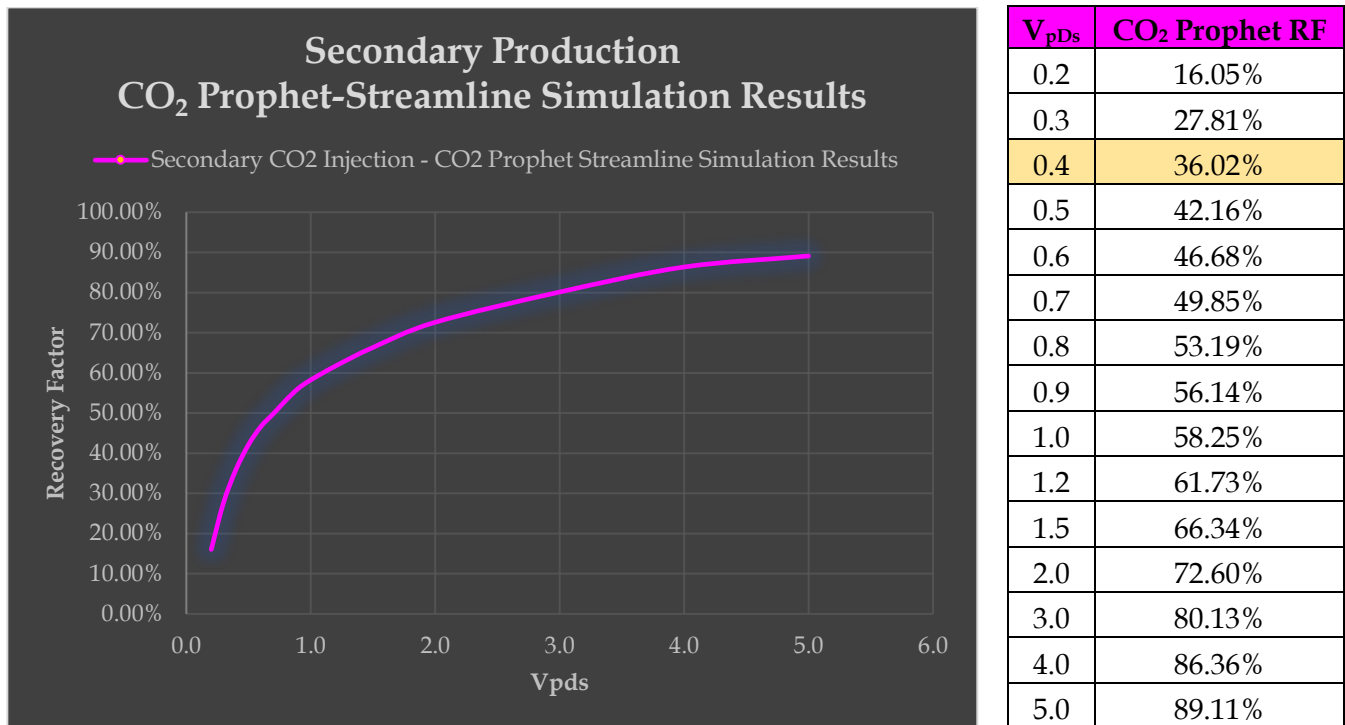
*Figure 4.4: Secondary Production Streamline Simulation Results - Oil Recovery vs Displaceable Volume*
*(Left : Plotted results , Right: Tabulated results – gas breakthrough at $V_{pds}$=0.4)*

By looking at the cumulative GOR produced column of the output DIGITOUT file with the simulation results, the breakthrough of gas in the production well can be defined. This can be observed due to the abrupt increase of the GOR and makes perfect sense since when the gas breakthrough occurs the gas

production increases a lot while the oil production stays constant or drops, thus leading to an increase in the cumulative GOR. Marked in the table of the results is the value of pore volumes injected which corresponds to the gas breakthrough.

Compared to the zero-dimensional model the results present a difference around 4% with streamline simulation giving, consistently, higher values of recovery. The comparative study is shown below on Table 4.8 and on Figure 4.4 diagrammatically.

| $V_{pDs}$ | Zero-Dimensional Mapping RF | CO2 Prophet RF | % Difference |
|-----------|-----------------------------|----------------|--------------|
| 0.2 | 17.49% | 16.05% | 1.44% |
| 0.3 | 25.92% | 27.81% | 1.89% |
| 0.4 | 32.30% | 36.02% | 3.72% |
| 0.5 | 37.40% | 42.16% | 4.76% |
| 0.6 | 41.63% | 46.68% | 5.05% |
| 0.7 | 45.24% | 49.85% | 4.61% |
| 0.8 | 48.35% | 53.19% | 4.84% |
| 0.9 | 51.09% | 56.14% | 5.05% |
| 1.0 | 53.51% | 58.25% | 4.74% |
| 1.2 | 59.11% | 61.73% | 2.62% |
| 1.5 | 64.04% | 66.34% | 2.30% |
| 2.0 | 69.88% | 72.60% | 2.72% |
| 3.0 | 76.73% | 80.13% | 3.40% |
| 4.0 | 80.24% | 86.36% | 6.12% |
| 5.0 | 82.00% | 89.11% | 7.11% |

*Table 4.7: Secondary Production Comparative Study – Zero-Dimensional Mapping versus CO₂ Prophet Results*
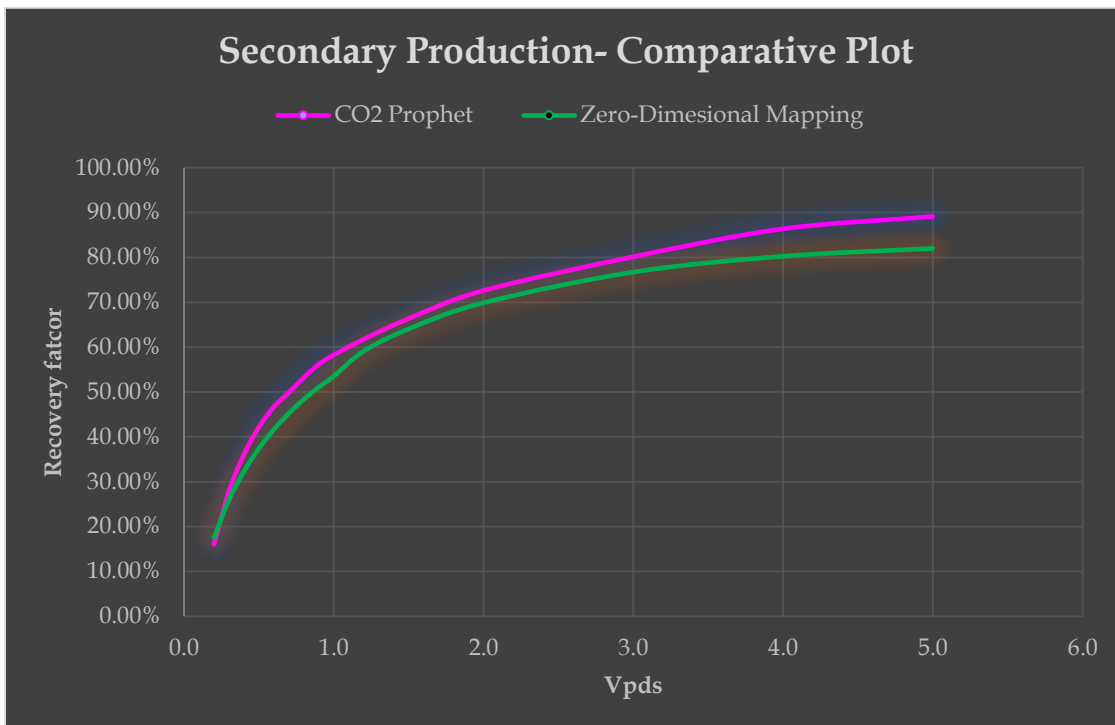


*Figure 4.5: Secondary Production Comparative Study – Plot Results*

## 4.2 Tertiary Production - $CO_2$ Injection

The second example of Green and Willwhite, is about $CO_2$ injection in tertiary production and refers to an already waterflooded reservoir. The example makes certain assumptions which will be revised and taken into account in order to make the best approach possible.

The key-assumptions made are:

- The oil resource target is assumed to exist in two different saturation conditions. In the part of the reservoir previously swept by water or other secondary recovery fluid, oil is at a residual saturation ($S_{or}$). In the remaining part of the reservoir, oil saturation is relatively high and exists at initial oil saturation ($S_{oi}$).
- The mobility ratio in a miscible displacement is typically more unfavorable than the value in a waterflood. Thus, sweep efficiency will be poorer in a tertiary miscible process than in the preceding secondary waterflood. The mobility ratio governing sweepout is the ratio of mobility in the solvent-invaded region to that in the region of water flow ahead of the tertiary oil bank.
- Residual oil from the prior waterflood is banked up into a tertiary oil bank by injected miscible solvent. At the leading edge of the oil bank, waterflood residual oil is mobilized and water is displaced with a sharp front. The tertiary oil bank is displaced by solvent with a sharp front. There may be an ROS, $S_{orm}$, after the solvent displacement. The water saturation through the oil and solvent banks is assumed to be a constant value, $S_{wt}$. The saturation would, in fact, vary across these banks, and the average value could be estimated from frontal-advance theory.
- A pseudodisplaceable PV injected is calculated and used that includes the oil bank and is defined by Equation 3.1.

### 4.2.1 Stalkup-Claridge Model Implementation on Microsoft Excel (Zero-Dimensional Mapping)

Keeping in mind the assumption made the problem is to be set in excel spreadsheet form. The steps followed are going to be straight forward as presented in Chapter 3. Generally, the procedure described in Chapter 3 is used until $V_{pDs}$ reaches the maximum desired value. Firstly, the displaceable volume $V_{pDs}$ is set and the $\Delta V_{pDob}$ and $V_{pDob}$ are calculated be Equations 3.3 and 3.2 respectively. The sweep efficiencies $E_{As}$ and $E_{Aob}$ are then calculated using the Claridge's Implementation Model by use of the normalized mobility ratio and $V_{pds}$ as well as the initial polynomial coefficients are used in order to reach the final solution. Finally, the recovered amount $N_p$ is calculated with Equation 3.4 and the procedure is repeated for the next $V_{pDs}$ value.

The next tables include the data used and the calculations made for the implementation of the procedure.

| A(ft²) | h(ft) | φ | k(md) | $S_{wc}$ | $S_{oi}$ | $S_{orm}$ | $\mu_o$(cP) | $\mu_s$(cP) |
|--------|-------|------|-------|----------|----------|-----------|-------------|-------------|
| 873000 | 20 | 0.18 | 120 | 0.25 | 0.75 | 0.05 | 1.5 | 0.06 |
| Bo | T(F) | P(psia) | $S_{orw}$ | $S_{ob}$ | $S_{wt}$ | $\mu_w$ | $kr_w$ | $kr_s$ |
| 1.15 | 120 | 2500 | 0.3 | 0.75 | 0.25 | 0.7 | 0.2 | 0.8 |

*Table 4.8: Tertiary Production - Initial Input Data*

| Initial Volumetric Calculations and Mobility Ratio Calculation | | | | |
|---|---|---|---|---|
| N(OOIP in ft³) | Displaceable Volume $V_{pd}$ | Mobility Ratio M | log(M) | Normalized log(M) |
| 146012.62 | 391800.53 | 46.67 | 1.6690 | 0.6673 |

*Table 4.9: Tertiary Production - Initial Volumetric Calculations and Mobility Ratio*

| Areal Sweep Efficiency $E_{As}$ Calculations - Claridge Model | | | | | | | | |
|---|---|---|---|---|---|---|---|---|
| $V_{pDs}$ | $\log(V_{pDs})$ | Norm $V_{pDs}$ | $A_4$ | $A_3$ | $A_2$ | $A_1$ | $A_0$ | $E_{As}$ |
| 0.1 | -1.0000 | 0.1505 | 3.3607 | -6.0385 | 0.4708 | 3.8448 | -1.5545 | **0.093** |
| 0.2 | -0.6990 | 0.3010 | 1.6331 | -3.0785 | 0.5546 | 1.4132 | -0.4068 | **0.192** |
| 0.3 | -0.5229 | 0.3891 | 1.0148 | -1.9107 | 0.4663 | 0.4535 | 0.1189 | **0.263** |
| 0.4 | -0.3979 | 0.4515 | 0.7573 | -1.3539 | 0.3472 | -0.0004 | 0.4154 | **0.318** |
| 0.5 | -0.3010 | 0.5000 | 0.6530 | -1.0714 | 0.2292 | -0.2264 | 0.6005 | **0.363** |
| 0.6 | -0.2218 | 0.5396 | 0.6223 | -0.9299 | 0.1211 | -0.3347 | 0.7232 | **0.401** |
| 0.7 | -0.1549 | 0.5731 | 0.6289 | -0.8668 | 0.0248 | -0.3773 | 0.8075 | **0.434** |
| 0.8 | -0.0969 | 0.6021 | 0.6544 | -0.8490 | -0.0597 | -0.3819 | 0.8668 | **0.463** |
| 0.9 | -0.0458 | 0.6276 | 0.6890 | -0.8581 | -0.1332 | -0.3638 | 0.9092 | **0.489** |
| 1.0 | 0.0000 | 0.6505 | 0.7268 | -0.8829 | -0.1968 | -0.3325 | 0.9398 | **0.512** |
| 1.2 | 0.0792 | 0.6901 | 0.8006 | -0.9543 | -0.2979 | -0.2512 | 0.9775 | **0.552** |
| 1.5 | 0.1761 | 0.7386 | 0.8880 | -1.0701 | -0.3971 | -0.1214 | 1.0012 | **0.601** |
| 2.0 | 0.3010 | 0.8010 | 0.9526 | -1.2134 | -0.4625 | 0.0534 | 1.0050 | **0.663** |
| 3.0 | 0.4771 | 0.8891 | 0.8253 | -1.2486 | -0.3693 | 0.1904 | 0.9884 | **0.744** |
| 4.0 | 0.6021 | 0.9515 | 0.4697 | -1.0187 | -0.1155 | 0.1004 | 0.9879 | **0.794** |

*Table 4.10: Tertiary Production - Areal Sweep Efficiency Calculations*

| Final Volumetric Sweep Efficiency $E_{Aob}$ Calculations - Claridge Model | | | | | | | | | | |
|---|---|---|---|---|---|---|---|---|---|---|
| $V_{pDs}$ | $\Delta V_{pDob}$ | $V_{pDob}$ | $\log(V_{pDob})$ | Norm $V_{pDob}$ | $A_4$ | $A_3$ | $A_2$ | $A_1$ | $A_0$ | $E_{Aob}$ |
| 0.1 | 0.056 | 0.156 | -0.8081 | 0.2465 | 2.1674 | -4.0219 | 0.5579 | 2.1892 | -0.7909 | **0.153** |
| 0.2 | 0.111 | 0.311 | -0.5071 | 0.3970 | 0.9741 | -1.8279 | 0.4536 | 0.3857 | 0.1600 | **0.269** |
| 0.3 | 0.167 | 0.467 | -0.3310 | 0.4850 | 0.6769 | -1.1454 | 0.2677 | -0.1679 | 0.5475 | **0.349** |
| 0.4 | 0.222 | 0.622 | -0.2061 | 0.5475 | 0.6214 | -0.9106 | 0.0986 | -0.3486 | 0.7446 | **0.409** |
| 0.5 | 0.278 | 0.778 | -0.1091 | 0.5959 | 0.6477 | -0.8502 | -0.0419 | -0.3832 | 0.8553 | **0.457** |
| 0.6 | 0.333 | 0.933 | -0.0300 | 0.6355 | 0.7014 | -0.8650 | -0.1555 | -0.3545 | 0.9205 | **0.497** |
| 0.7 | 0.389 | 1.089 | 0.0370 | 0.6690 | 0.7605 | -0.9124 | -0.2457 | -0.2983 | 0.9596 | **0.531** |
| 0.8 | 0.444 | 1.244 | 0.0950 | 0.6980 | 0.8157 | -0.9717 | -0.3162 | -0.2318 | 0.9829 | **0.560** |
| 0.9 | 0.500 | 1.400 | 0.1461 | 0.7236 | 0.8628 | -1.0327 | -0.3701 | -0.1638 | 0.9962 | **0.586** |
| 1.0 | 0.556 | 1.556 | 0.1919 | 0.7465 | 0.9002 | -1.0899 | -0.4099 | -0.0988 | 1.0031 | **0.609** |
| 1.2 | 0.667 | 1.867 | 0.2711 | 0.7860 | 0.9451 | -1.1834 | -0.4548 | 0.0137 | 1.0061 | **0.649** |
| 1.5 | 0.833 | 2.333 | 0.3680 | 0.8345 | 0.9434 | -1.2610 | -0.4573 | 0.1296 | 0.9995 | **0.695** |
| 2.0 | 1.111 | 3.111 | 0.4929 | 0.8970 | 0.7950 | -1.2343 | -0.3471 | 0.1901 | 0.9872 | **0.750** |
| 3.0 | 1.667 | 4.667 | 0.6690 | 0.9850 | 0.1519 | -0.7629 | 0.1031 | -0.0484 | 1.0005 | **0.818** |
| 4.0 | 2.222 | 6.222 | 0.7939 | 1.0475 | -0.7435 | 0.0436 | 0.6979 | -0.5797 | 1.0646 | **0.854** |

*Table 4.11: Tertiary Production - Pseudodisplaceable Volume and Volumetric Sweep Efficiency Calculations*

| Oil Recovery Calculations | | | |
|---|---|---|---|
| $V_{pDs}$ | $E_{Aob}$ | $N_p$ | RF |
| 0.1 | 0.153 | - | - |
| 0.2 | 0.269 | 6487.87 | 4.44% |
| 0.3 | 0.349 | 13140.98 | 9.00% |
| 0.4 | 0.409 | 18712.30 | 12.82% |
| 0.5 | 0.457 | 23521.27 | 16.11% |
| 0.6 | 0.497 | 27758.86 | 19.01% |
| 0.7 | 0.531 | 31549.97 | 21.61% |
| 0.8 | 0.560 | 34981.38 | 23.96% |
| 0.9 | 0.586 | 38116.06 | 26.10% |
| 1.0 | 0.609 | 41001.31 | 28.08% |
| 1.2 | 0.649 | 46161.95 | 31.62% |
| 1.5 | 0.695 | 52734.46 | 36.12% |
| 2.0 | 0.750 | 61539.24 | 42.15% |
| 3.0 | 0.818 | 74325.38 | 50.90% |
| 4.0 | 0.854 | 83434.17 | 57.14% |
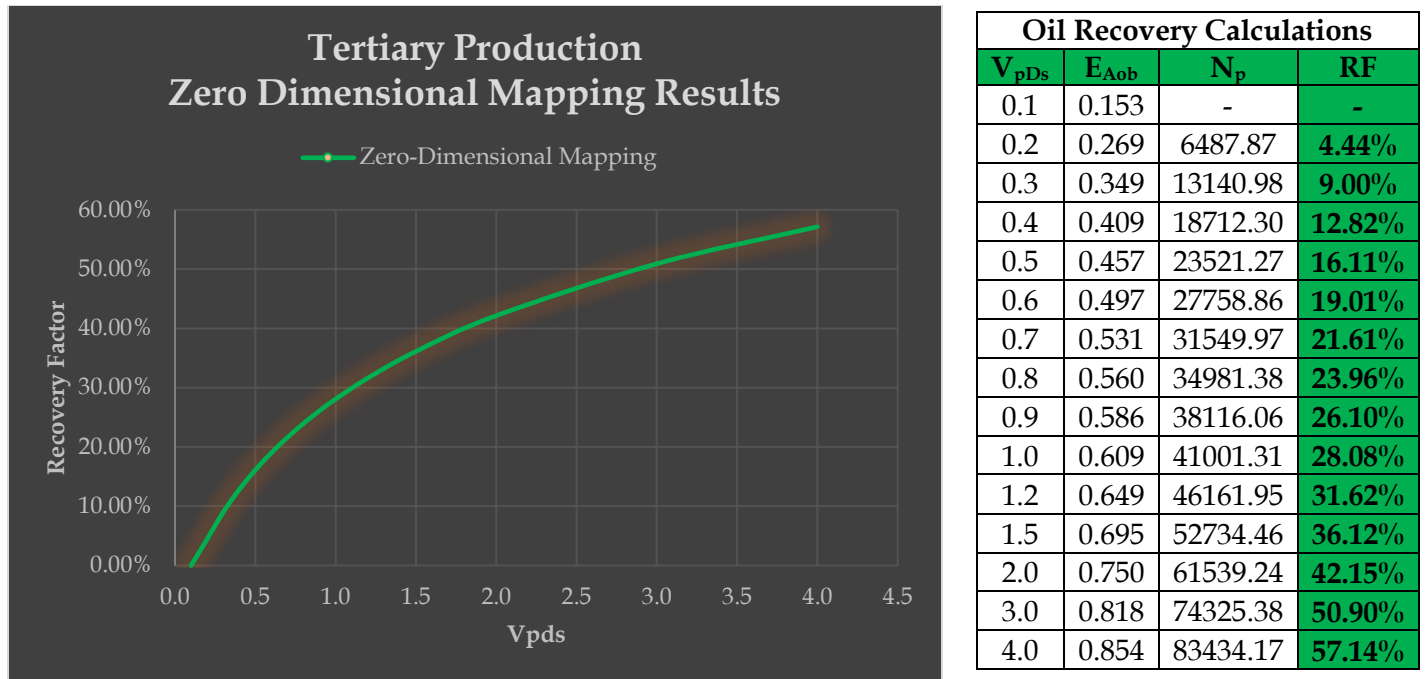
*Figure 4.6: Tertiary Production - Oil Recovery Calculation*

## 4.2.2 $CO_2$ Prophet Simulation Results – Tertiary Production

Before setting up the example in "$CO_2$ Prophet" some key points need to be underlined. The first assumption made actually divides the reservoir volume into two distinct parts:

1. The water-swept one where oil exists at Residual Oil Saturation ($S_{or}$)
2. The part not reached by the waterflood where oil exists at Initial Oil Saturation ($S_{oi}$)

This particular assumption cannot be implemented in "$CO_2$ Prophet" because the software does not have an option to split the reservoir into two distinct parts. In order to approximate that condition, the following assumption is made. Since the Zero-Dimensional Mapping is a Material Balance-like method the two different parts of the reservoir with different saturations are approached with a uniform reservoir existing at the average saturation of the two. If a percentage for the water swept reservoir is given then the average is weighted. Since no data are available for the particular example an equal split is assumed of 50% water-swept and 50% virgin reservoir. The procedure included also pseudodisplaceable volumetric calculations which in the streamline simulation method are not required. Only the initial data will be imported and the software will determine the path of the solution internally.

With no further due the data imported in the software are presented in the following Figures. Again, the Dykstra-Parsons coefficient is set to 0 since a single layer reservoir with uniform permeability is simulated. Again, the minimum miscibility pressure (MMP) is set with a value below 75% of the average reservoir pressure is chosen in order to ensure full miscibility due to lack of specific data. For the same reason, reasonable values are set for the black oil variables (API gravity, SG and water salinity) and for the GOR. The water viscosity, however now plays a significant role for the mobility ratio calculations and therefore receives the value of 0.7 as described in the book example.

*Figure 4.7:Reservoir Data for Tertiary Production- $CO_2$ injection*

Regarding the saturations tab as implemented previously, no change is done on the default values for any of the relative permeability curves. The only significant change is for the initial oil saturation which as explained before is set to the average value of the two reservoir parts, water-swept and virgin respectively. Since the values are $S_{orw}$=0.30 and $S_{ob}$=0.75 the value for the $S_{oi}$ chosen is :

$$S_{oi} = \frac{S_{orw} + S_{ob}}{2} = \frac{0.30 + 0.75}{2} = 0.525$$



*Figure 4.8: Saturations Data -Tertiary Production $CO_2$ Injection*

On the "Patterns and Rates" tab, a 5-spot Pattern is chosen. Next, on the "Amounts and Rates" menu, the volumes are chosen to be injected on a Volume Basis. Again, in order to be consistent with the example, for each $V_{pds}$ value defined in Table 4.13 an injected volume in hydrocarbon PV units ($V_{ph}$) is computed which is inserted as input in the model using Equation 3.1 Specifically:

| $V_{pDs}$ | 0.1 | 0.2 | 0.3 | 0.4 | 0.5 | 0.6 | 0.7 | 0.8 | 0.9 | 1.0 | 1.2 | 1.5 | 2.0 | 3.0 | 4.0 |
|---|---|---|---|---|---|---|---|---|---|---|---|---|---|---|---|
| $V_{ph}$ | 0.093 | 0.187 | 0.280 | 0.373 | 0.467 | 0.560 | 0.653 | 0.747 | 0.840 | 0.933 | 1.120 | 1.400 | 1.867 | 2.800 | 3.733 |

*Table 4.12: Tertiary Production -$CO_2$ amount injected in Hydrocarbon Pore Volumes*

Having set all required data, 15 simulations are run each one differing only in the final injected volume of $CO_2$. As mentioned before, the value chosen for the injection rate per day is not of great importance since the only difference it will make will be for the months needed to complete the injection so a relatively low amount of 1 MMscf/day is chosen. The results are exported in an Excel spreadsheet and presented below in tabulated and diagrammatic form. For the first point of $CO_2$ volume injected equal to 0.1 hydrocarbon pore volume, the software returned no result due to the fact that the value itself is so small that mobilizes actually nothing. This is quite reasonable and is in agreement with Green and Willwhite' results which also predict a very small recovery at this low value less than 1% of the OOIP. Marked in the table is the value of injected pore volumes for which gas breakthrough occurs.



| $V_{pDs}$ | $CO_2$ Prophet |
|---|---|
| 0.1 | - |
| 0.2 | 6.40% |
| 0.3 | 12.47% |
| 0.4 | 17.41% |
| 0.5 | 21.90% |
| 0.6 | 25.27% |
| 0.7 | 28.04% |
| 0.8 | 30.60% |
| 0.9 | 32.59% |
| 1.0 | 34.33% |
| 1.2 | 37.39% |
| 1.5 | 41.22% |
| 2.0 | 46.12% |
| 3.0 | 52.80% |
| 4.0 | 57.11% |
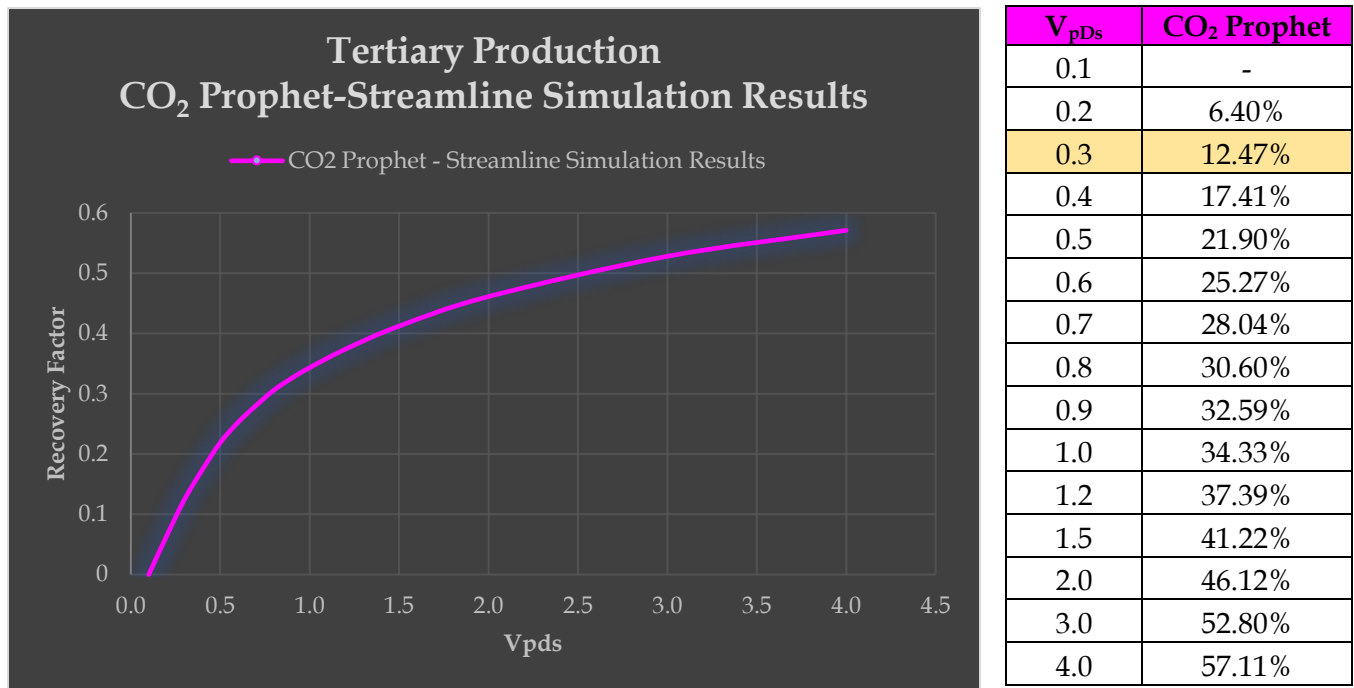
*Figure 4.9: Tertiary Production Streamline Simulation Results - Oil Recovery vs Displaceable Volume*
*(Left : Plotted results , Right: Tabulated results – gas breakthrough at $V_{pds}$=0.3)*

Compared to the zero-dimensional model the results present a difference around 4.6% with streamline simulation giving, consistently, higher values of recovery. The comparative study is shown below on Table 4.8 and on Figure 4.4 diagrammatically. Compared to the secondary production the difference is slightly more visible but definitely inside acceptable limits.

| VpDs | Zero-Dimensional Mapping RF | CO₂ Prophet RF | % Difference |
|------|---------------------------|----------------|--------------|
| 0.1 | - | - | |
| 0.2 | 4.44% | 6.40% | 1.96% |
| 0.3 | 9.00% | 12.47% | 3.47% |
| 0.4 | 12.82% | 17.41% | 4.59% |
| 0.5 | 16.11% | 21.90% | 5.79% |
| 0.6 | 19.01% | 25.27% | 6.26% |
| 0.7 | 21.61% | 28.04% | 6.43% |
| 0.8 | 23.96% | 30.60% | 6.64% |
| 0.9 | 26.10% | 32.59% | 6.49% |
| 1.0 | 28.08% | 34.33% | 6.25% |
| 1.2 | 31.62% | 37.39% | 5.77% |
| 1.5 | 36.12% | 41.22% | 5.10% |
| 2.0 | 42.15% | 46.12% | 3.97% |
| 3.0 | 50.90% | 52.80% | 1.90% |
| 4.0 | 57.14% | 57.11% | 0.03% |

*Table 4.13::  Tertiary Production Comparative Study – Zero-Dimensional Mapping versus CO₂ Prophet Results*
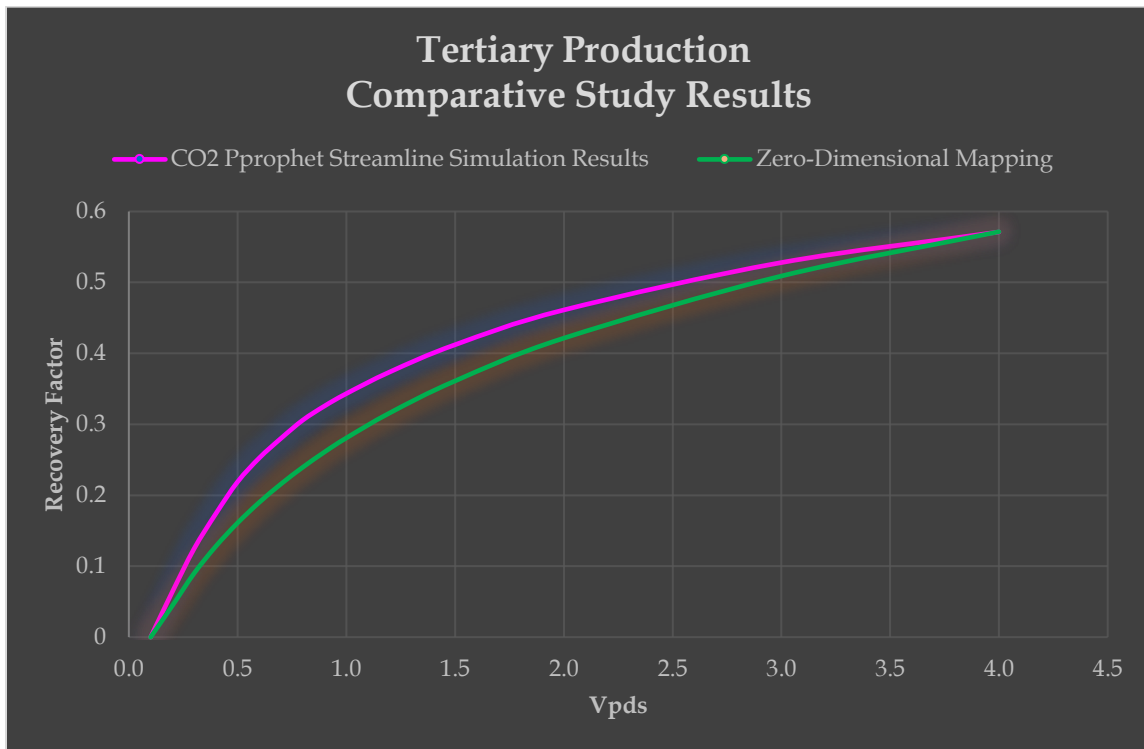


*Figure 4 .10: Tertiary Production Comparative Study - Plot Results*

# CHAPTER 5

# CO$_2$ Prophet – In depth investigation of software capabilities

## 5.1 Comparative Project Settings – Screening Tool Implementation

Since the way the screening tool works has been defined and its reliability has been tested on a basic level, a further investigation of the potential capabilities and uses of CO$_2$ Prophet will be conducted. In real case projects, huge uncertainties exist regarding several values which play a major role for the final value of recovery. For example, the Dykstra-Parsons coefficient is a variable whose value is quite uncertain but, at the end, it plays a definitive role. "CO$_2$ Prophet" can be used investigate the sensitivity of such uncertain input parameters, which is a something that the zero-dimensional model cannot handle. So, the aim of this chapter is to test the sensitivity of "CO$_2$ Prophet" results against uncertainty on various input parameters. For this purpose, another project similar to the ones presented on Chapter 4 will be set, regarding tertiary recovery, will be set. The test-project will be treated as presented previously and next, a series of extra information and charts, which can be produced by the outputs of "CO$_2$ Prophet" will be used.

The test-project (Project-T) is referring to tertiary recovery and is similar to the one presented on Chapter 4. In this project the reservoir is assumed to be quite larger than the previous ones with an area of 50 acres and thickness of 100 ft all of which are considered to be part of the pay zone. The average pressure is 4000 psia and the average reservoir temperature is 180 $^0$F. The main data required are presented in the Tables below:

| A(ft²) | h(ft) | φ | k(md) | S$_{wc}$ | S$_{oi}$ | S$_{orm}$ | μ$_o$(cP) | μ$_s$(cP) |
|--------|-------|-----|-------|----------|----------|-----------|-----------|-----------|
| 2182500 | 100 | 0.2 | 150 | 0.2 | 0.8 | 0.08 | 2 | 0.084 |
| Bo | T(F) | P(psia) | S$_{orw}$ | S$_{ob}$ | S$_{wt}$ | μ$_w$ | kr$_w$ | kr$_s$ |
| 1.4 | 180 | 4000 | 0.4 | 0.8 | 0.2 | 1 | 0.2 | 0.8 |

*Table 5.1: Project-T Initial Input Data*

| Initial Volumetric Calculations and Mobility Ratio Calculation | | | | |
|-----------------|------------------------------|------------------|---------|---------------------|
| N( OOIP) | Displaceable Volume V$_{pd}$ | Mobility Ratio M | log(M) | Normalized log(M) |
| 146012.62 | 391800.53 | 46.67 | 1.6690 | 0.6673 |

*Table 5.2: Project-T Initial Volumetric Calculations and Mobility Ratio*

Firstly, the screening tool developed in the previous chapter will be used exactly as it was used before. Therefore, the Claridge Model will be used and the required calculations are presented in the following tables.

| | | | Areal Sweep Efficiency $E_{As}$ Calculations - Claridge Model | | | | | | |
|---|---|---|---|---|---|---|---|---|---|
| $V_{pDs}$ | $\log(V_{pDs})$ | Norm $V_{pDs}$ | $A_4$ | $A_3$ | $A_2$ | $A_1$ | $A_0$ | $E_{As}$ |
| 0.1 | -1.0000 | 0.1505 | 3.3607 | -6.0385 | 0.4708 | 3.8448 | -1.5545 | 0.094 |
| 0.2 | -0.6990 | 0.3010 | 1.6331 | -3.0785 | 0.5546 | 1.4132 | -0.4068 | 0.192 |
| 0.3 | -0.5229 | 0.3891 | 1.0148 | -1.9107 | 0.4663 | 0.4535 | 0.1189 | 0.262 |
| 0.4 | -0.3979 | 0.4515 | 0.7573 | -1.3539 | 0.3472 | -0.0004 | 0.4154 | 0.317 |
| 0.5 | -0.3010 | 0.5000 | 0.6530 | -1.0714 | 0.2292 | -0.2264 | 0.6005 | 0.361 |
| 0.6 | -0.2218 | 0.5396 | 0.6223 | -0.9299 | 0.1211 | -0.3347 | 0.7232 | 0.399 |
| 0.7 | -0.1549 | 0.5731 | 0.6289 | -0.8668 | 0.0248 | -0.3773 | 0.8075 | 0.432 |
| 0.8 | -0.0969 | 0.6021 | 0.6544 | -0.8490 | -0.0597 | -0.3819 | 0.8668 | 0.461 |
| 0.9 | -0.0458 | 0.6276 | 0.6890 | -0.8581 | -0.1332 | -0.3638 | 0.9092 | 0.487 |
| 1.0 | 0.0000 | 0.6505 | 0.7268 | -0.8829 | -0.1968 | -0.3325 | 0.9398 | 0.510 |
| 1.2 | 0.0792 | 0.6901 | 0.8006 | -0.9543 | -0.2979 | -0.2512 | 0.9775 | 0.550 |
| 1.5 | 0.1761 | 0.7386 | 0.8880 | -1.0701 | -0.3971 | -0.1214 | 1.0012 | 0.599 |
| 2.0 | 0.3010 | 0.8010 | 0.9526 | -1.2134 | -0.4625 | 0.0534 | 1.0050 | 0.661 |
| 3.0 | 0.4771 | 0.8891 | 0.8253 | -1.2486 | -0.3693 | 0.1904 | 0.9884 | 0.742 |
| 4.0 | 0.6021 | 0.9515 | 0.4697 | -1.0187 | -0.1155 | 0.1004 | 0.9879 | 0.792 |

*Table 5.3: Project-T Areal Sweep Efficiency Calculations*

| | | | Final Volumetric Sweep Efficiency $E_{Aob}$ Calculations - Claridge Model | | | | | | | |
|---|---|---|---|---|---|---|---|---|---|---|
| $V_{pDs}$ | $\Delta V_{pDob}$ | $V_{pDob}$ | $\log(V_{pDob})$ | Norm $V_{pDob}$ | $A_4$ | $A_3$ | $A_2$ | $A_1$ | $A_0$ | $E_{Aob}$ |
| 0.1 | 0.080 | 0.180 | -0.7447 | 0.2782 | 1.8434 | -3.4543 | 0.5608 | 1.7224 | -0.5628 | **0.175** |
| 0.2 | 0.160 | 0.360 | -0.4437 | 0.4287 | 0.8348 | -1.5320 | 0.3956 | 0.1441 | 0.3144 | **0.296** |
| 0.3 | 0.240 | 0.540 | -0.2676 | 0.5167 | 0.6345 | -1.0023 | 0.1846 | -0.2801 | 0.6554 | **0.377** |
| 0.4 | 0.320 | 0.720 | -0.1427 | 0.5792 | 0.6329 | -0.8603 | 0.0070 | -0.3807 | 0.8210 | **0.438** |
| 0.5 | 0.400 | 0.900 | -0.0458 | 0.6276 | 0.6890 | -0.8581 | -0.1332 | -0.3638 | 0.9092 | **0.487** |
| 0.6 | 0.480 | 1.080 | 0.0334 | 0.6672 | 0.7572 | -0.9092 | -0.2411 | -0.3019 | 0.9579 | **0.527** |
| 0.7 | 0.560 | 1.260 | 0.1004 | 0.7007 | 0.8208 | -0.9779 | -0.3223 | -0.2250 | 0.9846 | **0.561** |
| 0.8 | 0.640 | 1.440 | 0.1584 | 0.7297 | 0.8733 | -1.0479 | -0.3816 | -0.1466 | 0.9984 | **0.590** |
| 0.9 | 0.720 | 1.620 | 0.2095 | 0.7553 | 0.9128 | -1.1118 | -0.4227 | -0.0733 | 1.0046 | **0.616** |
| 1.0 | 0.800 | 1.800 | 0.2553 | 0.7782 | 0.9388 | -1.1661 | -0.4486 | -0.0081 | 1.0063 | **0.638** |
| 1.2 | 0.960 | 2.160 | 0.3345 | 0.8177 | 0.9529 | -1.2411 | -0.4639 | 0.0941 | 1.0026 | **0.677** |
| 1.5 | 1.200 | 2.700 | 0.4314 | 0.8662 | 0.8930 | -1.2706 | -0.4195 | 0.1771 | 0.9928 | **0.721** |
| 2.0 | 1.600 | 3.600 | 0.5563 | 0.9287 | 0.6324 | -1.1361 | -0.2301 | 0.1584 | 0.9853 | **0.774** |
| 3.0 | 2.400 | 5.400 | 0.7324 | 1.0167 | -0.2485 | -0.4130 | 0.3722 | -0.2721 | 1.0252 | **0.836** |
| 4.0 | 3.200 | 7.200 | 0.8573 | 1.0792 | -1.3765 | 0.6519 | 1.1066 | -1.0041 | 1.1246 | **0.867** |

*Table 5.4: Project-T Pseudodisplaceable Volume and Volumetric Sweep Efficiency Calculations*

### Project-T
### Zero Dimensional Mapping Results

— Zero Dimesional Mapping
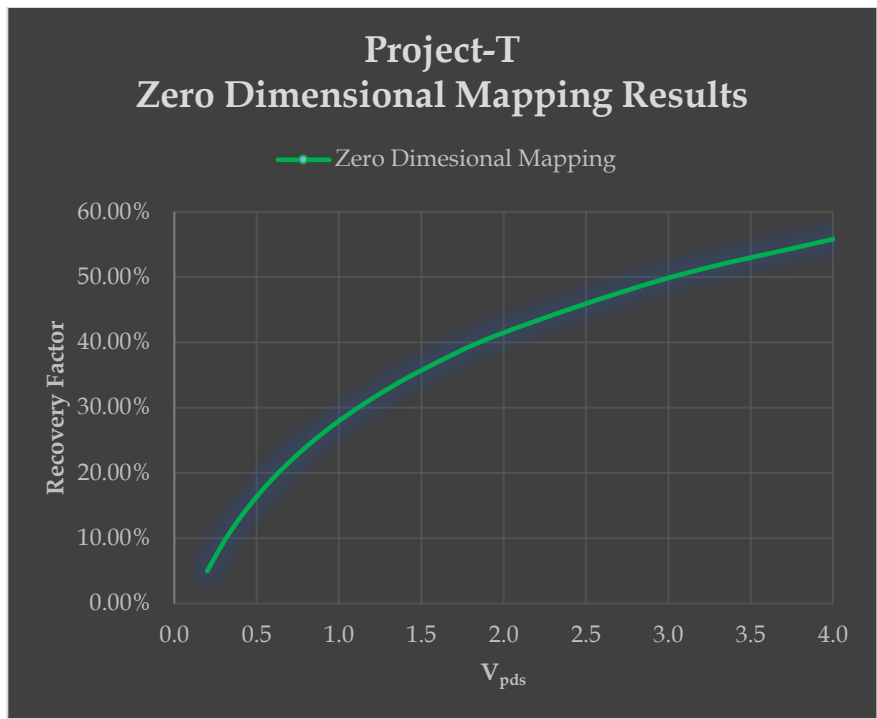
| Oil Recovery Calculations | | | |
|---|---|---|---|
| $V_{pDs}$ | $E_{Aob}$ | $N_p$ | RF |
| 0.1 | 0.175 | - | - |
| 0.2 | 0.296 | 66241.37 | 4.97% |
| 0.3 | 0.377 | 125737.33 | 9.44% |
| 0.4 | 0.438 | 175377.86 | 13.16% |
| 0.5 | 0.487 | 218109.04 | 16.37% |
| 0.6 | 0.527 | 255682.75 | 19.19% |
| 0.7 | 0.561 | 289239.19 | 21.70% |
| 0.8 | 0.590 | 319567.11 | 23.98% |
| 0.9 | 0.616 | 347237.19 | 26.06% |
| 1.0 | 0.638 | 372677.01 | 27.97% |
| 1.2 | 0.677 | 418113.81 | 31.37% |
| 1.5 | 0.721 | 475863.99 | 35.71% |
| 2.0 | 0.774 | 553027.66 | 41.50% |
| 3.0 | 0.836 | 664669.89 | 49.88% |
| 4.0 | 0.867 | 743881.04 | 55.82% |

*Figure 5.1: Project-T - Oil Recovery (Zero-Dimensional Mapping)*

The first part of the integrated screening tool is complete so the second part is the implementation on CO₂Prophet.The restrictions of the software apply in this case as well so even if we considered the reservoir to exist in two different parts (one reached by the previous waterflood where there is only residual oil left, and one not reached where oil exists at initial oil saturation), this split cannot be implemented on CO₂ Prophet, and therefore an average saturation of: $Soi = \frac{0.80+0.40}{2} = 0.60$ is used. This assumption is valid as mentioned before, since the Zero-Dimensional Mapping is a volumetric method and so averaging two parts into a uniform one is not introducing a significant error.

The data are introduced in the software. The Dykstra-Parsons coefficient is again set to 0 because a single layer reservoir with uniform permeability is assumed. The MMP is set to 2500 psia which satisfies the condition for full miscibility and reasonable values are chosen for the black oil variables. The water viscosity is chosen to be 1 cp while the oil viscosity is 2 cp. The imported data can be seen in Figure 5.1.
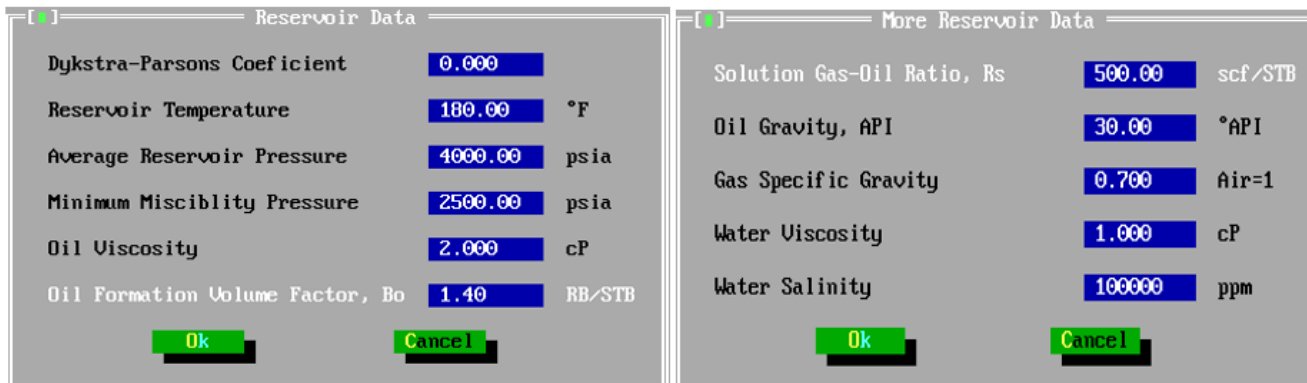
*Figure 5.2: Project-T - Reservoir Data*
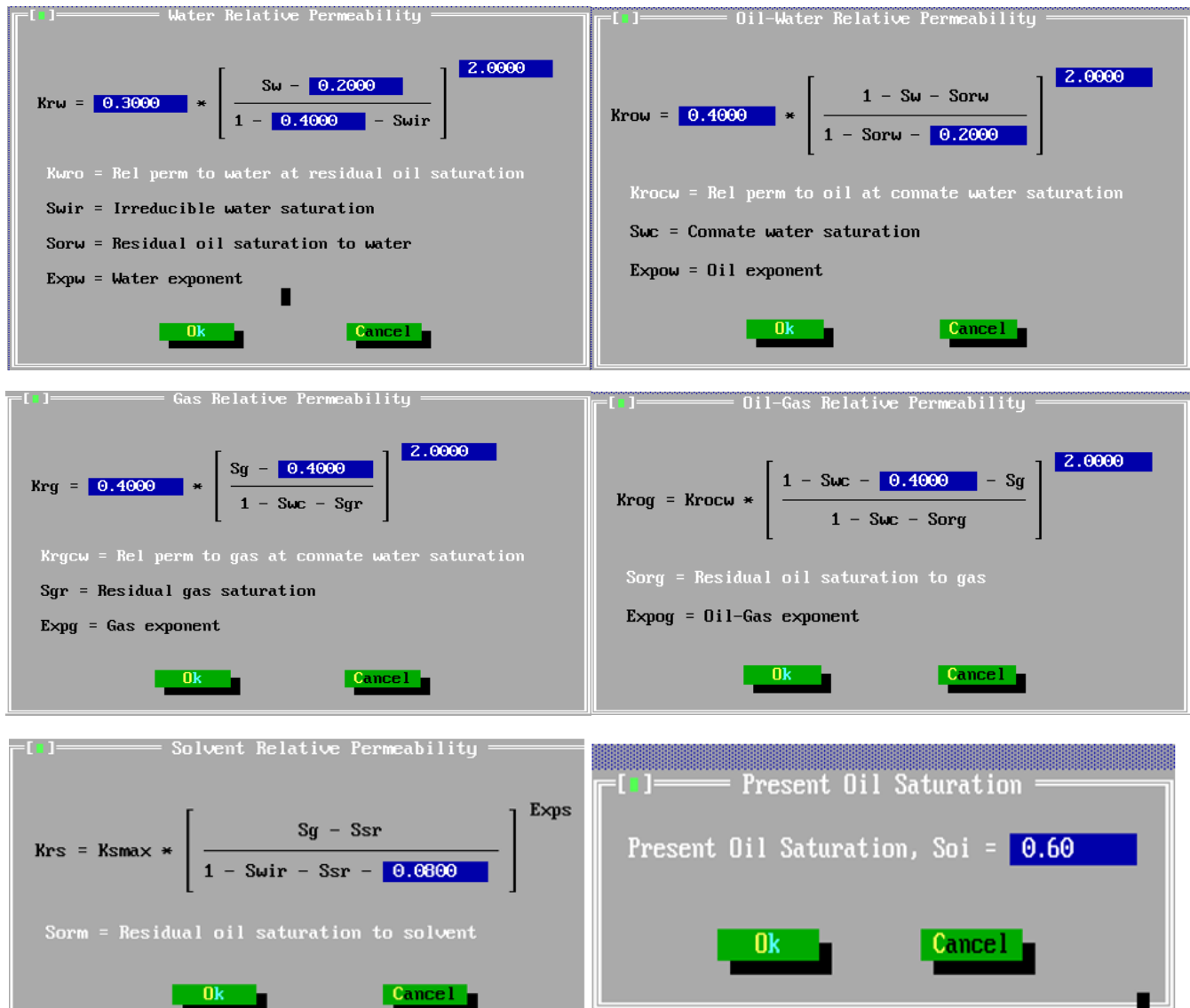
*Figure 5.3 Project-T - Saturations Data*

A 5-spot Pattern is chosen from the "Patterns" and the injection rates are chosen to be inputted on a Volume Basis on the "Amounts and Rates" tab. Once again, for each $V_{pds}$ value defined in Table 5.6 the injected volume in hydrocarbon PV units ($V_{ph}$) is computed which is introduced as input in the model using Equation 3.1.

| $V_{pDs}$ | 0.1 | 0.2 | 0.3 | 0.4 | 0.5 | 0.6 | 0.7 | 0.8 | 0.9 | 1.0 | 1.2 | 1.5 | 2.0 | 3.0 | 4.0 |
|---|---|---|---|---|---|---|---|---|---|---|---|---|---|---|---|
| $V_{ph}$ | 0.090 | 0.180 | 0.270 | 0.360 | 0.450 | 0.540 | 0.630 | 0.720 | 0.810 | 0.900 | 1.080 | 1.350 | 1.800 | 2.700 | 3.600 |

*Table 5.5: Project-T CO₂ amount injected in Hydrocarbon Pore Volumes*

The 15 simulations are run each one differing only in the final injected volume of CO₂. The oil recovery results are presented in the following figure both in tabulated and chart form. Marked on the table is the $V_{pds}$ value corresponding to the gas breakthrough.

| V$_{pDs}$ | CO2 Prophet |
|---|---|
| 0.1 | - |
| 0.2 | 7.18% |
| 0.3 | 12.97% |
| 0.4 | 17.74% |
| 0.5 | 21.62% |
| 0.6 | 24.89% |
| 0.7 | 27.50% |
| 0.8 | 29.70% |
| 0.9 | 31.61% |
| 1.0 | 33.28% |
| 1.2 | 36.84% |
| 1.5 | 39.66% |
| 2.0 | 44.18% |
| 3.0 | 50.66% |
| 4.0 | 55.28% |
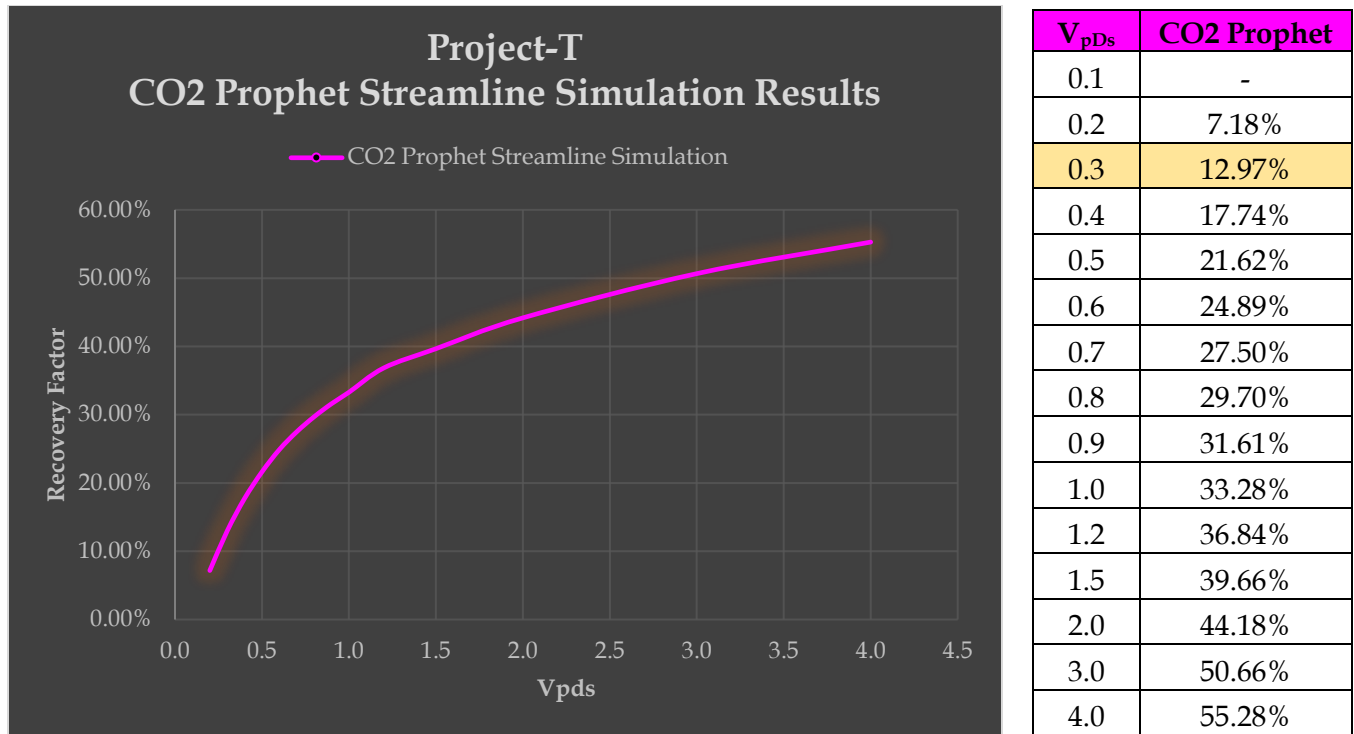
*Figure 5.4: Project-T Oil Recovery (CO$_2$ Prophet Streamline Simulation)*

The comparative table and plot, for the two parts of the screening tool is presented below. The observed differences are again quite low with an average of 4% and a maximum at 5.8% which is another proof that the developed screening tool works correctly. Again, the software consistently gives consistently more favorable values of recovery except for the final value which corresponds to quite high quantity of injected gas, which is highly unlikely to be implemented in a real project.

| V$_{pDs}$ | Zero-Dimensional Mapping RF | CO$_2$ Prophet RF | % Difference |
|---|---|---|---|
| 0.2 | 4.97% | 7.18% | 2.21% |
| 0.3 | 9.44% | 12.97% | 3.53% |
| 0.4 | 13.16% | 17.74% | 4.58% |
| 0.5 | 16.37% | 21.62% | 5.25% |
| 0.6 | 19.19% | 24.89% | 5.70% |
| 0.7 | 21.70% | 27.50% | 5.80% |
| 0.8 | 23.98% | 29.70% | 5.72% |
| 0.9 | 26.06% | 31.61% | 5.55% |
| 1.0 | 27.97% | 33.28% | 5.31% |
| 1.2 | 31.37% | 36.84% | 5.47% |
| 1.5 | 35.71% | 39.66% | 3.95% |
| 2.0 | 41.50% | 44.18% | 2.68% |
| 3.0 | 49.88% | 50.66% | 0.78% |
| 4.0 | 55.82% | 55.28% | 0.54% |

*Table 5.6: Project-T Comparative Study – Zero-Dimensional Mapping versus CO2 Prophet Results*
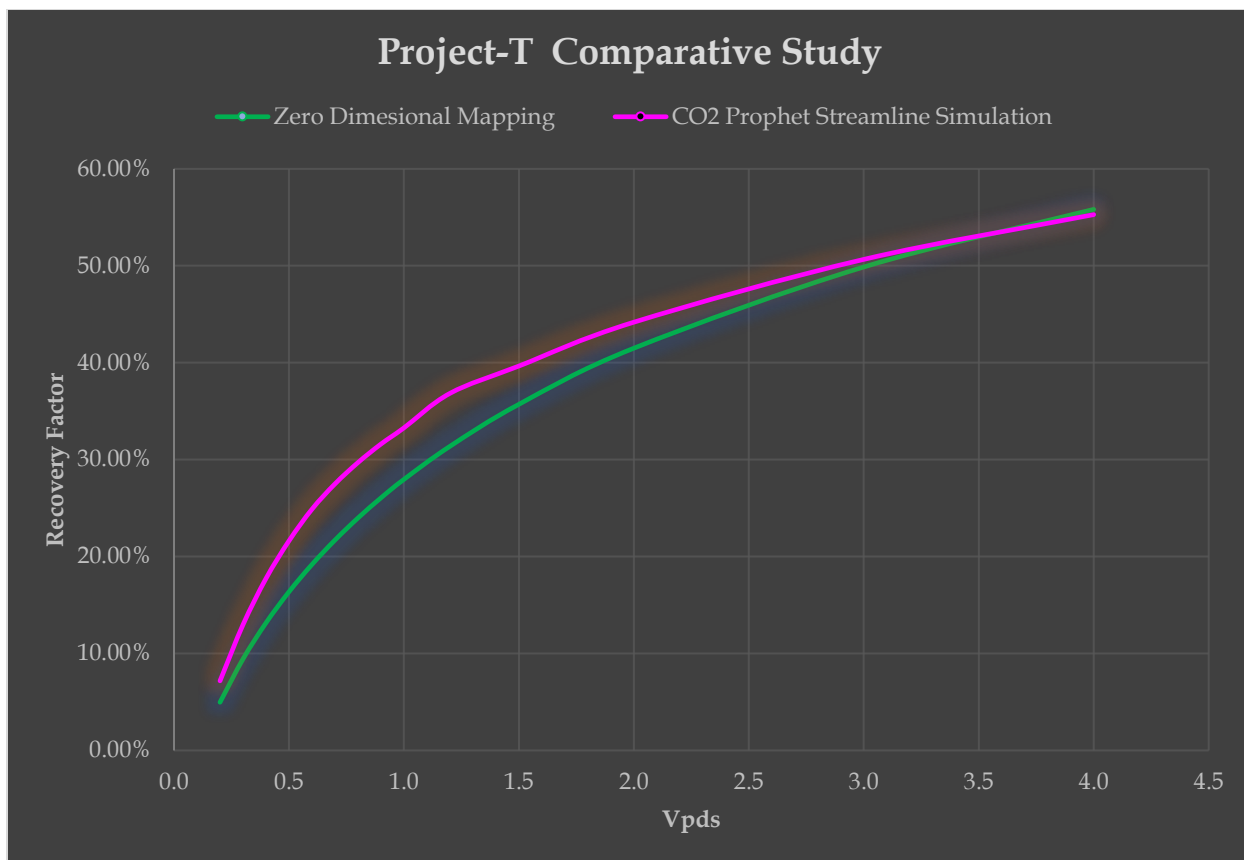
*Figure 5.5: Project-T  Comparative Plot (Zero-Dimensional Mapping vs CO2 Prophet Streamline Simulation)*

## 5.2 Project-T Case Studies – CO$_2$ Prophet

"CO$_2$ Prophet" has many more capabilities compared to the Zero-Dimensional model and can help in the development of case studies or serve as a powerful tool for the optimization procedure. In this chapter three case studies are going to be presented regarding three very important parameters of the problem which are all, most of the times very uncertain. These are:

- The Dykstra Parsons Coefficient (V).
- The number of layers existing.
- The minimum miscibility (MMP) estimate.

For each case study only one variable will be tested and all other variables of the problem will be kept constant in order to observe its effect. For each case study, three different values have been tested for the variable under study. The results will be presented in a tabulated and a diagrammatic form compared to the zero-dimensional mapping which was produced in the previous paragraph.

### 5.2.1 Dykstra Parsons Coefficient Case Study

The Dykstra Parsons Coefficient (V) is perhaps the most important variable when dealing with 2D models as it represents the permeability variation and therefore defines the degree of heterogeneity in a reservoir. The larger is its value, the more difficult it becomes for the fluid to reach the producing well and therefore the lower is the recovery. For the previous examples, single layered reservoirs were assumed and therefore V was equal to zero. This assumption however is very far from real because real reservoirs have many geological layers very different to each other which sum up to pretty high values of V. In general, values of V below 0.5 indicate low heterogeneity, a mediocre value can be 0.7 and highly heterogenous reservoirs can exhibit values close to 1. For the "CO$_2$ Prophet" software the V coefficient is of paramount importance and it is pointed out that it plays a major role in the final recovery.

For this case study, a 5-spot pattern is going to be used and the reservoir will be assumed to have 5 layers. Three different cases are going to be tested:

- V=0.5 (low heterogeneity)
- V=0.7 (medium heterogeneity)
- V=0.9 (high heterogeneity)

The values and the respective plot are going to be placed in a comparative table in order to observe how these changes affect the final recovery.

As expected, the oil recovery factor drops abruptly as the Dykstra-Parsons coefficient increases. The observed differences are of the order of 5-10% for sequential curves and should we focus on the two extremes, a huge difference of nearly 40% is observed. This proves the initial claim that the V coefficient is one of the key variables of the problem and thorough study needs to be conducted in order to either define the correct value or enclose the problem in viable limits that assure the minimum required recovery is secured. The comparative plot, which was quite quickly and easily produced, can be used in a real case problem in order to quickly visualize the extreme cases of maximum and minimum recovery

and decide whether or not the risk is worth taking. This is the actual power of "CO₂ Prophet" , that it allows the user to visualize the effects of a certain parameter on the  final recovery quickly and define the extreme conditions this parameter can possible create, in order to set limits to the problem.

| $V_{pDs}$ | Dyktsra-Parsons Coefficient (V) | | | |
|---|---|---|---|---|
| | **0** | **0.5** | **0.7** | **0.9** |
| | | | | |
| 0.2 | 7.18% | 7.69% | 7.39% | 7.04% |
| 0.3 | 12.97% | 10.67% | 9.39% | 8.49% |
| 0.4 | 17.74% | 12.84% | 10.84% | 9.52% |
| 0.5 | 21.62% | 14.57% | 11.97% | 10.33% |
| 0.6 | 24.89% | 16.15% | 12.96% | 11.00% |
| 0.7 | 27.50% | 17.61% | 13.85% | 11.57% |
| 0.8 | 29.70% | 18.96% | 14.69% | 12.08% |
| 0.9 | 31.61% | 20.23% | 15.49% | 12.49% |
| 1.0 | 33.28% | 21.41% | 16.23% | 12.86% |
| 1.2 | 36.84% | 23.50% | 17.60% | 13.49% |
| 1.5 | 39.66% | 26.25% | 19.57% | 14.23% |
| 2.0 | 44.18% | 30.18% | 22.13% | 14.78% |
| 3.0 | 50.66% | 35.77% | 25.71% | 15.81% |
| 4.0 | 55.28% | 40.05% | 28.85% | 17.26% |

*Table 5.7: Project-T - Dykstra Parsons Coefficient -Case Study Results*
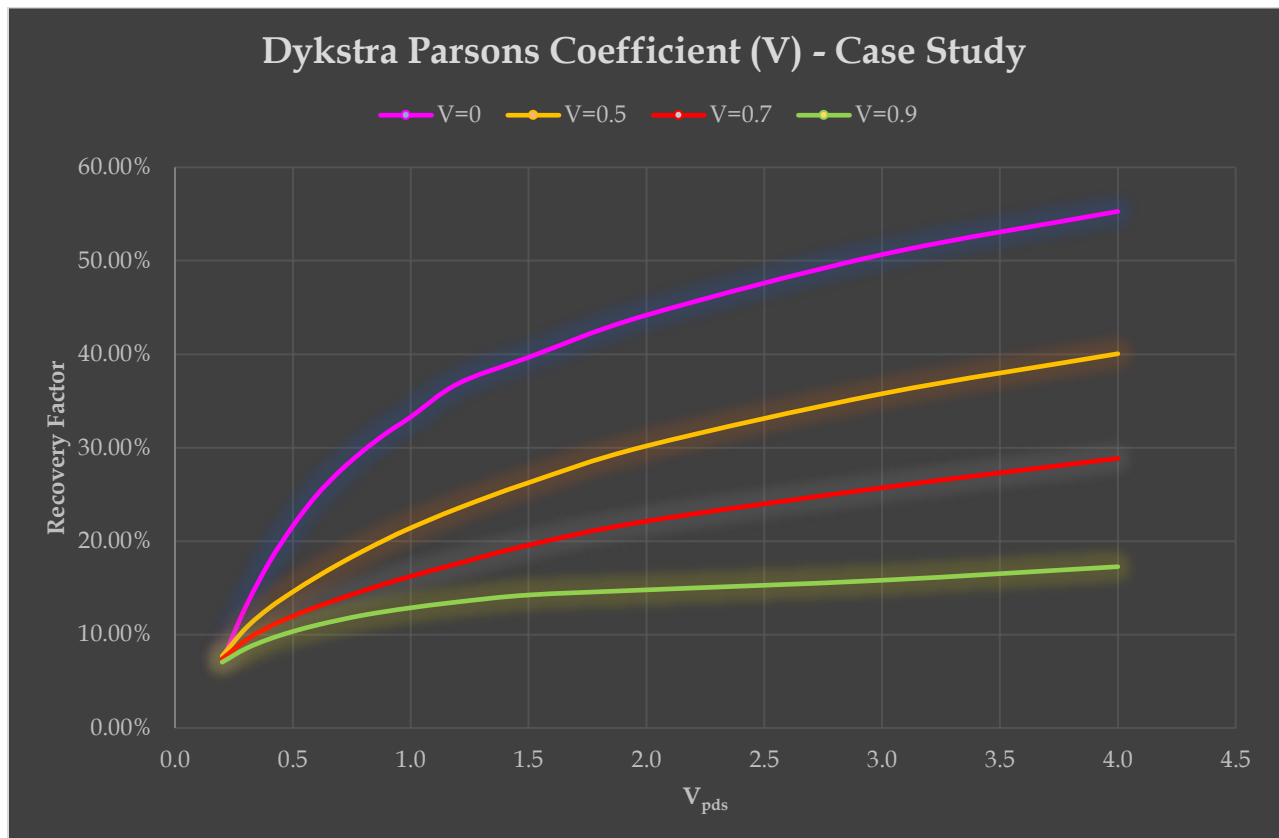


*Figure 5.6: Project-T - Dykstra Parsons Coefficient -Case Study Comparative Plot*

## 5.2.2 Existing Reservoir Layers - Case Study

Another important variable is the number of layers existing in the reservoir model. Usually, in real world problems, the geological study indicates the number of geological strata existing. However, there is a great chance for the reservoir to be in one quite big strata, or even that the results of the geological study are not crystal clear and do not clarify the exact number of layers existing in the reservoir. This needs to be dealt with caution as the heterogeneity of a reservoir is a function of the number of layers and of the way those layers communicate with each other or not. This uncertainty needs to be dealt with a case study that examines the problem in a close range of possibilities. Very few layers would mean easy flow for the fluids, when many different layers would raise the heterogeneity and therefore make it harder for the fluids to reach the production well.

For this case study, a 5-spot pattern is going to be used and the reservoir will be assumed to exhibit a Dykstra Parsons coefficient V=0.7, indicating medium to high heterogeneity (which is a pretty common case). For "CO$_2$ Prophet" the number of layers and the Dykstra Parsons coefficient are two variables related with each other that interact a lot. Three different cases, besides the initial one for single layer reservoir (which corresponds to V=0 by default) for the number of existing layers will be tested. These are:

- 3 layers (low heterogeneity)
- 5 layers (medium heterogeneity)
- 10 layers (high heterogeneity)

The produced results in terms of oil recovery are presented in a comparative table and the respective plot in order to observe how these changes affect the performance of the project.

| | Number of Reservoir Layers | | | |
|---|---|---|---|---|
| $V_{pDs}$ | 1 | 3 | 5 | 10 |
| | | | | |
| 0.2 | 7.18% | 8.40% | 7.39% | 6.22% |
| 0.3 | 12.97% | 11.18% | 9.39% | 7.63% |
| 0.4 | 17.74% | 13.22% | 10.84% | 8.82% |
| 0.5 | 21.62% | 14.64% | 11.97% | 9.92% |
| 0.6 | 24.89% | 15.82% | 12.96% | 10.91% |
| 0.7 | 27.50% | 16.82% | 13.85% | 11.82% |
| 0.8 | 29.70% | 17.71% | 14.69% | 12.64% |
| 0.9 | 31.61% | 18.52% | 15.49% | 13.40% |
| 1.0 | 33.28% | 19.25% | 16.23% | 14.08% |
| 1.2 | 36.84% | 20.57% | 17.60% | 15.30% |
| 1.5 | 39.66% | 22.32% | 19.57% | 16.95% |
| 2.0 | 44.18% | 24.74% | 22.13% | 19.45% |
| 3.0 | 50.66% | 28.70% | 25.71% | 23.67% |
| 4.0 | 55.28% | 31.72% | 28.85% | 27.01% |

*Table 5.8: Project-T - Number of Reservoir Layers -Case Study Results*
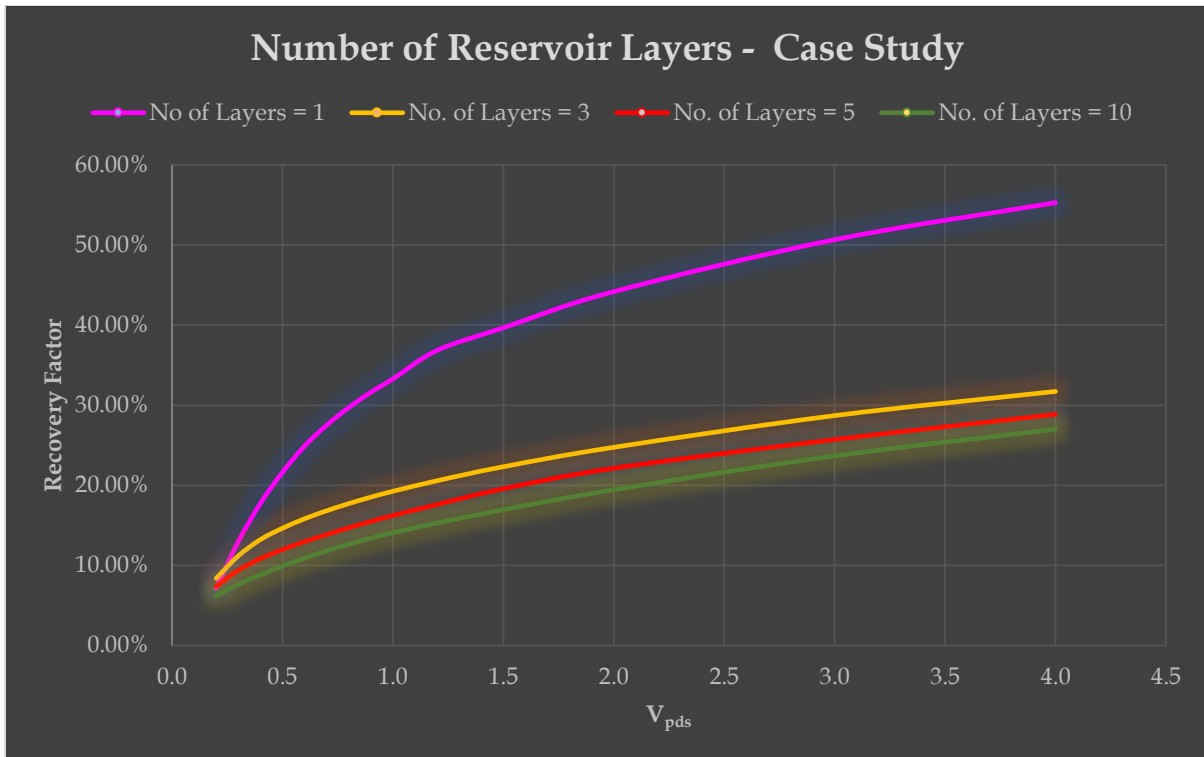
*Figure 5.7: Project-T - Number of Reservoir Layers -Case Study Comparative Plot*

It is quite clear from the graph that major difference appears between the single layered reservoir and the multilayered ones. The single layered reservoir is an idealized case that actually never happens in reality. Comparing the three realistic plots for the different number of layers, there are differences in recovery which actually reflect what was said initially, that as the number of layers rises the oil recovery drops. However, the differences observed are minor due to the fact that the Dykstra Parsons coefficient is the same for all cases which means that the permeability values are distributed the same way in all cases and therefore the "difficulty" that the fluids find (due to heterogeneity) is more or less the same. That is why, the differences observed are not big. In reality, the Dykstra-Parsons coefficient is actually a function of the number of layers and rises along with the number of them.

## 5.2.3 Minimum Miscibility Pressure (MMP) – Case Study

As discussed previously, defining the minimum miscibility pressure (MMP) can be done either experimentally or with empirical correlations. Both ways involve uncertainty which in the case of empirical correlations is quite high, leading sometimes in differences for the estimated value of the order of 1000 psia for the different correlations used. This in turn means that if the reservoir pressure and the MMP are close in range the concept of miscibility is debatable. In order to define the extremities of the induced uncertainty, case studies based on that particular variable can be conducted with "CO₂ Prophet".

All cases about to be examined correspond to a 5-spot pattern. For Project-T the average reservoir pressure is set to 4000 psia. For this case study three different values of the MMP will be tested, each corresponding to a different type of flow. These are:

- MMP=2500 (Miscible flow)
- MMP=5000 (Partially Miscible Flow)
- MMP=6000 (Immiscible Flow)

The three values chosen correspond to the different cases described in Chapter 3. A MMP of 2500 psia is less than the average reservoir pressure leading to full miscibility between the fluids. The ¾ of a MMP of 5000 psia is equal to 3750 psia meaning that the average reservoir pressure is higher than the ¾ of the MMP which leads to partial miscibility conditions. On the contrary, when the MMP is equal to 6000 the average reservoir pressure is less than its ¾ leading to fully immiscible flow.

The three different cases are plotted and presented in Table 5.9 and Figure 5.8 below.

| | MMP | | |
|---|---|---|---|
| $V_{pDs}$ | 2500 | 5000 | 6000 |
| | | | |
| 0.2 | 7.18% | 13.38% | 13.92% |
| 0.3 | 12.97% | 20.32% | 20.09% |
| 0.4 | 17.74% | 25.00% | 23.80% |
| 0.5 | 21.62% | 27.62% | 26.43% |
| 0.6 | 24.89% | 29.24% | 27.88% |
| 0.7 | 27.50% | 30.32% | 28.94% |
| 0.8 | 29.70% | 31.14% | 29.37% |
| 0.9 | 31.61% | 31.52% | 29.71% |
| 1.0 | 33.28% | 31.87% | 30.04% |
| 1.2 | 36.84% | 32.58% | 30.05% |
| 1.5 | 39.66% | 33.62% | 30.05% |
| 2.0 | 44.18% | 35.27% | 30.05% |
| 3.0 | 50.66% | 38.33% | 30.05% |
| 4.0 | 55.28% | 40.87% | 30.05% |

*Table 5.9: Project-T MMP estimate - Case study results*
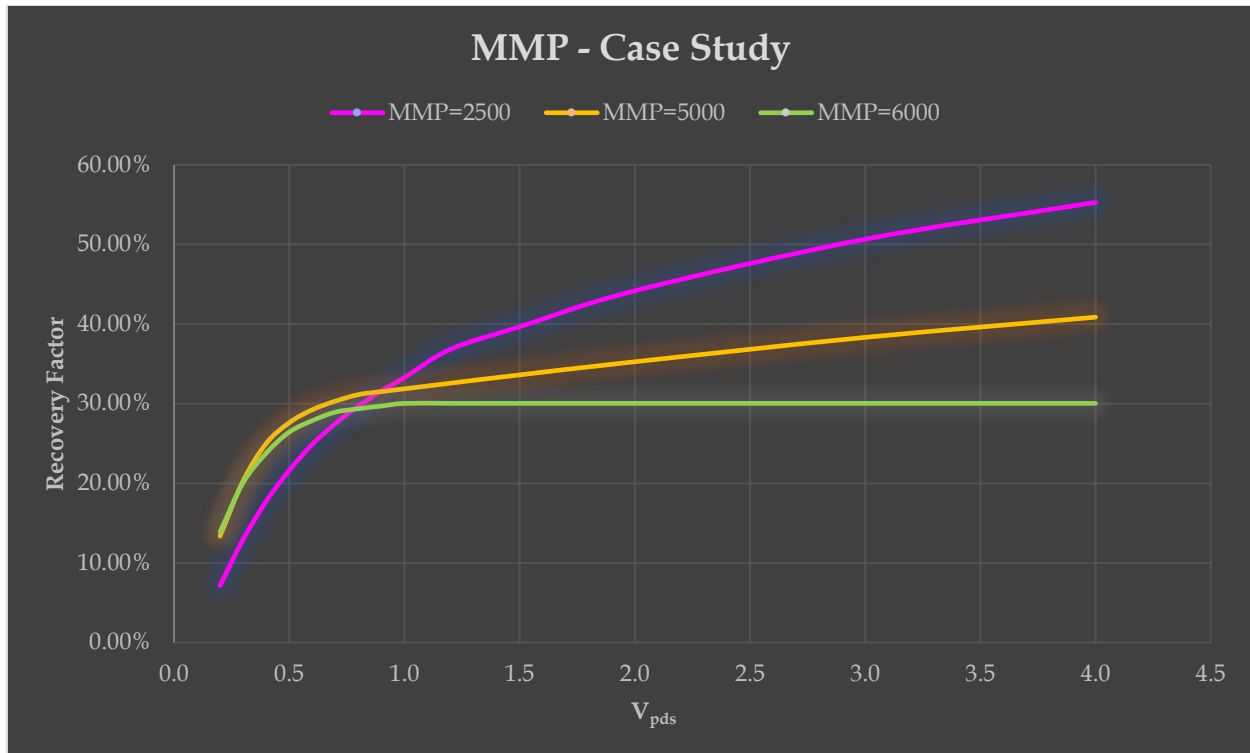
*Figure 5.8: Project-T MMP estimate - Case study comparative plot*

This case study presents an extreme case of uncertainty more than 1000 psia in the MMP. The three cases examined show that:

- Should full miscibility between fluids exist, the recovery will continue rising with a relatively high rate.
- Should partial miscibility exist, the recovery will continue rising but with a significantly lower rate, and tends to reach a plateau number as the volume injected rises. This happens because all the "miscible part" of the equation, is used as more fluid is injected.
- If the conditions correspond to immiscible flow, the two fluids ($CO_2$ and reservoir oil) do not mix at all and move independently, so once a certain amount is injected the reservoir is filled with gas that now does not allow oil to move at all but instead moves throughout the reservoir and gets produced.

This case study proves that the uncertainties of the MMP must be narrowed down enough in order to ensure the flow pattern at least. Should an estimate diverge from the real value significantly, the flow pattern might be different leading to completely different behavior of the recovery curve. "$CO_2$ Prophet" can be used to test and visualize the effect of low or high uncertainties in the MMP estimation.

# CHAPTER 6

# Conclusions and Recommendations for Future Research

## 6.1 Conclusions

The oil and gas industry has developed over the years very powerful tools in order to predict and simulate the oil recovery processes as accurately as possible. The apogee of this technology are the 3D Reservoir Simulators. These tools use very complex map and geo models and very accurate numerical methods to compute the unknown variables (finite elements – finite differences). However, due to exactly these facts, there are big limitations regarding the time required to complete the task at hand. The objective of this thesis was to establish a quick and reliable integrated screening tool in order to realize quickly whether there is need to use a reservoir simulator (e.g. when high recovery values are predicted) or there is no point in using the human and economic resources in order to set such a project.

The concept was to use two existing methodologies different than the numerical techniques implemented by the reservoir simulators and the combination of them to be the original screening tool. The first methodology was Zero-Dimensional Mapping, a volumetric technique based to the material balance principles which by the use of simple equations and relationships predicts a percentage of oil recovery. The second methodology was based on the Streamlines-Streamtubes simulation theory and was implemented by the commercial software $CO_2$ Prophet. Two scenarios were examined from the book of Green and Willwhite, regarding secondary and tertiary production via $CO_2$ injection respectively. The results have shown that:

1. The Zero-Dimensional Mapping need an implementation of the Claridge Diagram which, given the mobility ratio and the displaceable injected volume of $CO_2$, predicts the oil recovery. The model developed on Excel spreadsheet is considered to be quite good, as the rest of the procedure was relatively easy to follow and the results match the ones of Green and Willhite's.

2. $CO_2$ Prophet was proven quite accurate in predicting the shape of the recovery curvature showing that the theoretical background was very well programmed.

3. Comparison between the two approaches showed the following:
   - Qualitatively, both approaches predicted the form of recovery and were in good agreement with each other.
   - Quantitatively, CO2 Prophet predictions were consistently higher than those by the Zero-Dimensional Mapping. On average, for the secondary production there was a difference of approximately 4,02% with a 7,11% maximum deviation. The respective percentages for the tertiary production were 4,62% on average and maximum deviation of 6,64%.

In the sequel in order to explore the capabilities and potential of $CO_2$ Prophet another project was set. The concept was to make case studies for some key variables of such problems and see how the changes affect the total recovery. The variables that were tested was the Dykstra-Parsons coefficient (V), the number of existing reservoir layers and the minimum miscibility pressure (MMP) estimate. The results showed that:

i. Changes in the Dykstra Parsons coefficient are by far the most significant. This is to be expected this coefficient defines the distribution of permeability values and therefore the heterogeneity of the reservoir. The three values tested indicated that as V rises the total recovery factor drops. The biggest difference is observed when any curve is compared to the one for V=0 (corresponding to a homogeneous reservoir). In fact, this shows that in the unrealistic case of a homogeneous reservoir, the recovery would be significantly higher. The three realistic cases have reasonable differences of the order of 5-10% for sequential pairs. In the two extreme cases of V=0 and V=0,9 are compared, the differences are huge ranging from 15% up to 40%. This goes to show that the degree of heterogeneity plays a major role in 2D simulations and need to be treated carefully.

ii. The number of layers proved to be an important but not definitive factor, if the number is somewhat realistic. The case study conducted has shown that when the number of layers is more than 3, which actually activates the Dykstra-Parson coefficient, it actually plays a minor role in the recovery as the major part is taken by the V coefficient. Again, should the unrealistic case of single layered reservoir be taken into account, there are huge differences but only because in that case V=0 by default. Comparing the three realistic cases the differences observed were in the order of 2% for sequential curves and 5% for the 3- and 10-layers curve.

iii. For the case study of the MMP estimate, the differences observed were both in quality and quantity terms and that is because of the change in the flow patter. The value of the MMP and its relation to the average reservoir pressure defines whether the flow will be fully or partially miscible, or immiscible. Should this estimate exhibits uncertainty high enough to it is possible to compromise the flow pattern, serious errors regarding the predicted recovery could occur. Uncertainties on the MMP estimates are tolerable but the flow pattern must be crystal clear.

## 6.2 Recommendations for Future Research

This thesis presented the idea of a "screening tool" which will be used to test some cases quickly and give a first, rough estimation of recovery, in order to show whether further research is required or no reason for it exists. The methodology was established and tested by two examples. The idea has shown its potential and there is room for improvement is several aspects such as:

1. The same examples should be simulated by a 3D-Reservoir Simulator (e.g. Eclipse, REVEAL, etc.) in order to observe differences and deviations both qualitatively and quantitatively.
2. The case of WAG ($CO_2$ slug followed by water) should also be examined, as sole $CO_2$ injection is rarely used due to economic reasons.
3. More examples of secondary and tertiary production should be tested in order to establish the methodology and form a concrete idea of how it works. Different well patterns should be used in order to observe especially how the streamlines are affected and how the recovery alters.
4. $CO_2$ Prophet is a quite good software but can take a lot of improvement. New developments on it can be made in order to make it work both more accurately and quickly but also to make it more usable. For instance, the injected fluid can be defined by the user from a database of existing fluids with known basic properties. The principle is quite similar to the one used by a Compositional Reservoir Simulator. This will allow users throughout the world to use it since gas-floods in general will be simulated rather than pure $CO_2$ floods.

# References

D. W. Green and G. P. Willhite (2017): Enhanced Oil Recovery (Second Edition).

M.R. Thiele: "Streamline Simulation", 6th International Forum on Reservoir Simulation September 3rd-7th, 2001, Schloss Fuschl, Austria.

R.P. Batycky (SPE), M.J. Blunt (SPE) and M.R.Thiele (SPE), "A 3D Field-Scale Streamline-Based Reservoir Simulator", Stanford University, November 1997, SPE Reservoir Engineering.

R. Juanes and K.A. Lie, Numerical modeling of multiphase first-contact miscible flows. Part 2: Front-tracking/streamline simulation, frontmisc2.tex; 19/10/2006; 0:16; pages 1-27.

A. S. Al-Zawawi, M.E.Hayder, M.A. Baddourah, M.G.B.A.Karim and W. Hidayat, Saudi Aramco, "Using Streamline and Reservoir Simulation to Improve Waterflood Management", SPE Middle East Oil and Gas Show and Confrence, 2011,Manama-Bahrain 25-28 September.

T. Lolomari (SPE), K. Bratvedt (SPE), M. Crane (Schlumberger GeoQuest), William J. Milliken (SPE and Chevron Petroleum Technology Company), J.J. Tyrie (SPE and Schlumberger H-RT), "The Use of Streamline Simulation in Reservoir Management: Methodology and Case Studies", 2000, SPE Annual Technical Conference and Exhibition, Dallas, Texas, 1–4 October 2000.

R.O. Baker, F. Kuppe, S. Chugh, R. Bora, S. Stojanovic, Epic Consulting Ltd., R. Batycky, Streamsim Technologies, Inc., "Full-Field Modeling Using Streamline-Based Simulation: 4 Case Studies", 2001, SPE Reservoir Simulation Symposium held in Houston, Texas, 11–14 February 2001.

E. L. Claridge, "Prediction of Recovery in Unstable Miscible Flooding", 1972, *SPE J*. **12** (2): 143–155. SPE 2930-PA.

R. Habermann, "The Efficiency of Miscible Displacement as a Function of Mobility Ratio", 1960, Petroleum Transactions, AIME, Vol. 219, 264–72. SPE-1540-G.

Alexander Pappas, "Evaluation of Different Correlations for the definition of the Minimum Miscibility Pressure during the injection of $CO_2$/gases on oil reserves", 2019, Athens, Diploma Thesis.

F.I. Stalkup, "Displacement of Oil by Solvent at High Water Saturation", 1970, *SPE J*. **10** (4): 337–348. SPE-2419-PA.

F.I. Stalkup, "Miscible Displacement", 1983a. ,Vol. 8. Monograph Series. Richardson, Texas: SPE.

F.I. Stalkup, "Status of Miscible Displacement", 1983b, *J Pet Technol* **35** (4): 815–826. SPE-9992-PA.

F.I. Stalkup, "Displacement Behavior of the Condensing/Vaporizing Gas Drive Process" , 1987, SPE Annual Technical Conference and Exhibition, Dallas, Texas, 27–30 September. SPE-16715-MS.

L. Yarborough, and L. R. Smith, "Solvent and Driving Gas Compositions for Miscible Slug Displacement" ,1970, *SPE J*. 10 (3): 298–310. SPE-2543-PA.

W. F. Yellig and R. S Metcalfe, "Determination and Prediction of $CO_2$ Minimum Miscibility Pressures" 1980, J Pet Technol 32 (1): 160–168. SPE-7477-PA.

## References

H. Yuan and R.T Johns, Simplified Method for Calculation of Minimum Miscibility Pressure or Enrichment, 2005, *SPE J.*10 (4): 416–425. SPE-77381-PA.

D. Zhou, and F.M. Jr. Orr, "Analysis of Rising-Bubble Experiments to Determine Minimum Miscibility Pressures", 1998, *SPE J.* 3 (1): 19–25. SPE-30786-PA.

A.A. Zick,"A Combined Condensing/Vaporizing Mechanism in the Displacement of Oil by Enriched Gases",1986, SPE Annual Technical Conference and Exhibition, New Orleans, 5–8 October. SPE-15493-MS.